Politecnico di Torino

MSc Automotive engineering
A.a. 2022/2023
Sessione di Laurea Ottobre 2023

Development of a robot for the last-mile delivery

Supervisors:
Prof. Andrea Tonoli
Prof. Alessandro Scattina

Candidate:
Olga Iaconelli
S291464

Tutor:
Ing. Giacomo Mussino

Index

Figure index

Table index

Abstract

This work resumes and continues what has been done previously about the design of the Pacci drone. Pacci is the result of a project started in April 2022, it is an autonomous delivery robot, dealing with the last-mile delivery, which is the last segment of this path, it is the one in which many and different problems have been encountered.

In this work all the main researches about this topic and the problems that have been examined are collected and reported, since these constituted the starting point of the initial stages of design of the ground drone. Particular attention has been dedicated to the themes of sustainability, inclusivity and safety.

After this part, all the requirements, both functional and technical, have been outlined, analysing the devices that have been chosen for the traction system and energy storage, together with the stylistic choices and volumes definition.

The core of this work is represented by the study that has been conducted on the systems enabling the autonomy of the vehicle in driving and travelling among pedestrians, so that a first definition of sensors and controllers has been reported and then they have been integrated in the vehicle system model to test their behaviour.

Chapter 1

With this first chapter, the purpose is the one of placing the project that has been developed, about an autonomous delivery robot, in the present era, in relation to the always more demanding challenges that the technology has to face, to the past events that have changed the lifestyle of many people, to the idealised idea of future cities, that is becoming always more a fact, where everything can be obtained in no more than 15-minutes, to the interaction between humans and machines.

National Research Programme (PNR) 2021- 2027

On the 13th of July 2021 the National Research Programme (PNR) 2021- 2027 has been approved by the Economic and Financial Affairs Council of the EU (ECOFIN Council).

The document, reporting all the economic, social, scientific and technological objectives, highlighted the importance and the necessity of research and innovation in the field of digitalisation, industry and aerospace. The themes covered in this program are different: digital transition and industry 4.0, quantum technologies, high performance computing and big data, artificial intelligence, robotics, manufacturing industry innovation and the aerospace. In particular, for Italy, the digital transition represents a fundamental contribution to the overall economic and social development. In the document about "*The role of research and innovation in support of Europe's recovery from the Covid-19 crisis*" has been made clear, about the present situation, how "*The recovery should accelerate the digital and ecological transformation of our societies, with a particular focus on the European Green Deal and giving a clear signal to industry, investors and consumers*". For Europe, and in particular for Italy, this represents a greater challenge both in ecological and innovation fields which will drive to the achievement of 2030 Sustainable Development Goals. All these digital technologies must give birth to models of interaction between society and industry that are adaptive, customizable and even automatic, in this way it is possible to provide some digital services of great added value and to enable the development of new on-demand products.

The major obstacle that must be faced is the common belief that this innovation will bring to the substitution of workers with robots, this document is about to discuss also this point, making clear how it is fundamental the role played by the training courses that must be led in order to head in the correct direction of innovation; the OCSE recommend of "*Equipping workers with ICT skills needed for the digital transformation*", in this way workers can cooperate and deal with the digital technologies, making possible an optimization of some processes, in a view of safety and security of the workers themselves; these devices can operate in many situations that can result to be dangerous or too heavy for humans.

Some of the key words that often resonate in the document are "*interdisciplinary, intersectoriality and interinstitutionality*" to highlight how this innovation does not involve just one research field, because there is no distinction between one discipline end and another one beginning, they are all merged together, for this reason the objectives of this innovation are not just technological, but they will have a strong influence also on the socio-economic scenario, which must be prepared for this new advent.

The project that has been developed during the past months comes under the category of the digital transition and Industry 4.0 and it can be defined as part of the so-called "Human-centred services", since it has been thought with a particular focus on the necessities, the characteristic and the ability to adapt to all the users, the access to these kinds of services must be easy, safe and economically sustainable. It is a ground drone, which aims to solve the majority of the problems related to the last-mile delivery.

For what concerns the "Digital Technologies", three different areas can be identified: the first one concerns the "*Cyber Physical Systems*" which are all characterized by the integration between a physical system and a digital system with the aim of controlling this latter; the "*Software Systems*" which are software systems equipped with adaptability, interoperability and scalability for the management and interconnection of production, computing and storage equipment; then the "*Sensors and IoT*", field in which the utilisation of evolved sensors applied to the different environment of social and productive life is introduced. According to this classification, our project merges all these systems in a device for which the interaction between the physical and the digital systems results to be fundamental, the adaptability and interoperability, together with multi-tasking ability, for what the delivery services can be concerned, are some of the guidelines that were followed; then, all these tasks cannot be operated without a strong connection between external signals and their manipulation, so that evolved sensors are necessary, even in a view of optimization, customization and reliability of the services that this device can carry out.

Some of the objectives, that are reported in this program, were clear from the initial stages of the design of the concept, they are reported in the following:

- *"Development of technological solutions aimed at extending access to digital services to all categories of citizens, with particular reference to vulnerable groups, people with disabilities, people with less digital skills;*

[…]

- *Development of biometric technologies for access to personalised services;"* [1]

These represent just two of the cornerstones around which our project has been developed together with the purpose of making use of electric vehicles in order to fight the effects on urban emission. It has been estimated by ISPRA (Istituto Superiore per la Protezione e la Ricerca Ambientale) that, in 2019, the transport sector was responsible of 25,2% of the greenhouse gases emission and among this percentage, the 92,6% was due to the road transport.

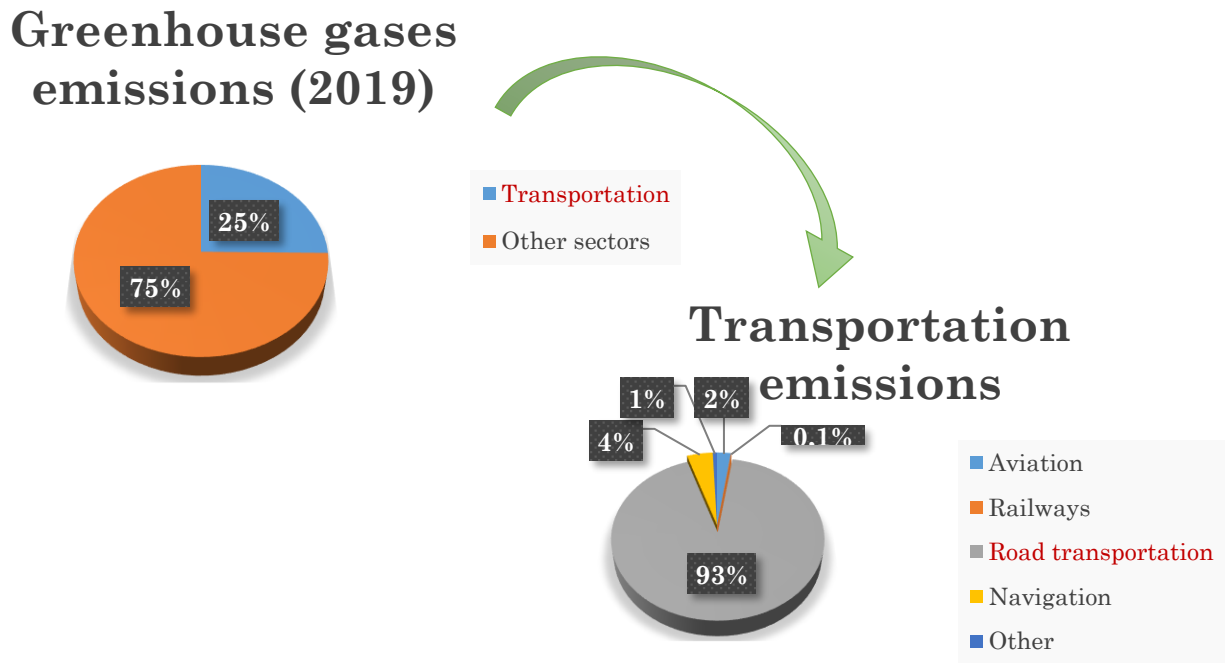

Figure 1 : Greenhouse gases emissions in 2019 and Transportation emissions, ISPRA, 2021

The other objective is what has been called "Design for all", which means the realization of a device with an inclusive design, capable to satisfy the needs of people with reduced mobility, in terms of delivery. In Italy it has been estimated that the people with reduced mobility are about 5,2% of the total population, with a growth forecast of 25% in 2060. According to surveys, most of them prefer not to buy on the internet because of the problems related to the fastness of delivery service, increasing, in this way, the number of missed deliveries. With this project, the drone can wait for the customer to come to the door and pick up his or her order, because, having the rover a reduced number of parcels to deliver and providing a detailed localisation to the buyers, it is not a problem for it to wait some more minutes to complete its

operations. Also for this reason our project proposes to minimise the number of missed deliveries, also taking notice of the fact that each return costs about 15 euros to the delivery companies. An additional potential issue that this device can solve could be the fact that according to the projections, there will be an increase of the deliveries up to 200% until 2030, but our system will be able to satisfy the rising number of shipments, with a minimum impact on urban traffic and emissions. For what concerns the environment in which the people and the drone can "walk" side by side, the aesthetic plays a fundamental role. It must be integrated in an urban environment and must not annoy or hold up pedestrians, it must be as much as possible user-friendly.

15-minute cities

The pandemic left the awareness that the whole urban areas must be re-though in a more sustainable and resilient way; in this scenario, the definition of 15-minute city was born, as a kind of necessity, with the particular aim of preserving the quality of life beyond the fractures that the virus left behind it.

What is a 15-minute city?

The definition of 15-minute cities has been first explained by Carlos Moreno, who can be regarded as its very first author and won the Obel Award in 2021; to him "*the 15-minute city rides on the concept of "chrono-urbanism", which outlines that the quality of urban life is inversely proportional to the amount of time invested in transportation […]. He advocates for an urban set-up where locals are able to access all of their basic essentials at distances that would not take them more than 15 minutes by foot or by bicycle. […] Residents will be able to enjoy a higher quality of life where they will be able to effectively fulfil six essential urban social functions to sustain a decent urban life. Those include living, working, commerce, healthcare, education and entertainment*." [2]

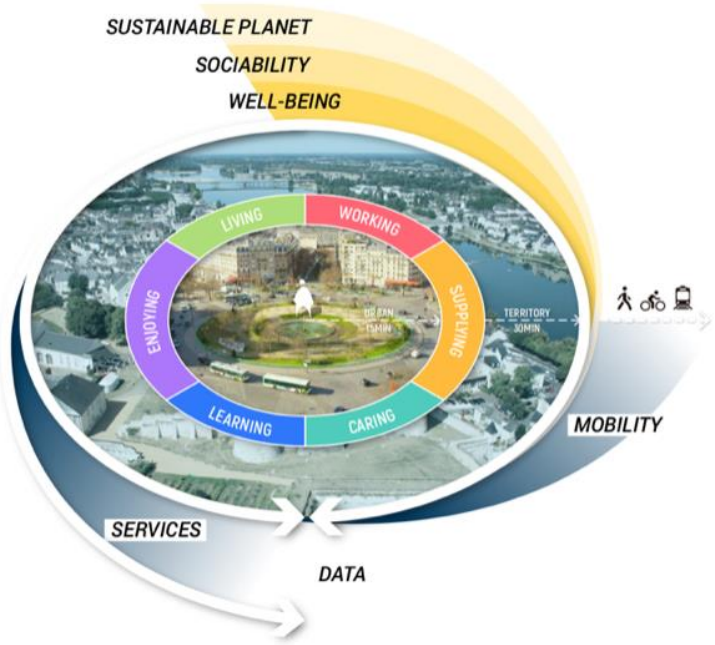

Figure 2 : 15-minute city, Carlos Moreno

The project that is going to be discussed is about to be placed in a smart city of this kind: it has been thought in a prospective in which the efficient services offered by the urban transportation infrastructure can be exploited in order to fasten the delivery service. In a city like Turin, it has been observed that each 5-10 minutes a bus serves a certain urban area, so that the cooperation with the drones could result to be quite satisfying, in order to not increase the urban traffic and to make these systems operate in a faster way. The purpose is trying to make the delivery service so efficient that it will take 15 minutes from the bus stop to the customer house to deliver an on-line order and it can be possible. In the following images the whole process is reported.

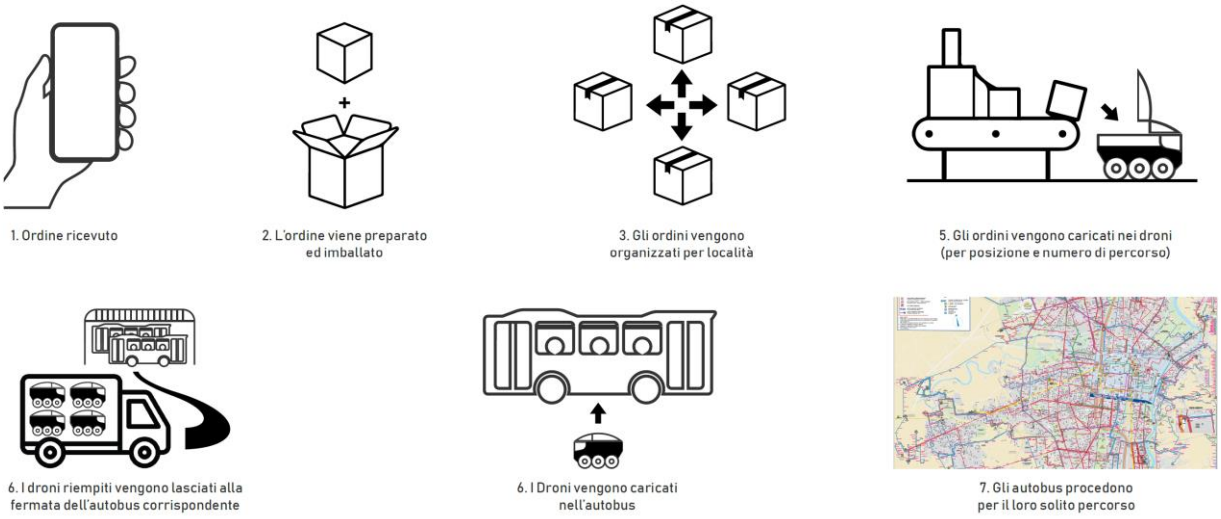

Figure 3 : First part of the delivery process

In the first icon the customer has decided to buy an item from the e-commerce site, so that the order has been received, as soon as it arrives to the warehouse, it must be processed and then it will be packed. A logistic system is thought to organize the packages according to the location in which they must be sent and, according to this, the drone will be filled up. This will be then brought to the bus terminal corresponding to the bus line which will serve the urban area in which the delivery has been requested; the drone will be loaded in the bus peak, that has been called "backpack", so that it will not hold up the people taking the bus. The GPS system makes possible to localize the drone so that it will get off at the nearest bus stop to the customer. Once it is on the ground, it will automatically send a notification to the person who will be served in order to make him aware of the incoming purchase. The drone will serve an area of 1km^2 and it can bring a maximum weight of 30 kg. It will drive to the customer's house, where he or she can pick up the item by means of recognition systems based on biometric data.

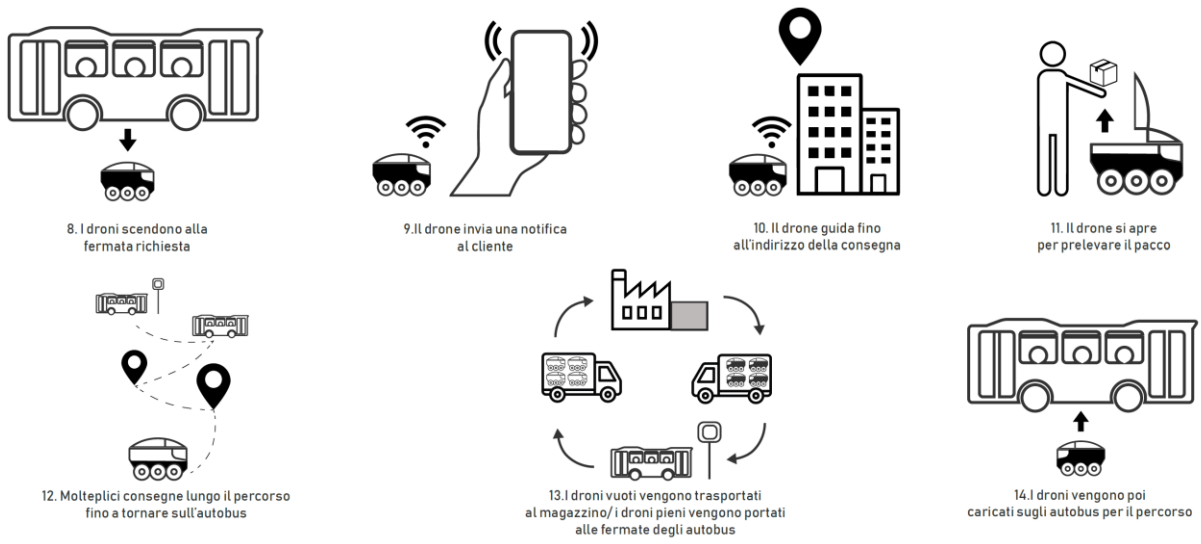

Figure 4 : Second part of the delivery process

Once the parcel has been delivered, the drone can plan to collect some returns, if they are present on its path, and then come back to the nearest bus stop. A bus will take it and bring it to the bus terminal where it will be withdrawn and delivered to the warehouse, where other full drones will be ready to be collected.

Delivery services during pandemic

The pandemic showed the resiliency of delivery services. These resulted to be fundamental in order to limit or eliminate the danger of contagion. Some solution, similar to the one that is proposed in this document, were developed in this period, especially for the healthcare environment, to move medicines between hospital wards; some other were thought to bring home food from grocery stores or for the meal delivery services; other devices were designed also to collect garbage from sidewalks. The pandemic transformed in an irreversible way many aspects of the economic and social scenario; for what concerns these kinds of services, the necessity to get essential goods, staying at home, made indispensable people to learn how to use and interact with e-commerce and online purchases, moreover, many restaurants, markets and warehouses had to adapt to this new scenery, so they started to deliver their products or make use of the delivery services that were already existing. Nowadays, most of them continue having a kind of e-commerce, noticing that this can be an extra service that is much appreciated by the customers. The project that is going to be presented ranks among this challenging scenario, in which an increasing number of online orders shipment must be satisfied. Taking into consideration an urban setting like Turin, it has been estimated that, if these drones would operate on a working turn from 9 in the morning to 18 in the evening, taking into consideration that every 5-10 minutes a bus will stop for the drop-off of its passenger, a number of about 300 parcels can be potentially shipped in an area of about 1 km^2, considering the most severe situation in which all the 4 drone, filled with the maximum number of orders, will serve the same zone.

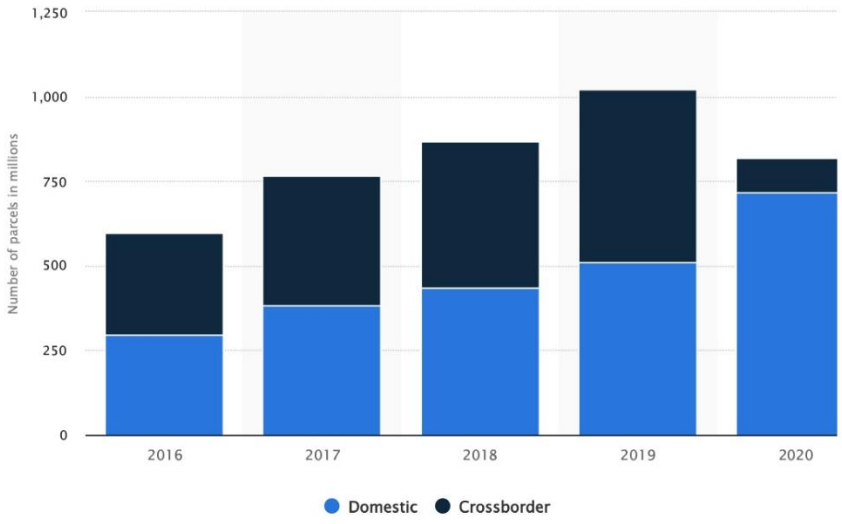

Figure 5 : Number of parcels delivered in Italy from 2016 to 2020, by type, Statista Research Department, 2022[3]

In this diagram the number of parcels delivered in Italy from 2016 to 2020 are reported, it can be noticed how the domestic parcels had and is still having a growing

trend with a big increase registered in 2020, with 718 million orders delivered to customers' houses.

LIP project: PACCI for the last mile

LIP stands for "Product Innovation Laboratory" and from this, the project that will accomplish all of the tasks mentioned until now and will solve most of the problems related to the last-mile delivery, was born with the name of Pacci. It is a ground drone that is capable of travelling autonomously in an urban setting to deliver parcels and collect returns. This will rely on the urban transport infrastructure, by means of an additional component, the backpack, that must be added to the bus in order to move the drone from the bus terminal, typically in the suburban area, to the city centre. The path that brought to the definition of this concept started in April 2022 thanks to the initiative of "Di Bartolo" Design Research Centre, CIM4.0 SMTC, the European Institute of Design IED and Politecnico of Turin.

The students from "Transportation Design" of IED dealt with the aesthetic and visual part, while the students from Politecnico of Turin dealt with the engineering part, designing the devices to make it possible for the drone to move in an urban environment, to drive autonomously and to deliver the parcels in a way that could be easily accessible and safe. In particular, in the following chapters, the development part about virtual dynamic simulation will be outlined.

This has been a very interesting training experience, the different worlds of designer and engineers merged and worked together since the initial stages of the definition of this concept. From my side, working together has been quite compelling and not without many debates. The way designers approached this project was totally different from the one of engineers, that is typically more schematic. Apart from this challenging situation, a good relationship has established between us which lies outside the project itself.

On the 12th of September the final presentation of the Pacci concept has been shown in the suggestive and particular scenery of the FCA Heritage Hub in Turin.

Chapter 2

In this chapter the project that brought to the definition of the Pacci drone is presented, together with some analyses about some guidelines that have been defined during the initial stages, well in advance with respect to the definition of shapes and what came immediately after, and, in particular, about the interaction with the external environment, so its level of autonomy and safety, the different requirements that must be satisfied in order to not result dangerous for other people, passing through some considerations about an initial regulation that could represent, the starting point for future homologation of fully autonomous vehicles and finally to the most important user interaction, which results to be a fundamental aspect to make the delivery service effective and efficient.

Pacci

Pacci is a ground drone of reduced dimensions which can travel autonomously among people, without annoying or scaring them; due to the colours that have been chosen, the different textures, its rounded and harmonious shape, it gives the impression of a harmless and friendly robot. Lightings make easily understandable what are the compartments which are full (red colour) or empty (green colour), moreover, the led screen will switch on whenever the costumer get closer to the drone, giving all the information about the parcel that he or she has to pick up, so that the interaction with users will be even easier.

Figure 6 : Rendering of Pacci travelling in a pedestrian area

The idea of designing this little robot was born with the aim of solving the problems related to the last-mile delivery, that is the last segment of the delivery path items must travel to get to consumer's house. This last, results to be the most problematic phase, because it is the one that in terms of emissions is the most pollutant and it is the one that in large part contributes to the urban traffic, noticing also how much the request of delivery services is rapidly increasing. From this, the idea of taking advantage of a well-structured and proven system, that is the one of urban transportation; the challenge now is to think about a way to transport in an efficient way the different drones, without affecting the maximum capacity of the buses.

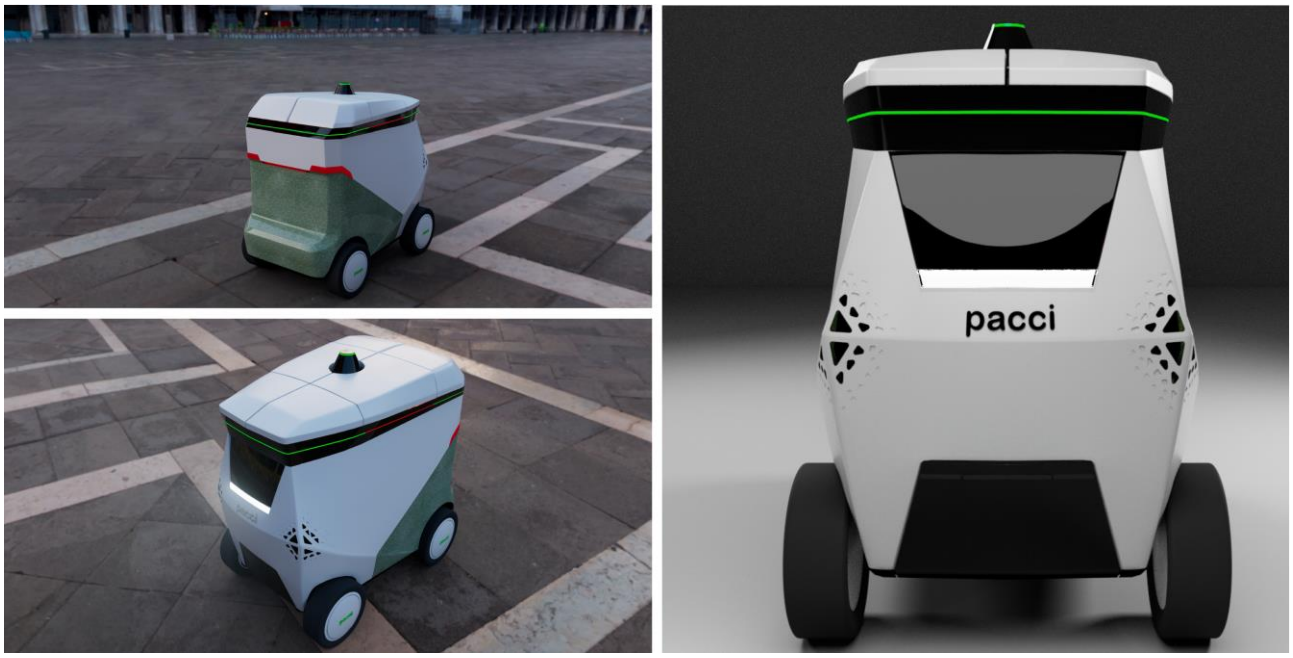

Figure 7 : Rendering of Pacci from different prospective

So that, the backpack has been designed; it is an additional part that will be hooked up to the bus, in this way the drone transport will not compromise the bus capacity in terms of passengers, so that the drone can be moved also during rush hours. This peak can bring up to 3 or 4 drones simultaneously per each travel, it has a ramp that can be opened by the bus driver together with the bus doors; in this way the drone can autonomously get on or off according to the accomplishment of its mission.

Figure 8 : Rendering of the peak with the drone getting on it at the bus stop

Autonomy level

The field of autonomous robots is expanding very fast and many sectors are pursuing to involve these systems, apart from delivery, there are also industries, homes, disasters management, hospitals, military and many others which decide to rely on them in the prospective of optimization, to perform tasks that can result to be dangerous or time consuming for humans.

The "Recommended Practice J3016" of SAE reports the precise definitions of the six levels of driving automation, from Level 0 of no automation to Level 5 of full driving automation.

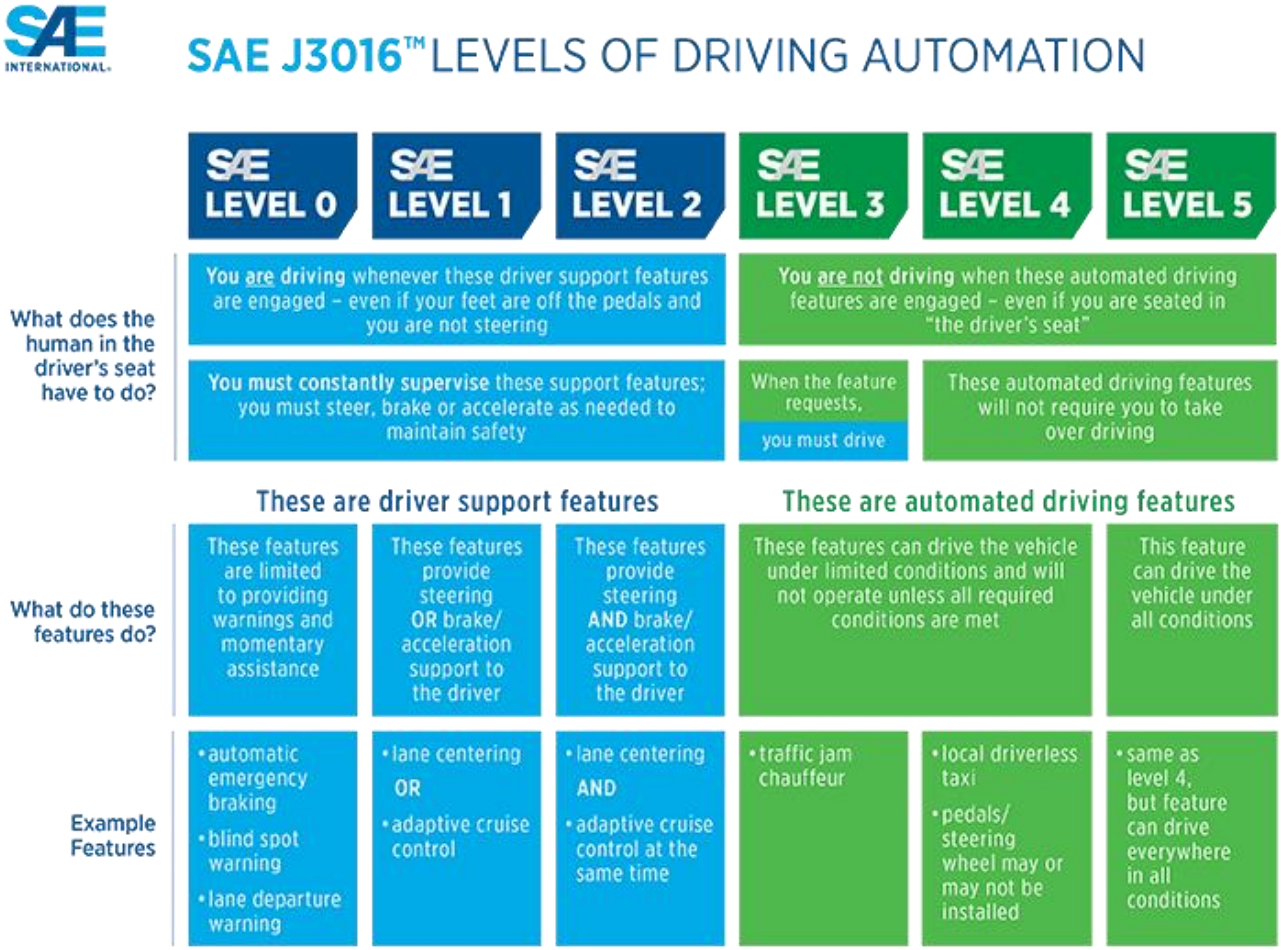

Figure 9 : SAE J3016: Levels of driving automation

The level 0 is the one in which the driver has the full-control of the vehicle, in this classification fall all the devices that are limited to providing warnings and momentary assistance, like the automatic emergency braking, the blind spot warning or the lane departure warning; vehicles provided with level 1 of driving automation are the ones in which driver support features provide steering or braking or acceleration, in this category falls devices like lane centering or adaptive cruise control, both steering and braking and acceleration features are provided to the driver in the 2nd level of driving automation. All these three levels require that the driver is constantly driving the vehicle and the features must be always supervised by him. Going on, there is the level 3, the driver is asked to drive when requested by the feature, but the functionalities provided to this kind of vehicles are such that they can drive autonomously in most of the ordinary situations, while the driver can be asked to drive in some particular scenarios; vehicles provided with level 4 of autonomous driving can drive by themselves, but these are provided with all the devices that are necessary to drive it, so that the driver can take the control of the vehicle whenever he or she finds it necessary; finally, the last one is level 5, the vehicle in this case can drive autonomously and the driver can be seen as a passenger, this level 5 is typical of the future MaaS autonomous vehicles (Mobility as a Service).

According to the SAE classification reported above, Pacci falls into the 5th level of automation. An autonomous robot has to deal with the environment surrounding it and it must face the different scenarios that can be present in front of it; it has to work without the intervention of human supervisors for extended periods, in order to do this, it must be able to take the information provided by sensors, to perceive what is around it in a sufficient large spectrum, to localize itself precisely in any scenario and to deliver an optimised action plan to accomplish its mission; all these tasks must be performed in real time and in complete safety. This drone has been thought to operate also in case of fault of one or more sensors, so that a certain redundancy has been taken into consideration and also strategies to work in a situation like that.

Safety

"An automated/ autonomous vehicle shall not cause any non-tolerable risk". The most important topic is the one related to safety, especially because this drone has to deal with an environment strongly affected by the presence of humans, both on foot or by some means of transportation. The World Forum for Harmonization of Vehicle Regulations (WP.29) for automated self-driving cars purposes to realize their potential, especially to improve road traffic, they must be brought to market in a way that gives road users confidence in their safety. WP.29 aims to deliver safe road vehicles in a consistent manner and to provide a framework that will help foster collaboration and communication between those involved in their development and monitoring.

The common principles that must be pursued are

- *System Safety:* risk-free for driver or other road users and compliance to road traffic regulations*;*
- *Failsafe Response:* the ability of detecting failures or when the conditions for ODD/OD are not met anymore and switch to a minimal risk condition autonomously;
- *Human Machine Interface (HMI)/ Operator Information:* driver engagement wherever the driver could be involved and in case of automated vehicles this regards the interaction with other road user;
- *Object Event Detection and Response (OEDR):* the ability of detection and recognition of obstacles or events and fast response to them;
- *Operational Design Domain (ODD/OD):* set of specific conditions the vehicle has to deal with during the automated driving mode;
- *Validation for System Safety:* robust design and validation process according to which the system is able to comply with the external environment according also to road traffic regulations;

- *Cybersecurity:* protection against cyber-attacks in accordance with established best practices for cyber vehicle physical systems*;*
- *Software Updates:* updated must occur as needed in a secured way and after-market repairs and modifications must be provided as needed;
- *Event data recorder (EDR) and Data Storage System for Automated Driving Vehicles (DSSAS):* function according to which data related to the system status are collected and recorded. [4]

In Italy a road regulation for Autonomous Vehicles of level 3 and successive ones does not exist; consumers are not allowed to use these vehicles on public roads and testing is permitted only under specific permissions of level 3 and 4 AVs. Even homologation results to be quite difficult for level 5 AVs, because a specific procedure has not been defined yet; it exists a procedure called "temporary homologation" for the experimental testing of prototypes, but this one has not the same aim as the standard homologation cycles, due also to the fact that the procedure of the homologation of vehicles provided with ADAS and driving software must provide more requirements, so it cannot be the same as the one of driven vehicles, where humans are constantly monitoring and modifying its behaviour. Despite the great improvement of the technologies in this field, the big step forward in the development of this systems, the legislative framework seems to be the major obstacle to overcome; the major concern is about which or who is the responsible in case of failure or in case of an accident.

In 2018, the strategy paper "*On the road to automated mobility: An EU strategy for mobility of the future*" was published by the European Commission and in this document the intention to make Europe leader in the world of the development of connected and automated mobility was declared. Another important issue concerns the storage of data collected during the different phases of training of automated vehicles, the United Nations Economic Commission for Europe, UNECE finalised at the end of 2022 the "*Regulation on Storage System for Automated Vehicles (DSSAD)*". [5]

This is paving the way for the future of mobility, especially in urban area, where the issue of traffic and pollution, as a consequence, is suffered the most, so 2023 represents a decisive year for the development of smart mobility.

Human-machine communication

With the acronym “HMI” all the interfaces between a human and a machine are indicated, in the most various fields, it could indicate the touchscreen on the dashboard of a car by means of which the driver can set different options regarding the vehicle, or it can be the screen by means of which an operator sets the commands to execute certain operations of some mechanical components on a computer numerical control machine. In this case the HMI is represented by the touch screen positioned in the front part of Pacci, this is necessary to communicate with the consumers who has to pick up or return his or her parcel. It has been thought to be easily understandable by users and in order to do this some additional lightings have been added indicating which of the compartments are full or empty. The communication does not concern only the relationship between the consumer and the drone, but comprehend also all the information that Pacci can provide to the drivers and pedestrians around it, like the indication of the direction it has to take or something similar, for this reason it has been equipped by some light projections on the ground that are thought to indicate the path that the drone will follow. In this way the people around the vehicle can predict what direction the drone will take.

From the customer side, instead the smartphone also represents a fundamental device to communicate with the Pacci drone, to understand the scheduling of the delivery and, eventually, also to re-program it. Once the drone has arrived to one of its destinations, the smartphone is necessary to scan a QR-code which will permit the opening of the item to pick up. Once this action has been concluded, the lid on the roof of the Pacci drone will close and the light around it will change its colour, updating its status from full to empty.

Chapter 3

The purpose of this chapter is to focus more on the technical aspects of the Pacci drone, first of all an initial taxonomy about autonomous delivery systems is presented, with the aim of trying to qualify in which category the Pacci drone could fall, then a fast representation of some of the most famous projects about delivery robots and vehicles and wherever they are already operating is reported, to arrive to the outlining of the entire process of design of the Pacci drone. First of all, the requirements have been clearly illustrated, the general ones and the more technical ones, then, this latter part, that has been widely analysed by a colleague from "Product Design", has been briefly discussed, defining all the devices that were necessary to the transmission of motion and energy storage, that constitutes the base from which starting to define the control system and the devices necessary to the autonomous driving; these latter topics will be discussed in the following chapter.

State of art

The efforts of robotics, nowadays, have seen the realisation of many prototypes of autonomous vehicles that are addressed to a variety of operations: in everyday life, from food-delivery, to the collection of waste, in the industrial environment from the transportation of tools along the supply chain, to the robots used to move objects from warehouse to the packaging area, in the healthcare environment for the transportation of medical supplies. All these applications have made been possible thanks to the development of the devices for hardware and software that make a vehicle able to travel autonomously.

For what concerns the delivery services, a taxonomy segmentation of the different ADVs has been published by the World Economic Forum, this was necessary since "*delivery has become a highly attractive application of automated driving systems,*

spurred by a surge in online shopping and grocery delivery that is increasing the load on middle and last-mile logistics", as Michelle Avary, Head of Automotive and Autonomous Mobility, said. [6] This taxonomy aims at describing the risk factors using sub-categories, to allow stakeholders to distinguish between different models and sizes of robots, vehicles or drones. First of all, distinction has to be made clear between the Personal Delivery Devices (PDDs) and Automated Delivery Vehicles (ADVs): the first one is a ground based autonomous vehicle, which can drive autonomously or commanded remotely, typically it is very small and it can bring goods just for one customer at a time, it can operate in public spaces, but cannot fully use the road as a car or a truck, it can travel on sidewalks, parks, campuses and pedestrianized urban areas; it can also be used in warehouses, shops and distribution hub. Differently, the ADV are based on conventional vehicle, van or truck and for this reason they can make fully use of roads and highways; their application can be in urban, residential or extra-urban environments. Moreover, the dimensions are much bigger than the one of PDD. According to this we can identify Pacci more related to PDDs category than ADVs. The PDDs sub-categories can be differentiated according to weight or maximum speed. The first sub-category identifies small PDDs if the weight is up to 100 kg, middleweight PDDs if it is between 101 and 250 kg and large PDDs if the weight is larger than 251 kg. According to maximum speed, it can be identified an ultra-low speed PDD if its maximum speed is lower than 5 km/h, a low speed PDD if this is between 6 and 15 km/h and high speed PDD if its maximum speed is higher than 15 km/h. According to this classification Pacci is a small, high speed PDD, in fact its weight is lower than 100kg and its maximum speed is about 30 km/h. Actually, if the rigorous definition is considered, Pacci cannot be classified as a PDD, because it has been projected to serve more than one costumer, but since its maximum speed and its weight are limited, it cannot be classified neither as an ADV; this taxonomy, in fact, is not intended to be an exhaustive categorization of all the possible applications of automated driving systems, so according to the path that the drone can travel, it is correct to put Pacci under the PDD category.

(A): Amazon scout

(B): Piaggio Gita

(C): Starship Robot

(D): Yape

Figure 10 : Examples of Personal Delivery Devices: Amazon Scout by Amazon (a); Gita by Piaggio (b); Starship Robot by Starship Technologies (c); Yape (d).

The first picture represents Amazon Scout, a self-driving robot endowed with six-wheels of reduced dimensions, that are large enough to accommodate small and medium-sized parcels; it travels around the neighbourhood delivering items to Amazon Prime customers and this service has been already introduced in different locations around the US, even if with a supervisor, who must set the route to the destinations. In the second picture a quite different concept has been developed by Piaggio Fast Forward, with Gita, a rounded self-driving robot equipped with artificial intelligence; it can be regarded as a personal assistant, it can be loaded with small items and by means of an AI algorithm, it will always follow its owner. Another example is Starship from Starship Technologies, a six-wheeled ground drone, which can travel autonomously within a 6 km range, it can bring up to two bags from grocery stores in its compartment and in 2017 Dominos entered into a partnership with Starhip Technologies to use these robots as PDD. Last one is Yape, a very recent prototype that has been tested in Milan, it is a ground drone that takes care of last-mile delivery, it can be loaded up to 10 kg, can travel autonomously for about 80 km and can reach a maximum speed of 6 km/h.

(E): Nuro

(F): Robomart

(G): Udelv

Figure 11 : Examples of Automated Delivery Vehicles: Nuro (e); Robomart (f); Udelv (g).

In these images are reported some ADVs: the first picture represents Nuro, a self-driving delivery robot, designed to carry more goods and makes possible to perform more deliveries; it has been thought to travel in the neighbourhood, so it has to be extremely safe for pedestrians; in 2021 a partnership with Domino's has started to deliver pizza in Houston. In the second picture a kind of small grocery store on wheels is reported, it is Robomart, a self-driving robot able to control refrigeration and temperature in its compartment; once customers want to buy something from it, they can request for the nearest Robomart by means of the dedicated app, this ADV will reach the person so to let him or her to pick the food he or she desires, simply unlocking the doors by means of their phone. In the third picture there is Udelv, a driverless, multi-stop delivery vehicle, endowed with modular cargo; it can deliver a variety of items and it can cover also the middle-mile delivery on road, its purpose is the *high volume delivery being eco, business and customer-friendly*. It is operative from 2017 in California, Arizona and Texas.

In the following chapter the design of the hardware of Pacci drone will be illustrated. The core of this phase was to have clear in mind all the operation that this drone has to carry out and also all the obstacles and difficulties that it would meet during its path.

Definition of the requirements

The project has been defined from scratch, the very initial stages are represented by the inventive and imaginary part, a kind of brainstorming about anything that can be used as a mean of transportation, in this phase the central core, in fact, was the one of carrying objects or humans or whatever the brain could imagine. After this phase, a partial idea of what we were going to design was coming out. The research phase came soon after, based on real data, collected from different articles, and on the needs that were made explicit and that the current service cannot satisfy. Starting from all these information, a first definition of the requirements was carried out as an answer to the problems that emerged during the research phase.

Needs	Solution
Storage due to the increasing number of online purchases	Subdivide the total volume of delivery items in smaller volumes on reduced areas so that the delivery mission can be accomplished in a faster and simpler way.
Sustainability	Make use of small battery electric vehicles.
Urban congestion reduction	Make use of small vehicles capable of travelling autonomously on mixed scenario (pedestrian area or roads), which will rely on urban transportation infrastructure.
Costs of returns minimization (time and money)	Implement a strategy according to which returns can be managed in an efficient and cheaper way.
Missed deliveries reduction	Real time updates of the shipment progress and possibility of update the shipment address up to 20 minutes before delivery.
Inclusivity	Personalized delivery system according to the needs of each user: due to the reduced volume of purchase, the drone can wait some more minutes than a standard delivery service.
Safety	The delivery robot has to travel in a mixed scenario, in the urban area, but also on sidewalks and shoulders, it must be safe, it has to not annoy or scare people.

Table 1 : Functional requirements for Pacci delivery robot

Once these functional requirements have been defined, the technical requirements must be defined around them.

Requirement	Solution
Sharing of urban and pedestrian scenario	Reduced dimensions to be physically non-invasive: 105cm x 105cm x 55cm.
Battery electric vehicle	Dimensioning of a Lithium-ion battery on a defined standard-type driving cycle.
Motion devices	In-wheel electric motors; Inflated tyres; Disc brakes; 4-steering wheels; McPherson suspension.
Autonomous driving	Proprioceptive sensors; GPS; LiDAR; Stereocamera; Control system.
Interaction with the user	Touchscreen display; Lightings; App.

Table 2 : Technical requirements for Pacci delivery robot

To resume all the requirements a summary picture has been reported in the following with particular focus on the technical aspects of the ground drone.

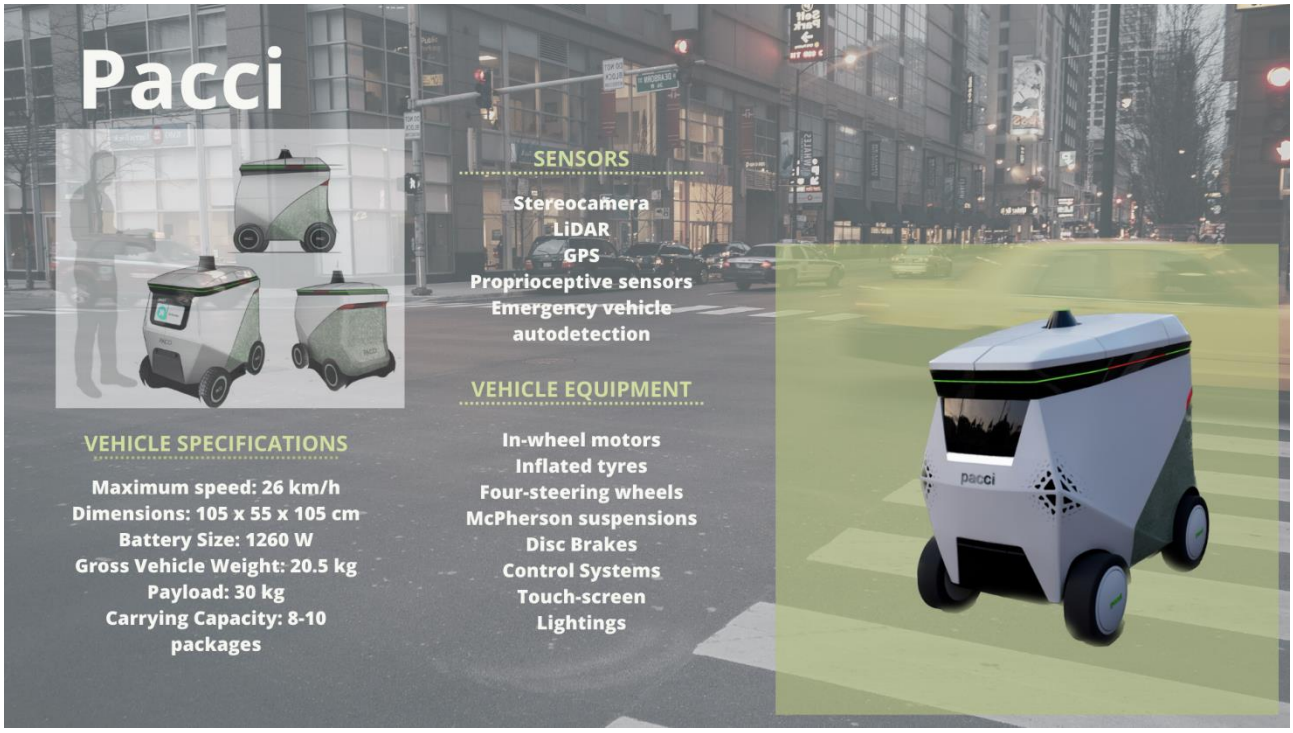

Figure 12 : Main Features of Pacci drone

Design phase

For each of the requirement that has been listed previously, an accurate research and study of the specific needs has been carried out, some of them are reported in the following chapter.

Dimensions and volumes

Research on the delivery service, revealed that the vast majority of packages delivered are typically of small-medium sizes (up to 5 kg), so that, from these dimensions, it was possible to establish the overall dimensions and carrying volumes of the drone.

Small packages:	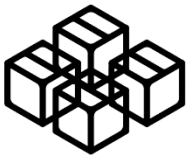	25 x 35,3 x 5 cm
Medium packages:		37 x 29.4 x 12.8 cm
Large packages:	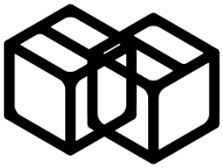	25 x 29 x 40 cm

Figure 13 : Standard sizes of packages up to 5 kg

The idea was to keep a modest size of the drone, and, according to the data about standard sizes of packages, check the best size to accommodate the largest possible number of packages, but without exceeding some limit dimensions derived from ergonomic tables. This latter choice has been discussed in order to design a robot that was thought to share the same environment with pedestrians, so to be as much as possible integrated in this kind of scenario, without annoying or scaring people around it. Finally, the overall dimensions of the drone have been chosen, as reported in the following figure.

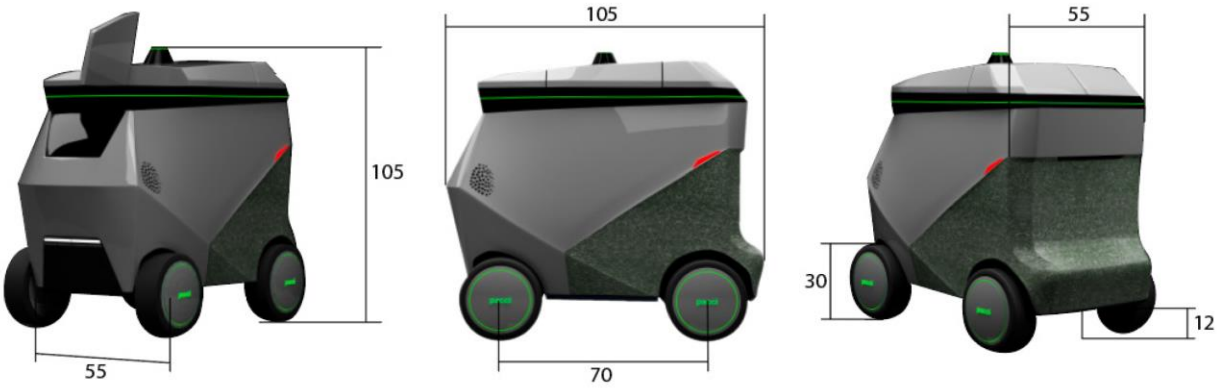

Figure 14 : Overall dimensions of Pacci drone (all the reported dimensions are in cm)

According to these representations, in the worst case in terms of capacity, Pacci can be loaded by *6 large packages*, for a total payload of *30 kg*. As can be noticed by the sketches reported above, there are some other interesting features of Pacci drone, like, for example, the lids on the roof, they were inspired by some lockers that can be found around cities, and that are necessary to accomplish more than just one delivery and to keep safe each parcel, so that the customer can pick or place just his or her order, so that the service will be efficient, intuitive and free from any possible error. Moreover, to facilitate the extraction of parcels, with a particular attention to people affected by reduced mobility, a system of small pistons has been placed under the compartment containing the parcel, to bring this at the level of the roof so to help the customer to pick it.

A special attention has been devoted in the choice of the shapes and colours. The purpose was to reflect the choices and the requirements also in the aesthetic aspect of the Pacci drone, for this reason the rounded shape gives the impression of a friendly robot and with an eye on passive safety, they have been designed in order to reduce as much as possible the severity of an accidental impact with a pedestrian; in the rear part a particular texture made of recycled fabric has been inserted to resemble the sustainability value that was one of the most important goals. Lightings have been positioned all around the drone roof, in order to make it clearly visible even in foggy days and to indicate the compartment that are free or already occupied by a parcel. In the front part the touchscreen has been placed to interact with user and give him or her instruction about the item to be delivered or returned.

Battery design

To design the battery, it has been defined a standard cycle in an area of 1 km^2 , which could represent all the possible situations that the drone can face in its operating life, it is reported below.

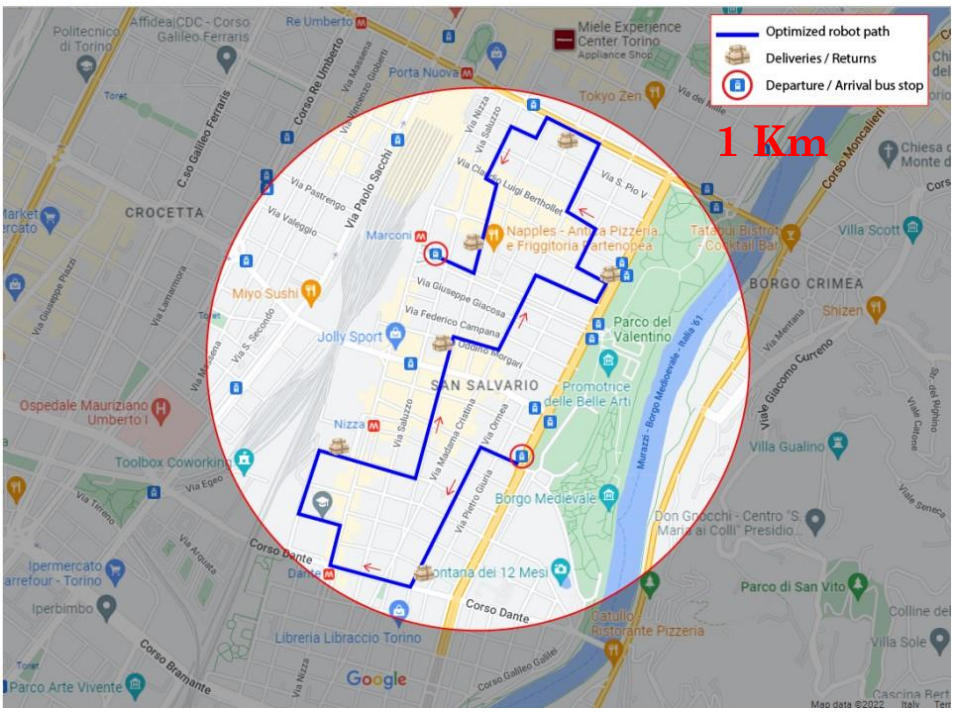

Figure 15 : Standard cycle simulation in San Salvario district, Turin

The starting point of this path is the bus stop near Parco del Valentino, in San Salvario district, the Pacci drone will drop off the bus peak and it will travel mainly on sidewalks, being in a residential area. This driving profile will present many speed changes due to diversity of the path (presence of pedestrians, ramps, obstacles), it will stop at the traffic lights for about 40 to 60 seconds, short stops of about 5-7 seconds are considered whenever the drone has to wait for a pedestrian to cross in front of it, longer stops instead are dedicated to the delivery mechanism and, according to the customer need, these can take from 2 to 5 minutes. At the end of its working turn, the Pacci drone will get to the nearest bus stop in order to take the bus and drop down at the bus terminal, where some operators will bring it to the warehouse, to change the battery with a charged one in case of battery swap or to charge it and fill it again with items, so to start another delivery mission.

The standard cycle counts 6 missions along its path, for a total of three and a half kilometres travelled by the Pacci drone on mixed scenario, with an average speed of 8.5 km/h and a duration of 1493 seconds. The traction system has been sized under these circumstances, also taking into consideration the possibility of regenerative braking. The battery in the end will result a little over-sized in order to make possible to work in more severe circumstances, where regenerative braking could be disabled, the Pacci drone will travel at its maximum power, with a slope of 15%.

The battery that has been chosen count a total number of *50 Lithium-ion cylindrical cells* and among these *10* are *in series*, while *5* are *in parallel*, with a power equal to *1260 W*. Its dimensions will be *210 x 107 x 70 mm* and its total mass will be of *6,5 kg*. All the battery specifics are listed in the table below.

Parameter	**Value**	**Units**
Number of cells in series	10	-
Number of cells in parallel	5	-
Total number of cells	50	-
Nominal voltage	36	V
Capacity	24	Ah
Rated discharge current	35	A
Instantaneous maximum discharge current	75	A
C-rate charge	0.35	-
C-rate discharge	3	-
Contained energy	864	Wh
Usable energy	690	Wh
Power	1260	W
Volume	210x107x70	mm
Weight	6.5	kg
BMS additional weight factor	1.5	-

Table 3 : Battery Pack Specifications

Single cell

Battery module 10S5P

Final assembly

Figure 16 : Battery layout

Electric motor choice

For what concerns the choice of the electric motor, a fail-safe oriented decision has been taken; in fact, it has been opted for 4 in-wheel electric motors in order to guarantee that the drone could continue to travel even in a condition in which one electric motor could not operate anymore because of some faults, having the other three electric motors, the drone can continue independently its working cycle, until it returns back to the warehouse. Always according to the standard cycle that has been defined previously, the maximum requested power, torque and speed have been derived taking into account just two traction wheels, in order to guarantee a fail-safe behaviour in case of fault of the other two electric motors. Once these parameters have been evaluated the choice was oriented toward a *three-phase brushless DC motor*.

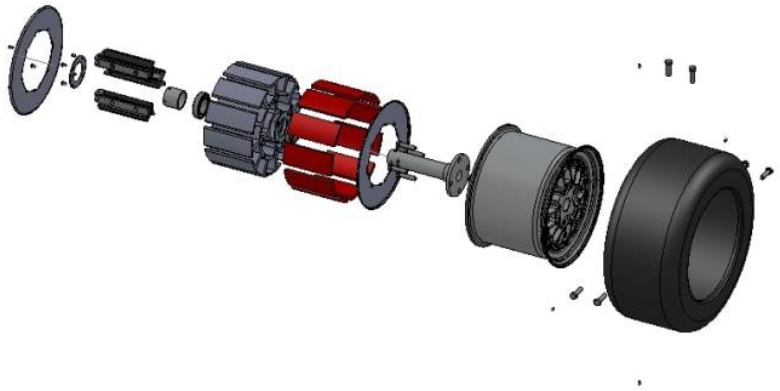

Figure 17 : In wheel brushless DC motor

The model that has been chosen is the *HJ-017 Bldc motor* and its characteristics are reported in the table below

Parameter	**Value**	**Unit**
Voltage	36	V
Rated power	250	W
Peak power	300	W
Peak torque	11.6	Nm
Max speed	650	rpm
Max efficiency	84.5	%
Dimensions (diameter)	220	mm
Weight	3.3	kg

Table 4 : Data-sheet of HJ-017 Bldc motor

After the motor has been chosen, it has been tested in three different situations: vehicle driving on a flat road in 4WD, vehicle driving on a flat road in 2WD and vehicle driving on an inclined road of 15% in 4WD; these tests gave all satisfactory results, for this reason it was the one chosen for the Pacci drone.

Tyres choice

For the wheel design, it has been opted for inflated tyres, that are able to further damp out vibration coming from the ground, especially because the Pacci drone has been though to face also some uneven paths, where dirt and gravel can be present, or streets paved with cobblestones, typical of the city centre and main squares.

The wheels have been dimensioned according to the need that Pacci has to travel on sidewalks and shoulder, to overcome possible obstacles, to easily get on and off steps, without capsizing, in particular their diameter has been evaluated taking into consideration the maximum diameter of the electric motor that is positioned inside each wheel, together with the braking system and the sensors necessary to monitor the speed of each wheel. The diameter of the wheel resulted to be equal to 320 mm, the tyres commonly used for e-scooter have been considered suitable for this application.

Figure 18 : Example of inflated tyre for e-scooter

Imposing the equilibrium of the forces at the contact point between the wheel and the step, it was possible to compute the maximum height of the step that can be overcame by the drone in 4WD mode, that resulted to be equal to 70mm, and the maximum breakover angle that can be faced without that the floor panel could slide on the ground while getting on or off a ramp, that resulted to be equal to 36°.

Ground clearance	120	mm
Maximum step height	70	mm
Breakover angle	36	deg

Table 5 : Summary table about the study on the wheels

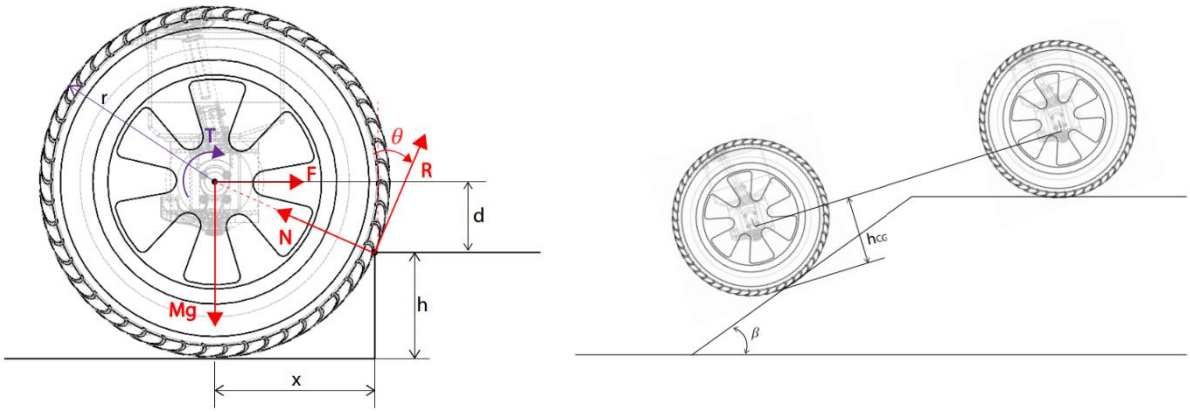

Figure 19 : Study of the maximum step and of breakover angle

Suspension design

The suspension system of the Pacci drone has to guarantee the stability of the vehicle, to avoid damages of the payload, maybe due to overturn or to uneven paths; moreover, they must be compact, due to size limitation of the vehicle, and must assure a sufficient insulation from the irregularities of the ground that the Pacci drone could face during its missions. Taking into consideration these two aspect, the McPherson suspension resulted to be the most suitable and it is the one that has been chosen also due to its design simplicity, compactness and cost, they can act independently one from the other, without the need of having a common axle to connect them, it has been proven that the forces coming from the ground are better distributed on the body part and are lower in comparison to another type of suspension and a higher stroke is allowed with respect to other types of suspensions.

The geometric parameters and the rotation centres have been evaluated and are reported in the following table:

Parameter	Value	Unit	Parameter	X	Y	Z	Unit
Lower arm	152	mm	Instant centre (x-y)	0	982	183	mm
Suspension length	230	mm	Instant centre (z-x)	503	0	240	mm
King pin angle	13	deg	Roll centre	0	250	51	mm
Caster angle	15	deg	Pitch centre	350	0	173	mm

Table 6: Suspension parameters

They are represented in the following figures.

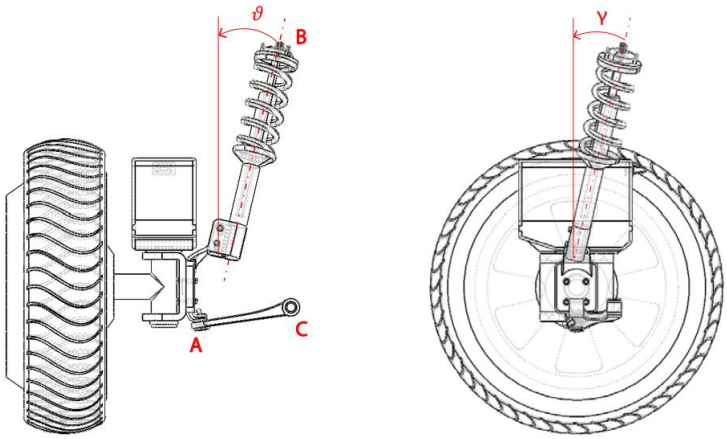

Figure 20: Geometry of the McPherson suspension

In this figure above the lower arm length is the one between the points A and C, the suspension length is the overall distance between A and B, the caster angle is the one reported with the Greek letter γ.

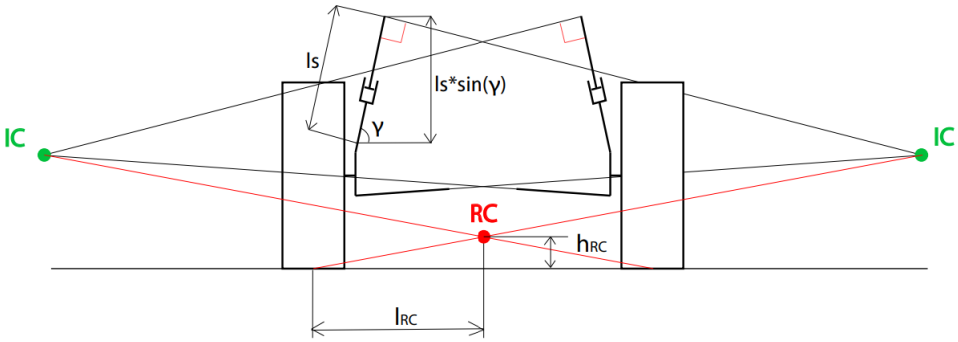

Figure 21: Geometry and articulation points (x-y plane)

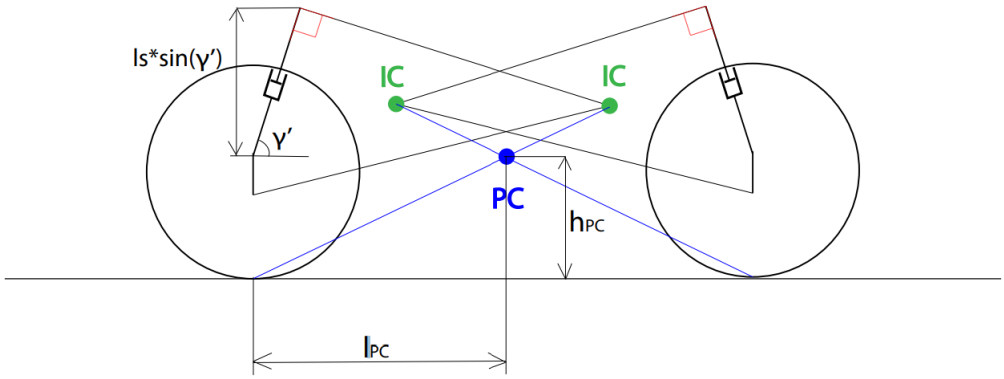

Figure 22: Geometry and articulation points (x-z plane)

In the two figures above, instead, the rotation centres can be individuated. The instant centre of rotation is marked with the letters IC both in the X-Y plane and in the X-Z plane, the roll centre is marked with RC and it is reported in the geometry on the X-Y plane and the pitch centre is reported in the geometry on the X-Z plane with the letters PC.

In the figure below the representation of McPherson suspension applied on the wheel assembly of the Pacci drone is reported.

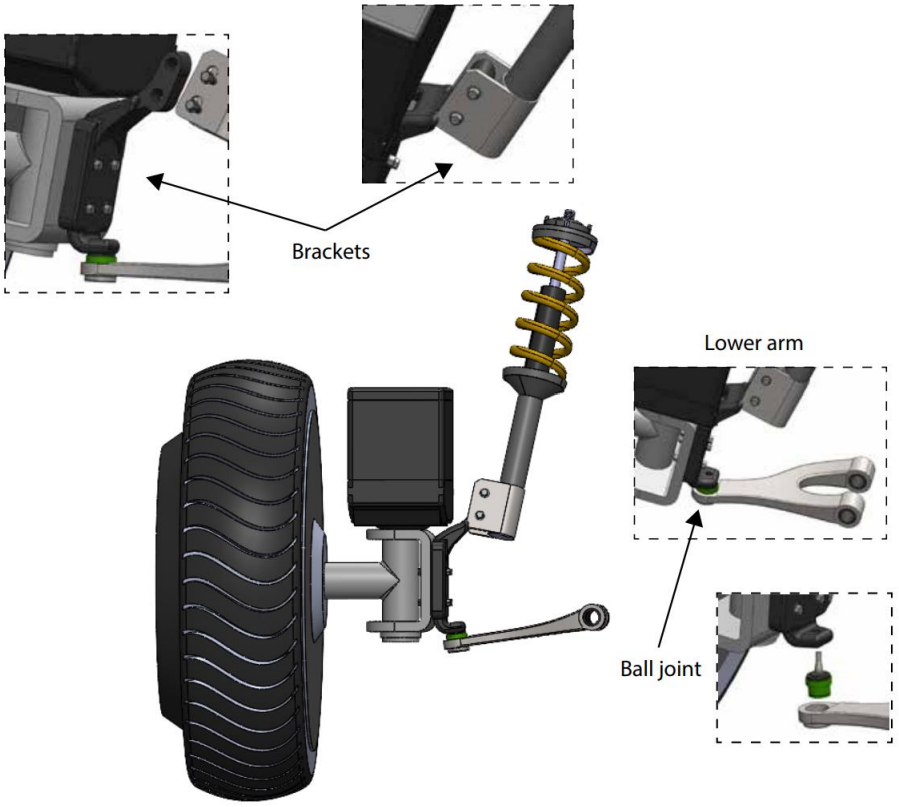

Figure 23: Suspensions system components

Once the best choice in terms of suspensions has been discussed, together with the evaluation of the geometry, the stiffness can be evaluated. The Pacci drone can be modelled by means of a 2 DOF quarter car model, assuming that the tyre can be modelled by means of a linear spring, the spring and the damper modelling the suspension can be assumed to have a linear behaviour, a natural frequency of 2 Hz has been imposed. The stiffness of the suspension resulted to be equal to $2408\ N/m$. The analyses that followed the one of the stiffness, aimed at the computation of the maximum stroke, starting from some considerations about the vertical forces acting on the suspension while braking or steering, then a maximum stroke of $75\ mm$ resulted to be quite satisfactory for the operations the Pacci drone has to carry out.

Steering system

The steering system that has been selected for the Pacci drone is the one with independent wheel steering, in practice, the 4 wheels can be commanded independently by different actuators. This choice has been made taking into consideration an agile movement of the drone between the different obstacles that it could meet on its path; this has to be as much as possible easy and fast to actuate with small steering radius, so that the Pacci drone could move and change direction also in small areas like sidewalks or shoulders. The actuators, mentioned before, are the so-called servomotors, positioned on each wheel on the C bracket, as reported in the figure below.

Figure 24: Steering mechanism of the front wheel (on the left) and of the rear wheel (on the right)

Also the servomotors have been dimensioned, taking into consideration the maximum torque that can be exerted at the ground level, so at the end the servomotor has to deliver a maximum torque equal to *11 Nm,* with a power output at least equal to *36 W*. The following step of the design of the suspension system was the dimensioning of the wheel arch and the determination of the steering angles. After this phase it was possible to realize a first 3D representation of the Pacci drone base, considering all the components that have been chosen and analysed in the previous paragraphs, it is reported below.

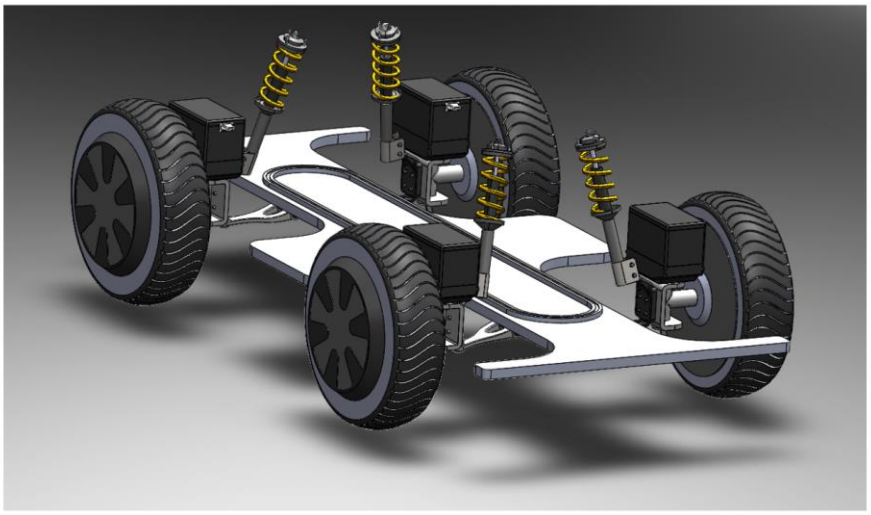

Figure 25: 3D design of the pacci drone base

Braking system

According to what can be seen on a similar system, which is the one of the e-scooters, the choice ranged among different types of brakes:

- Disc brakes;
- Drum brakes;
- Regenerative brakes;
- Electronic brakes.

The disc brakes consist of a rotor, a metal disc, which is attached to the moving part of the wheel, so it moves together with the electric motor, and a caliper which is mounted on this metal part, once brakes are activated, the pads inside the caliper are pushed on the rotor and exerting a certain amount of friction, this will cause the rotor to stop. Furthermore, the activation system of the brakes can be hydraulic, semi-hydraulic or mechanical; the working principle of the first kind relies on building up pressure inside the cables, which are filled with oil, to activate the calipers, this type of brake is the most reliable and effective, it can be easily and better controlled and provide a fast response. The second kind is the semi-hydraulic brakes and are quite similar to the previous type, except for the fact that instead of using a hydraulic line to activate the calipers, they use cables; finally, the mechanical disc brakes are the most common, the calipers are actuated by means of cables and by shortening or releasing them, the brake will be actuated or deactivated. This kind of brakes offers more friction, but with a behaviour that cannot be so regular and linear, moreover they can be suitable on lever actuated brakes, in the case of the Pacci drone, the cables to activate the

brakes can be difficult to be properly managed by an autonomous system. Among these three types of disc brakes the hydraulic ones seem to be the preferable choice.

The following option was the one of considering the drum brakes; in this case the braking system is isolated from the external environment and consists of a drum and braking pads, that, whenever they are activated, are pushed toward the external surface, exerting friction between the surfaces, this will cause the braking action. They are usually cable-actuated, can suffer from overheating and the braking performance is less effective than the one that can be offered by a disc brake. Moreover, this kind of brakes must be located inside the wheel, and in the case of the Pacci drone this option cannot be taken into consideration, since the EM is already positioned there.

The regenerative brakes option has been taken into consideration as an additional way of braking, that can help to recover some energy and recharge the battery whenever the Pacci drone is not travelling at its maximum power; this because this kind of brakes are not so effective like a disc brake and the regenerative braking can be implemented without adding weight or maintenance.

The electronic brakes can be activated by shortening the terminals of the EM, so that a certain resistance to the rotation is generated; this kind of brakes do not exert a strong braking force and their performance can be poor.

At the end of this discussion, it seems clear that the disc brakes are the best option to offer an effective braking action, that can be easily controlled and regulated also in wet conditions, they do not add too much weight to the system and can be easily adjusted and maintained. This system can be coupled with regenerative braking, which helps in recovering energy.

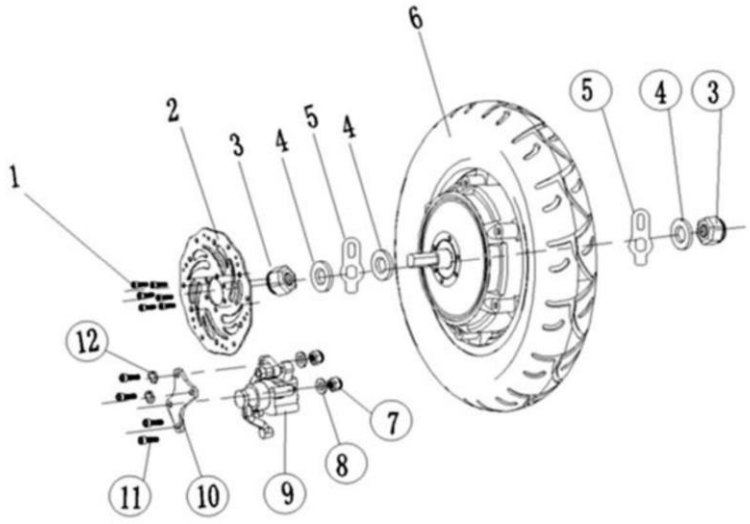

Figure 26: Schematic representation of a disc brake

In the picture above the metal disc is marked with 2, the caliper assembly with its screws is reported with number 9 and 10; these will be mounted on the wheel assembly, reported with the number 6.

Due to the presence of the EM inside the wheels and due to the modest speed that this vehicle can reach, for sake of packaging, it has been opted to provide the front axle with in-wheel electric motors and rear axle with mechanical disc brakes. This choice has been carried out to avoid the risk of oversteering, slippage, vehicle rollover and spinning, since, in case of emergency braking, the risk of losing adherence is much reduced.

In order to design a sufficiently effective braking system for this type of vehicle, it is necessary to compare the braking torque that the disc brakes are capable to develop with the peak torque that the E-motor can deliver.

From *Table 4,* in which all the parameters regarding the E-motor are collected, it can be seen that the peak torque reported is equal to 11.6 Nm, consequently, the braking torque must be equal to this value in order to ensure an effective braking manoeuvre.

$$T_{EM,peak} = T_{braking};$$

The braking torque can be computed as the product of the friction coefficient between braking pad and rotor, the braking pressure, the pad area and the middle point at which this force can be exerted. As first computation, it has been stated that the dimension of the arm cannot be larger than 120 mm, due to the established dimensions of the wheel, since it has been opted for the most conservative choice.

$$T_{braking} = \mu \cdot p_{braking} \cdot A_c \cdot r_d;$$

Assumptions:

$$T_{braking} = 11.6\ Nm;$$

$$120\ mm < r_d < 110\ mm;$$

$$\mu = 0.3 \div 0.5;$$

$$p_{braking} = 0.6\ MPa.$$

As a consequence:

$$A_c \sim 403\ mm^2.$$

This dimension results to be compatible with the design of the wheel system, since it can be imagined as a pad of rectangular shape with sides of about 10 mm per about 40 mm on a disc of 240 mm of diameter.

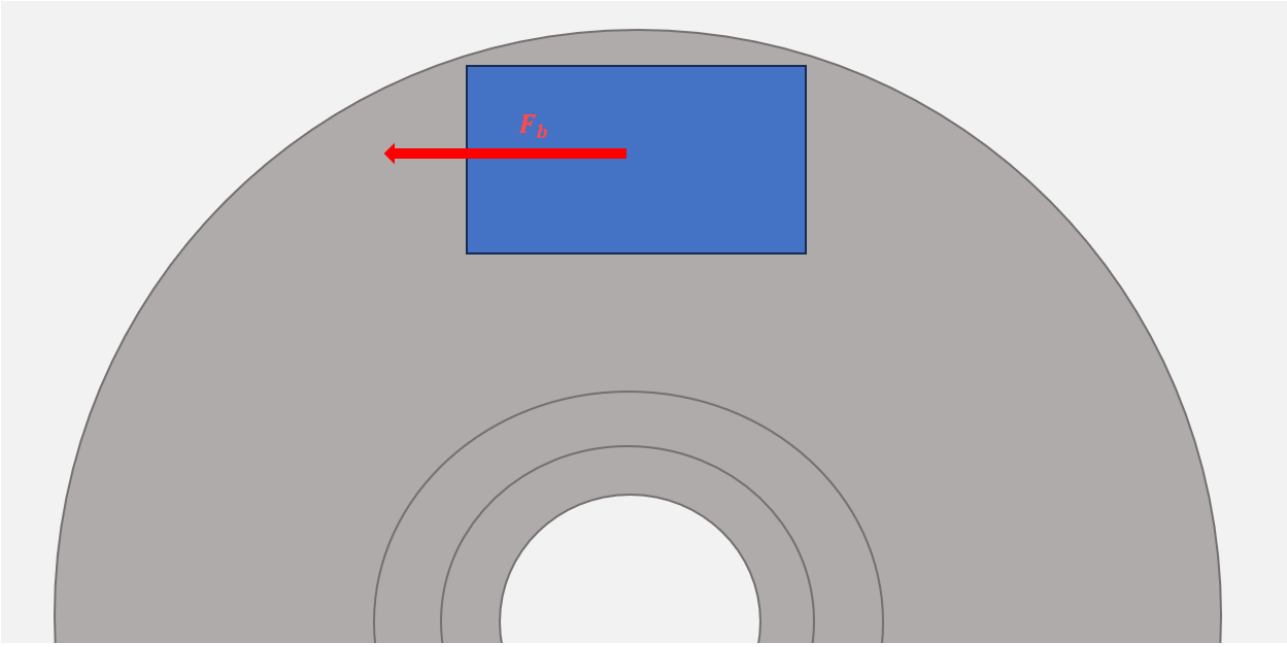

Figure 27: Scheme of disc brake

In *Table 7* all the parameters concerning the adopted braking system are reported:

Rear brakes		
Parameter	Value	Unit
Working pressure	0.6	MPa
Friction coefficient	0.4	-
Braking pad	403	mm^2
Disc diameter	240	mm
Disc thickness	3.5	mm

Table 7: Brakes parameters

HMI

With the acronym HMI, it is intended the human-machine interface, which results to be of great importance for Pacci to accomplish its missions. For this purpose, a touch-screen has been positioned in the front part of the Pacci drone, this has to help the user to easily comprehend what has to be done in order to pick up or deposit his or her order. The communication with the users is fundamental for a "Human-centred service" and for this reason also a personalized app has been projected with the aim of making the delivery service more accessible and customable according to the needs of each customer.

Figure 28: Example of HMI on the Pacci drone screen

In the following sequence of images it is shown an example of how the communication between the Pacci drone and the user is performed in a common delivery situation.

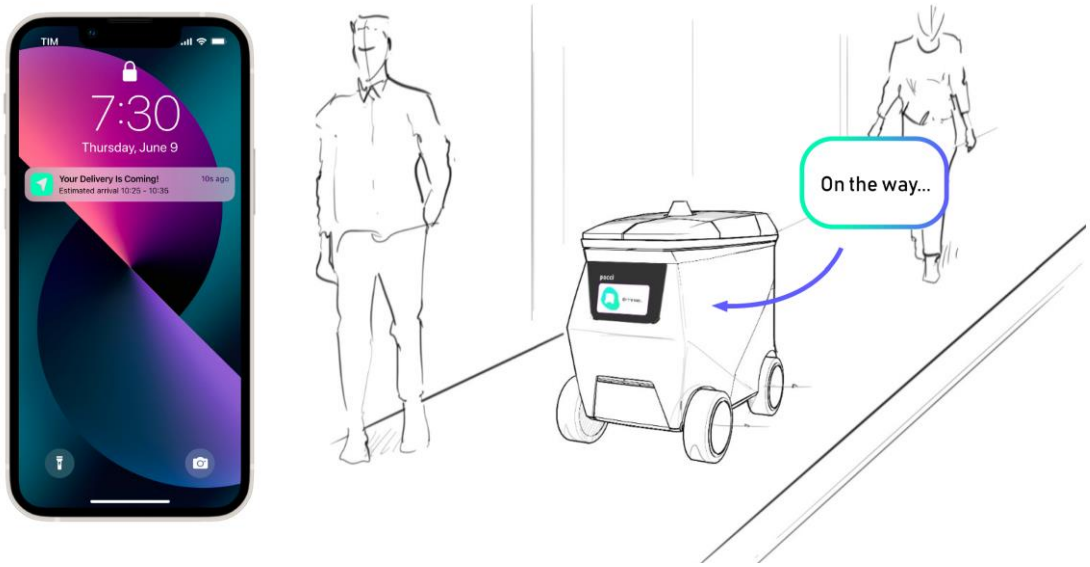

Figure 29: The drone is reaching the user after getting off the bus

Here the drone is sending automatically a notification to the first user that is going to be served, from the notification to the delivery phase no more than 15-minutes must be taken.

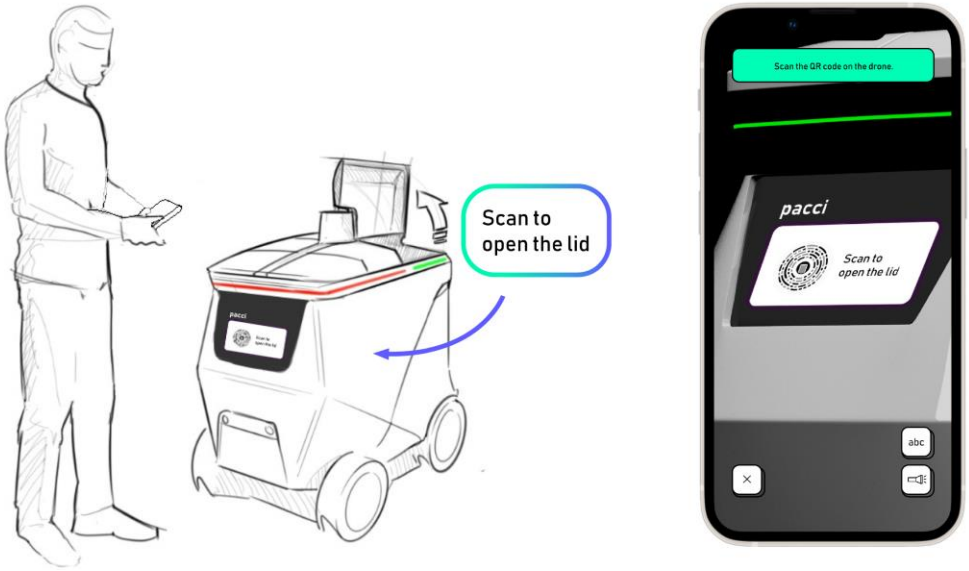

Figure 30: The user picks up the item from the Pacci Drone

Once the drone has met the customer, this one will pick up his or her order, by means of a personalized QR-code that he or she can scan from the mobile-phone, the lid that accommodates his or her item will open.

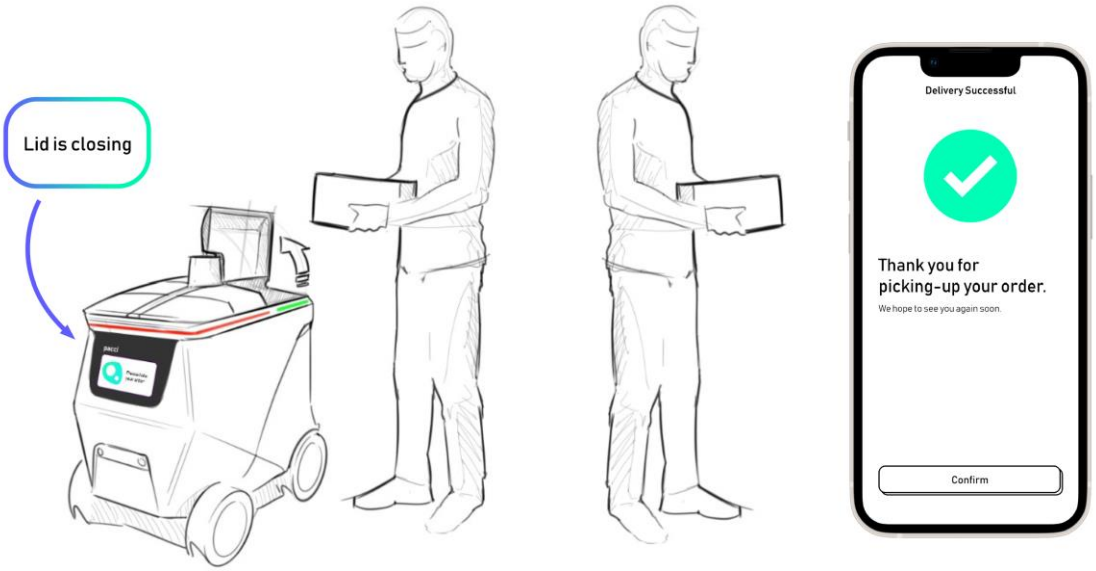

Figure 31: End of the delivery process

Once the customer has picked up the order, the lid will automatically close and a notification will be sent on the smartphone to update the delivery process status and to confirm the positive outcome.

Chapter 4

In this chapter the part related to the development of the system devoted to the autonomous driving is illustrated. Firstly, all the sensors and devices needed for the detection of the environment are outlined, then, the choice of the controller will be discussed, followed by the mathematical model that has been assumed to represent the dynamic behaviour of the vehicle, the driving model that has been implemented in order to actuate the driving system according to the driving scenario. Finally, some simulations are shown with possible trajectories that the Pacci drone could face in order to verify that the choices that have been made until this point result to be consistent and validated by means of MATLAB / Simulink software.

Vehicle dynamics

The science of vehicle dynamics is very broad and it investigates many aspects that are related to any kind of vehicle. The aim is the one of improving performance, handling and comfort studying the behaviour of the variables that affect these factors in different operating conditions; imagining a road as a long line, the vehicle must be an object with a clear heading direction, which must be driven in a precise way controlling simultaneously the yaw rate, the magnitude and direction of the vehicle speed. In order to do this, the vehicle is endowed with many systems that make possible to move it, to change its direction, to stop it and also to provide damping coming from the ground irregularities. To study the vehicle dynamic behaviour, it is

positioned in a Cartesian plane and three main aspects can be studied, according also to the mathematical model describing the vehicle itself; they are longitudinal dynamics, lateral dynamics and vertical dynamics.[7]

The longitudinal dynamics studies the motion of the vehicle along its longitudinal axis and it takes into consideration all the factors affecting the acceleration and braking manoeuvres, that are rolling resistance, the possibility to travel on a certain slope, the aerodynamic resistance, the load transfer and pitching.

The lateral dynamics studies the vehicle motion in its lateral direction; it includes all the aspects related to the stability of the vehicle whenever it performs cornering manoeuvres, so the roll motion, the lateral load transfers, the cornering behaviour.

The vertical dynamics involves all the disturbances related to the irregularities of the ground that can be transmitted to the vehicle; this aspect of dynamics is mainly related to the stability and comfort. It constitutes the main field to design the suspensions system, since it is in charge of damping out the vibrations coming from uneven roads, so that the tire remains attached to the ground to ensure vehicle stability.

Before starting, it is necessary to have an estimation of the position of the centre of gravity of the Pacci rover when it is fully loaded (30 kg of payload), according to the following expression:

$$CoG_{(x,y,z)} = \frac{\sum_{i=1}^{n} m_i(x,y,z)_i}{\sum_{i=1}^{n} m_i}$$

In order to compute the coordinates of the Centre of Gravity in this case, the rover has been subdivided in different components with their own masses, m_i, and centres of gravity position, x_i, y_i and z_i. The final result is reported in the table below:

CoG coordinates [mm]	
X	420
Y	0
Z	385

Table 8 : CoG coordinates of the Pacci drone

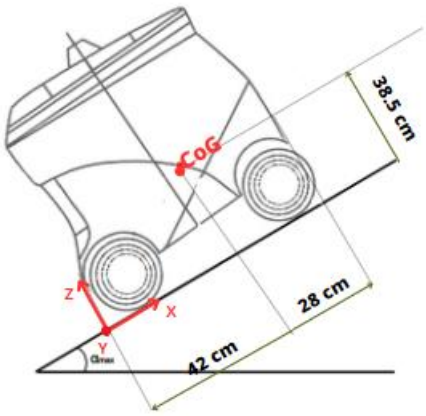

Figure 32: Schematic of CoG position

In the end a summary of the parameters describing the main characteristics of Pacci rover is reported in the following:

Vehicle parameters		
Data	*Value*	*Unit*
Total mass	70	kg
Distance CoG – front axle	0.42	m
Distance CoG – rear axle	0.28	m
Distance CoG – ground	0.385	m
Yaw moment of inertia J_z	160	kg·m^2
Cornering stiffness C_f	39156	N/rad
Cornering stiffness C_r	39156	N/rad
Suspension parameters		
Sprung mass	15.25	kg
Unsprung mass	5	kg
Stiffness of the spring	2408	N/m
Tire stiffness	78957	N/m
Optimal damping	139.6	Ns/m
Wheel assembly parameters		
Wheel radius	0.15	m
Mass at full load	79	kg
Frontal area	0.48	m^2
Wheelbase	0.70	m
Track	0.55	m
Drag coefficient	1.05	-

Table 9: summary of the main parameters of Pacci drone

Design loads

Having the coordinates of the centre of gravity and in particular its height, it is possible to compute the maximum longitudinal accelerations, both in traction and in braking, and the maximum lateral acceleration because it is quite sure that these are limited by capsizing and rollover, respectively.

In order to compute the maximum longitudinal acceleration in traction of an All-Wheel-Drive vehicle, as Pacci, it is necessary to introduce some assumptions, according to which, the vehicle is able to generate longitudinal forces on all the tires, in a condition of maximum adherence, then, it is stated that the vehicle accelerates from null speed and that the gradeability of the road is null.

$$\mu_{x1} = \mu_{x2} = \mu_{xmax}; \qquad V_{in} = 0; \qquad \alpha = 0.$$

From the first assumption,

$$m\dot{V} = F_{x1} + F_{x2} = \mu_{x1}F_{z1} + \mu_{x2}F_{z2};$$

From the second assumption, instead

$$m\dot{V} = F_{x1} + F_{x2} = \mu_{x1}F_{z1} + \mu_{x2}F_{z2} = \mu_{xmax}(F_{z1} + F_{z2})$$

The sum of the normal loads on front axle and rear axle is equal to the overall weight of the vehicle itself, due to the fact that the gradeability and initial speed have been stated equal to zero, so

$$m\dot{V} = \mu_{xmax}mg;$$

According to these considerations, the maximum acceleration allowed by the tire is given by

$$\dot{V} = \mu_{xmax}g.$$

The other limit to the maximum longitudinal acceleration, both in traction and braking, is given by the capsize limit; this is due to the fact that a certain amount of normal load transfers from the front to the rear axle, while in braking, a certain amount of normal load transfers from the rear to the front axle:

$$F_{z1} = mg\frac{b}{l} - m\dot{V}\frac{h}{l};$$

$$F_{z2} = mg\frac{a}{l} + m\dot{V}\frac{h}{l}.$$

Capsize in traction is obtained when the front axle is totally unloaded, so

$$F_{z1} = 0;$$

Capsize in braking is obtained when the rear axle is totally unloaded, so

$$F_{z2} = 0;$$

From these considerations, the maximum acceleration before reaching the capsize limit, in traction and braking, respectively, is given by

$$\dot{V} = g\frac{b}{h};$$

$$\dot{V} = -g\frac{a}{h};$$

Between these two limits given by tire adherence and capsize, the minimum one will prevail, stating the limit that will be reached first and which cannot be overcome.

$$a_{x,max,traction} = g\min\left(\mu_{x,max}, \frac{b}{h}\right);$$

$$a_{x,max,braking} = g\min\left(\mu_{x,max}, \frac{a}{h}\right);$$

In this first estimation, the maximum friction coefficient for the tire is assumed quite reasonably $\mu_{x,max} = 1$.

In order to compute the maximum lateral acceleration, the lateral forces generated during cornering must be considered. As done previously, some assumptions must be introduced: the vehicle is able to generate lateral forces on all the tires, in a situation of maximum adherence, then, the vehicle accelerates from null speed and that gradeability of the road is null, too.

The tire limit must be considered as follows

$$m\dot{V} = F_{y1} + F_{y2} = \mu_{y1}F_{z1} + \mu_{y2}F_{z2};$$

From the second assumption

$$\mu_{y1} = \mu_{y2} = \mu_{ymax}$$

$$m\dot{V} = F_{y1} + F_{y2} = \mu_{y1}F_{z1} + \mu_{y2}F_{z2} = \mu_{ymax}(F_{z1} + F_{z2}) = \mu_{ymax}mg;$$

So that,

$$\dot{V} = \mu_{ymax}g;$$

The other limit to the maximum lateral acceleration while cornering, is given by the rollover limit, due to the fact that a certain amount of normal load transfers from the right wheels to left wheels or from left wheels to right wheels according to the curve: For example, if the vehicle is turning to the right

$$F_{z,l} = mg\frac{c}{2} + m\dot{V}h;$$

$$F_{z,r} = mg\frac{c}{2} - m\dot{V}h;$$

The rollover limit is reached whenever $F_{z,r} = 0\ N$, so:

$$\dot{V} = g\frac{c}{2h};$$

Between the two limits given by tire adherence and rollover, the minimum one will prevail, stating the limit that will be reached first and which cannot be overcome.

$$a_{y,max} = g\ \min\left(\mu_{y,max}, \frac{c}{2h}\right);$$

The results that have been obtained are here reported:

$$a_{x,max,braking} = 7{,}13\ \frac{m}{s^2}; \qquad a_{x,max,traction} = 9{,}81\ \frac{m}{s^2}.$$

The capsizing limit, while braking, is reached before the tire limit; in traction, instead, the longitudinal acceleration is not limited by this behaviour, since maximum adherence is reached first.

$$a_{y,max} = 7\frac{m}{s^2};$$

For what concerns the maximum lateral acceleration, this is limited by rollover.

This behaviour was expected since the vehicle appears to be quite short and not so elevated and these thresholds depend on the dimensions of the vehicle: distance between the centre of gravity and the front axle, the distance between the centre of gravity and rear axle, the position of the centre of gravity with respect to the symmetry axle of the vehicle and the distance between the centre of gravity and the ground, as it can be seen in the previous formulae.

Load transfer due to rolling

As the roll centre does not coincide with the centre of gravity, a roll motion must be considered and it is the result of the lateral forces applied to the centre of gravity multiplied by the distance between the centre of gravity and the roll centre.

As can be seen in the suspension system design, the roll centre position is computed and in the following *Table 10* it is reported the coordinates with respect to the reference frame of the vehicle:

Roll centre position		
X [cm]	Y [cm]	Z [cm]
25	0	5.1

Table 10: Coordinates of the roll centre

Recalling that the height of the centre of gravity is equal to 38,5 cm, the distance between these two points results to be equal to 33,4 cm and this is the arm that, multiplied by the lateral forces applied to the vehicle body, results in rolling motion.

Before starting with the evaluation of the amount of vertical load that is transferred to front and rear axles, it is necessary to evaluate the rolling stiffness of the suspension. Knowing that the kind of suspensions that have been chosen are of a McPherson type, and the load distribution at steady state has been stated to 60%/40%, it is possible to evaluate the rolling stiffness analysing the response to vertical vibrations. It has been individuated 2 HZ as a reasonable choice for the natural frequency of Pacci's suspension, a quarter car model with 2 DOF has been taken into account, and, knowing that this frequency is equal to

$$\omega_s = \sqrt{\frac{K_s}{m_s}},$$

it is possible to get the rolling stiffness of the suspension at full load.

Generally, off-road vehicles tend to have a lower rolling stiffness compared to on-road vehicles in order to enhance their ability to face uneven terrain. This could be the case.

Moreover, it has been assumed to adopt the same rolling stiffnesses for both front and rear suspensions, and this is

$$K_R = 2408\ N/m;$$

$$K_{R_1} = K_{R_2} = 1204\ N/m;$$

At this point, it is possible to proceed with the computation of load transfer due to rolling.

At first, it must be stated the condition in which the rolling motion wants to be evaluated, since this can be done for different amounts of lateral load. In this case it has been decided to evaluate it when the maximum lateral load is applied to the vehicle body, in order to get the maximum amount of vertical load that can be transferred; this can be gained by the maximum lateral acceleration before rollover limit is reached. The maximum lateral force that the vehicle body can withstand is equal to 490N. The total load transfer is given by two contributions: the one which gives rolling motion and the non-rolling contribution, these respectively:

$$\Delta F_{z_{1,2}} = \Delta F_{z,R_{1,2}} + \Delta F_{z,nr_{1,2}};$$

$$\Delta F_{z,R_{1,2}} = \frac{M_{R1,2}}{t} = F_y \frac{d}{t} \frac{K_{R1,2}}{K_R}, \qquad where\ K_R = K_{R1} + K_{R2}$$

$$\Delta F_{z,nr_{1,2}} = F_{y1,2} \frac{h_{R1,2}}{t};$$

In the conditions that have been just outlined, the amount of load transfer between front and rear due to rolling motion, is about 150N.

In the following, the same consideration has been studied for different amounts of lateral force and the results here reported:

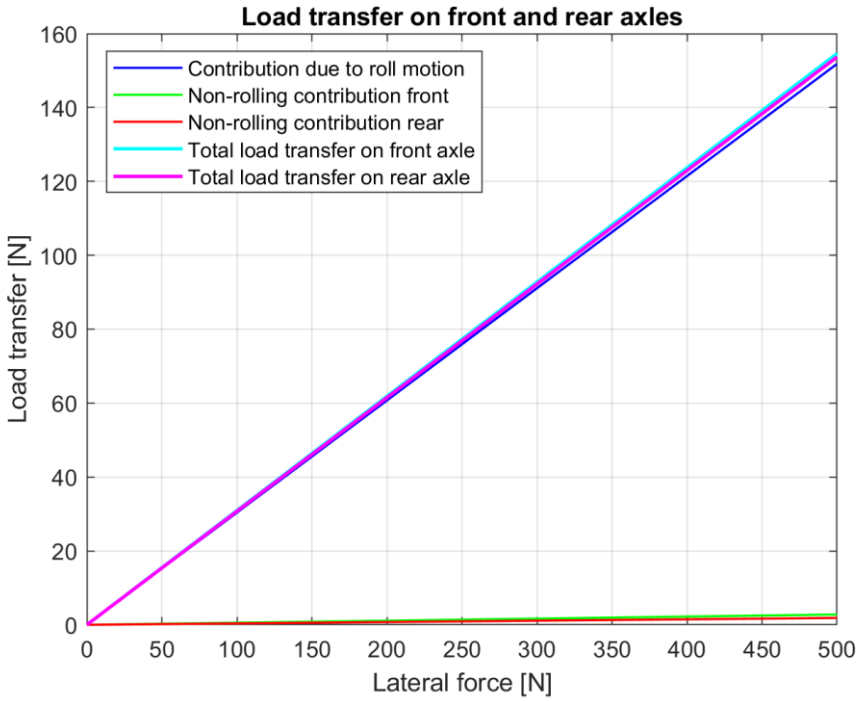

Figure 33: Load transfer between front and rear axles

As it can be noticed, the non-rolling contribution is so small, that it can be neglected.

Cornering dynamic behaviour

The analyses of lateral dynamic behaviour of Pacci have been carried out, in order to understand its limits while cornering.

The starting point is the study of the kinematics of steering manoeuvre, then the curvature gain can be analysed depending on the physical characteristics of the Pacci rover, at different speed, so that a minimum radius of curvature can be identified, together with the oversteering or understeering behaviour of the rover while facing a curve.

Kinematic steering

In this condition, the vehicle is assumed to be a rigid body and this kind of manoeuvre is performed at very low speed, so that the velocities of the of the wheels lie in their midplane and the sideslip angle is so small that can be neglected. In this situation, the wheels cannot exert any cornering force to balance the centrifugal force that pushes the vehicle outside of a lane while cornering at higher speeds.

The curvature gain of a vehicle that is facing a curve at low speed is defined as

$$\frac{1}{R\delta} = \frac{1}{l};$$

As it can be seen, it is independent from the steering angle and the curvature of the path, it depends just on the wheelbase of the vehicle.

Dynamic steering

When the speed of the vehicle is not negligible, the steering manoeuvre can be defined as dynamic steering. Differently from the kinematic one, the sideslip angles developed by the wheels are no more null or very small and this because the wheels have to counterbalance the centrifugal force that pushes the vehicle outside the lane while cornering.

It has been assumed that the vehicle is travelling on a circular and flat path, so that the radius of curvature can be considered constant, at constant speed. Moreover, the radius R is much larger than the wheelbase of the vehicle, consequently, the sideslip angles can be considered small.

The equilibrium of the forces in the lateral direction can be written as follows, neglecting any aerodynamic influence to motion and any aligning torque.

$$\frac{mV^2}{R}\cos(\beta) = \sum_{\forall i} F_{xi}\sin(\delta_i) + \sum_{\forall i} F_{yi}\cos(\delta_i).$$

The equilibrium around the centre of gravity, instead, can be written as

$$\sum_{\forall i} F_{xi} \sin(\delta_i)\, x_i + \sum_{\forall i} F_{yi} \cos(\delta_i)\, x_i = 0.$$

According to the assumptions that have been made at the beginning, the angles β and δ_i are small, so that the forces can be rewritten as

$$\sum\nolimits_{\forall i} F_{yi} = \frac{mV^2}{R};$$

$$\sum\nolimits_{\forall i} F_{yi} x_i = 0.$$

Starting from these expressions and discretizing between front and rear axle, it is possible to obtain another quantity of interest, which is the curvature gain. Before starting with its computation, it is necessary to compute the so-called understeering coefficient and according to this it is possible to obtain a first evaluation of the cornering behaviour of the vehicle (oversteering or understeering attitude).

$$K_{us} = \frac{mg}{l^2}\left(\frac{b}{C_1} - \frac{a}{C_2}\right);$$

In addition, it is necessary to compute the cornering stiffnesses and it is possible to evaluate how they change according to the load transfer between right and left tire until a saturation region is reached.

The cornering stiffness is affected by the shape of the contact patch, which can vary according to the physical properties of the tire, like material or structure, and the vertical load. It is given by computing the secant to the lateral force vs sideslip angle curve. In this case, dry asphalt has been assumed.

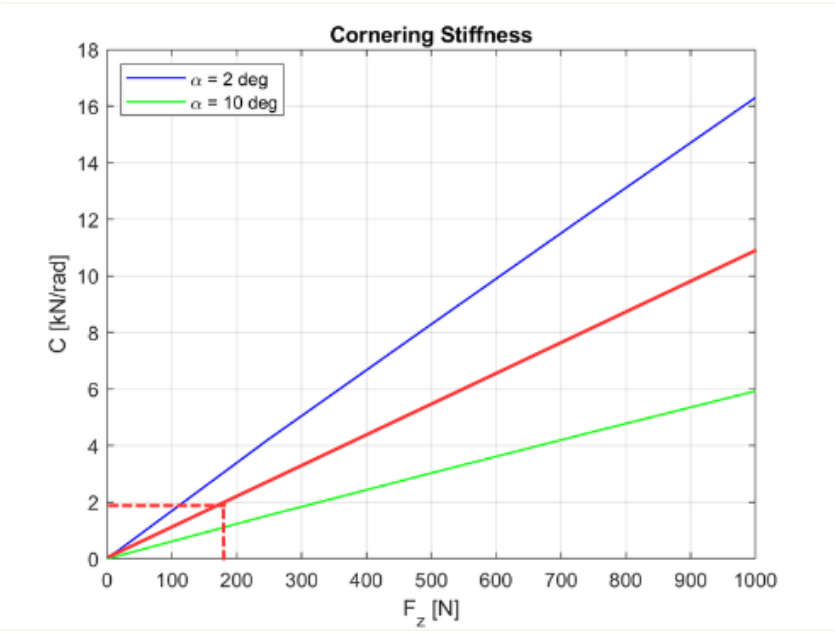

Figure 34: Cornering stiffness

As it can be noticed, increasing the sideslip angle, the cornering stiffness decreases, as expected. In this case two sideslip angles have been taken into consideration, to get the so-called bilinear approximation, which recalls the curve of the cornering stiffness with a first linear region and then a saturation one, in which the cornering stiffness cannot increase anymore. This will result in a modification of the cornering behaviour of the vehicle itself. In this particular case, instead, this modification of the cornering behaviour is not visible, since the cornering stiffness will linearly increase with the increasing of the load on the single wheel.

Coming back to the computation of the understeering coefficient, the cornering stiffness has been assumed equal for the front and rear axles, here the dotted line accounts just for one tyre, so it has been obtained:

$$C_1 = C_2 = 4\ \frac{kN}{rad};$$

With this assumption, it seems evident that the understeering coefficient will depend just on the distance between centre of gravity and front axle and centre of gravity and rear axle; having that $b > a$, $K_{us} > 0$, so the vehicle will be understeering.

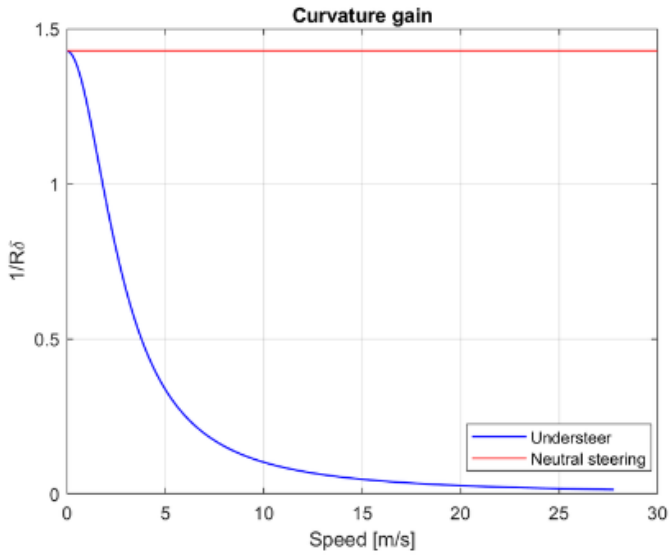

Figure 35: Curvature gain

As can be noticed in the *Figure 35* above, the actual attitude of the rover is highlighted in blue: with the increasing of the speed, the vehicle will be capable of facing a curve with increased radius of curvature, so increasing δ, R will increase, too. In red colour, instead, the neutral steering behaviour is marked. The curveture gain, in this latter case, will remain constant with the increasing of the vehicle speed.

Taking into consideration the maximum lateral acceleration, limited by rollover, it is possible to get an estimation of the minimum radius of curvature that the vehicle can withstand. This latter for different amounts of speed is reported in the *Figure 36* below:

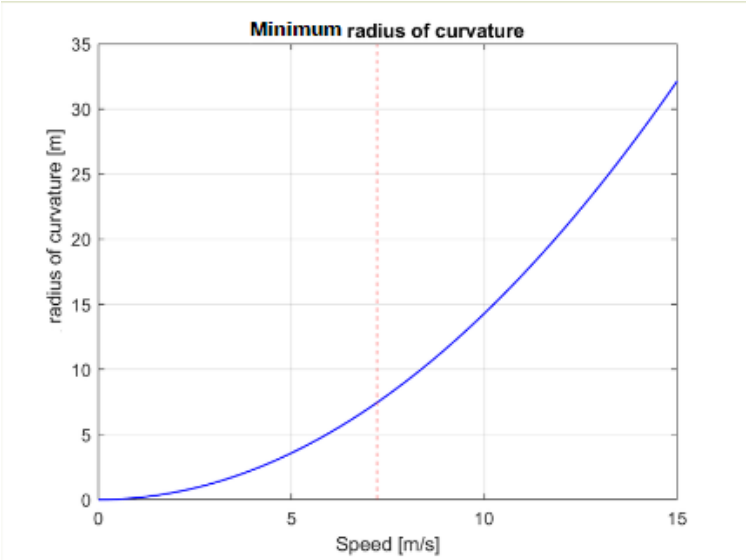

Figure 36: Minimum radius of curvature

In red dotted line, it is reported the maximum speed that can be reached by the vehicle on a flat road and at full load. All the points that are below the blue curve are feasible for the Pacci rover.

Nevertheless, none of the above considerations can bring to a substantial increasing of the cornering behaviour and of the lateral dynamics of the vehicle that has been analysed. Due to the marked understeering behaviour of the vehicle, it has been opted for a 4-wheel steering mechanism, to enhance the capability of promptly avoid obstacles and be reactive to the sudden change of trajectory of any kind of obstacle that could be present on roads, pedestrian paths and so on. In *Chapter 5* the behaviour of this vehicle provided with 4-wheel steering is simulated on Matlab-Simulink environment.

Vehicle models

Vehicles can be analysed from different points of view, the pure geometrical one, the kinematic one and the dynamic one, for each of these levels of study, a different vehicle model can be taken into consideration.

The first one is the geometric model and it consists of a simple model with just information about its position. No speed or accelerations are considered, but just geometrical parameters, such as vehicle dimensions.

The second one is the kinematic model and, as in the previous case, also here just geometrical parameters are taken into consideration; as the name resembles, in this simple model there are information regarding vehicle speed and its direction, which make reference to both a local and a global reference system.

The third model is more complex and it is the dynamic model, its level of complexity can increase according to the amount and the type of variables that can be analysed. Here geometric and dynamic parameters must be considered, such as dimensions, mass, inertia etc. It considers all the forces applied to the vehicle, both internal and external, from this model, it is possible to obtain a complete handling model of the vehicle. [8]

For this purpose, this latter is the model that is going to be used throughout all the dissertation.

Quarter car model

It is the simplest dynamic model, it is based on the assumption that the vehicle is completely symmetrical with respect to the longitudinal and vertical axis, so the behaviour of one fourth of the system can be studied, since the other tree fourth will replicate the same behaviour. This model is considered to describe the vertical behaviour and for this reason it has been used in the previous stages to investigate the characteristics of the suspensions.

Also, this kind of model can be further discretized according to the level of complexity and to the assumptions that can be introduced.

The first one is the simplest model, it consists of sprung mass and the suspension modelled by means of a damper and a linear spring in parallel, while the wheel is represented by a massless rigid body. This model is typically adopted to study the vertical behaviour of the vehicle in a range up to 3 Hz. The following model is the one that is typically adopted and it is a 2 DOF model; it comprehends the sprung mass and the suspension system represented by the parallel of a spring and a damper, like in the previous case, plus an additional mass, which is the unsprung mass accounting for the wheel hub, the wheel rim, the braking system and all what stands below the main spring; this mass is connected to the ground by means of a radial spring in parallel to a radial damper, representing the compliances of the tyre. This model is typically used to study the phenomena up to 25-30 Hz. The next model is the 3 DOF model and can be considered as a 2 DOF model to which the mass of the tire with its compliances, represented by an additional parallel of a spring and a damper, are added; this model is considered whenever phenomena up to 100-120 Hz are considered.

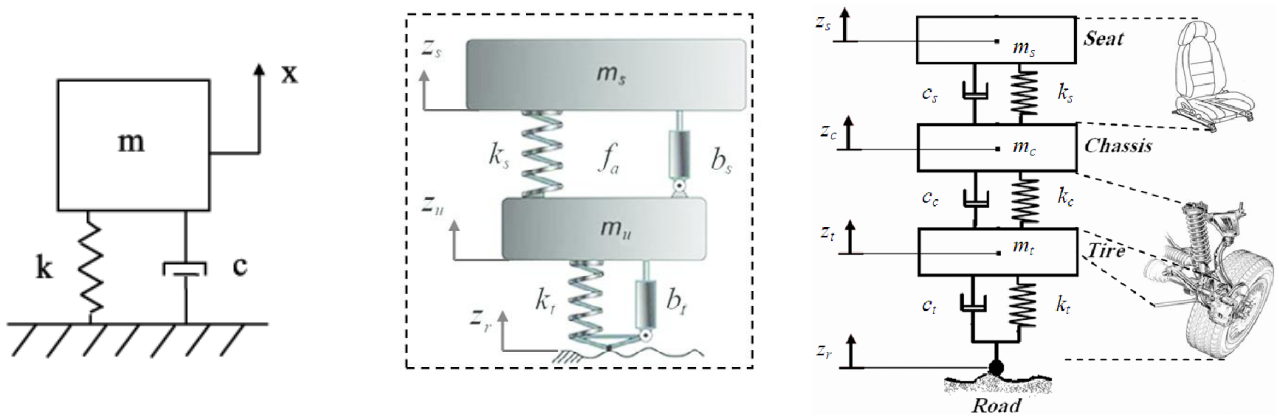

Figure 37: 1DOF quarter car model, 2 DOF quarter car model, 3 DOF quarter car model

These following models can be considered together in the same system, constituting the half car model, suitable to study pitch, roll and heave motion of the vehicle.

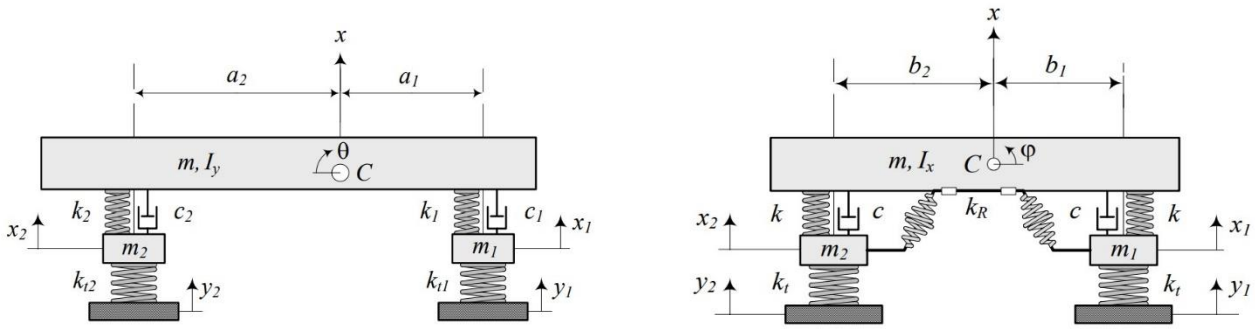

Figure 38: Half car models

The model on the left represents half vehicle, which is symmetrical with respect to the longitudinal axis, so that the unspung masses are representative of what is on the front and on the rear part of the vehicle, this model takes into consideration a certain degree of inequality between front and rear, due also to the possibility of load transfer between these two parts. This model is suitable to study the pitch and heave motion of the vehicle. The model on the right, instead, considers the vehicle that is symmetrical with respect to the vertical plane, so that a certain degree of inequality can be

considered between the left and right part of the vehicle; this model is suitable to study the roll and heave motion of the vehicle.

A full car model can be considered, modelling each unsprung mass for the 4 corners of the vehicle, as reported in the following *Figure 39*.

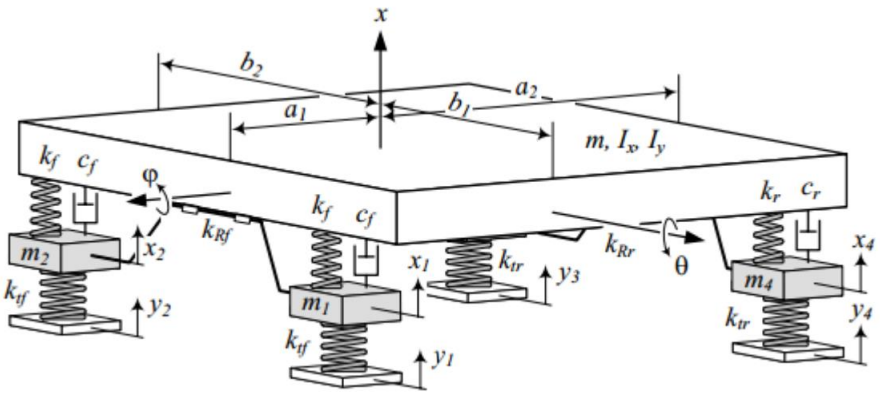

Figure 39: Full car model

All these models comply with the following general law:

$$[\boldsymbol{M}]\{\ddot{\boldsymbol{z}}\} + [\boldsymbol{C}]\{\dot{\boldsymbol{z}}\} + [\boldsymbol{K}]\{\boldsymbol{z}\} = \boldsymbol{F}$$

This latter represents a further simplification of the law obtained by means of the Lagrange equation

$$\frac{d}{dt}\left(\frac{\partial \mathcal{L}}{\partial \dot{q}_i}\right) - \frac{\partial \mathcal{L}}{\partial q_i} + \frac{\partial \mathcal{F}}{\partial \dot{q}_i} = \frac{\partial \delta L}{\partial \delta q_i}$$

All the parameters are going to be explained and developed considering a 2 DOF quarter car model, but this energy method can be applied to a variety of models.

- $\mathcal{L}$ is the Lagrange operator, given by the difference between the kinetic energy and the potential energy.

$$\mathcal{L} = T - U$$

$$T = \frac{1}{2} m_s \dot{z_s}^2 + \frac{1}{2} m_u \dot{z_u}^2$$

$$U = \frac{1}{2} k_t (z_u - z_r)^2 + \frac{1}{2} k_s (z_s - z_u)^2$$

- $\mathcal{F}$ represents the dissipative function and it contains the energy dissipated by the dampers

$$\mathcal{F} = \frac{1}{2} c_t (\dot{z_u} - \dot{z_r})^2 + \frac{1}{2} c_s (\dot{z_s} - \dot{z_u})^2$$

- δL is the virtual work exerted on the system by the external forces

$$\delta L = F \cdot \delta z_s$$

- q_i represents the vector of the variables and in this case

$$q_i = \begin{Bmatrix} z_s \\ z_u \end{Bmatrix}$$

DST model

The Dynamic Single-Track model, also called bicycle model, is represented by a scheme in which the right and left part of the vehicle are condensed on the central longitudinal plane of the vehicle itself, so right and left wheel are represented by one wheel for each axle. Thanks to this model it is possible to describe the longitudinal and lateral behaviour of the vehicle and it can be valid whenever some simplifications can be assumed, in particular, for the linear single track model:

- The speed of the CoG of the vehicle is constant along the trajectory;
- Lifting, Rolling and pitching motions are going to be neglected;
- The mass of the vehicle is concentrated in its CoG;
- Since the front and rear tire will be represented as a single tire per each axle, the contact patch lies along the centre of the axle, too;
- The pneumatic trail and self-aligning moment, resulting from the slip angle of the tire will be neglected;
- The load distribution between front and rear tire is considered constant;
- As a result of considering constant velocity, the longitudinal forces acting on the tire will be neglected.

In this case of non-linear Single-Track model, instead:

- The vehicle body in assumed as a rigid body;
- The front and rear wheels are characterized by a certain speed and force acting on tire;
- A certain steering angle is considered;
- The air resistance must be taken into consideration;
- Brake torques can be also provided. [9]

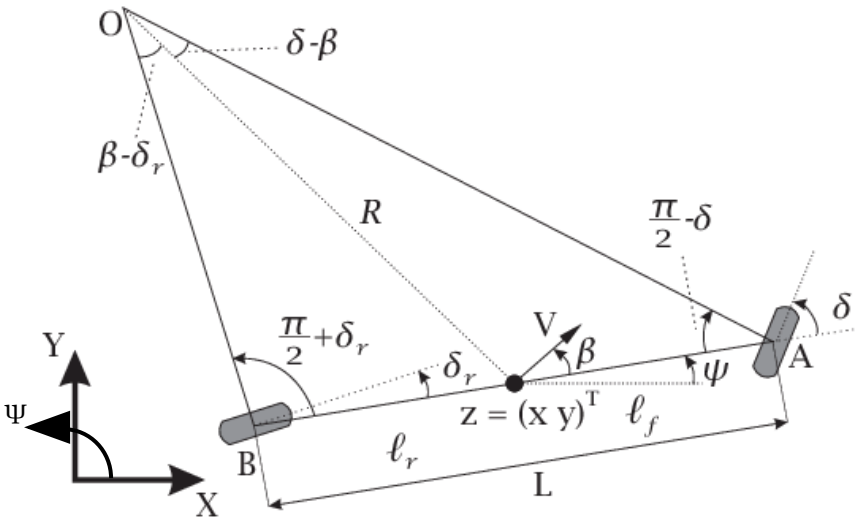

Figure 40: Linear single track kinematic model

Here:

- v_{CG} is the speed of the centre of gravity of the vehicle;

- δ is the steering angle of the front wheel (it is possible to have δ_f and δ_r if both front and rear wheels are steering wheels);
- v_f and v_r are the speed of the front and rear tire;
- α_f and α_r are the sideslip angles of the front and rear tire;
- β is the sideslip angle of the vehicle and it is the angle between the vehicle speed and its longitudinal axis;
- l_f and l_r are the distance between the CoG of the vehicle and the front or rear axle, respectively, the sum of the two will give the wheelbase.

Considering a dynamic model, instead, the following forces are also reported:

- $F_{x,f}$ and $F_{x,r}$ are the longitudinal forces exerted between the contact patch of the tire and the ground, they can be positive if the vehicle is in traction mode or negative if the vehicle is in braking mode;
- $F_{y,f}$ and $F_{y,r}$ are the lateral forces exerted between the contact patch of the tire and the ground and are the one responsible for the cornering behaviour of the vehicle.

Looking at the figure above, it can be noticed that now the behaviour of the vehicle can be described according to the coordinates that are the longitudinal one, x, the lateral one, y, and the angle ψ.

Developing some trigonometric considerations about the bicycle model reported above, it is possible to obtain the equations describing the kinematics of the model.

Considering the triangles that have as common side the radius of curvature R

$$\frac{\sin(\delta - \beta)}{l_f} = \frac{\sin\left(\frac{\pi}{2} - \delta\right)}{R}$$

$$\frac{\sin(\beta)}{l_r} = \frac{1}{R}$$

From these two, it can be obtained that

$$\tan(\delta)\cos(\beta) - \sin(\beta) = \frac{l_f}{R} \qquad and \qquad \sin(\beta) = \frac{l_r}{R}$$

Summing these two equations

$$\tan(\delta)\cos(\beta) - \sin(\beta) = \frac{l_f + l_r}{R}$$

Inserting this formula in the one of the yaw rate, given by the ratio of the speed of the CoG of the vehicle over the radius of curvature, it can be obtained that the yaw rate will be equal to

$$\Psi = \frac{v \cdot \cos(\beta)}{l_f + l_r} \cdot (\tan \delta);$$

While the other two equations can be obtained simply looking at the *Figure 40* above

$$\dot{x} = v \cdot \cos(\psi + \beta);$$

$$\dot{y} = v \cdot \sin(\psi + \beta);$$

Due to the assumptions that have been introduced, which are the one of having a vehicle represented by a rigid body and the one of having reduced speed, this model can result satisfactory to be applied to the Pacci drone, as will be done in the following paragraphs.

Non-linear full vehicle model

In environment like the one of CarSim or ADAMS Car it is possible to implement a full vehicle model, which is used for several vehicle dynamic studies, it is much more complex than the 2 DOF bicycle model, because it includes more components of the vehicle assembly.

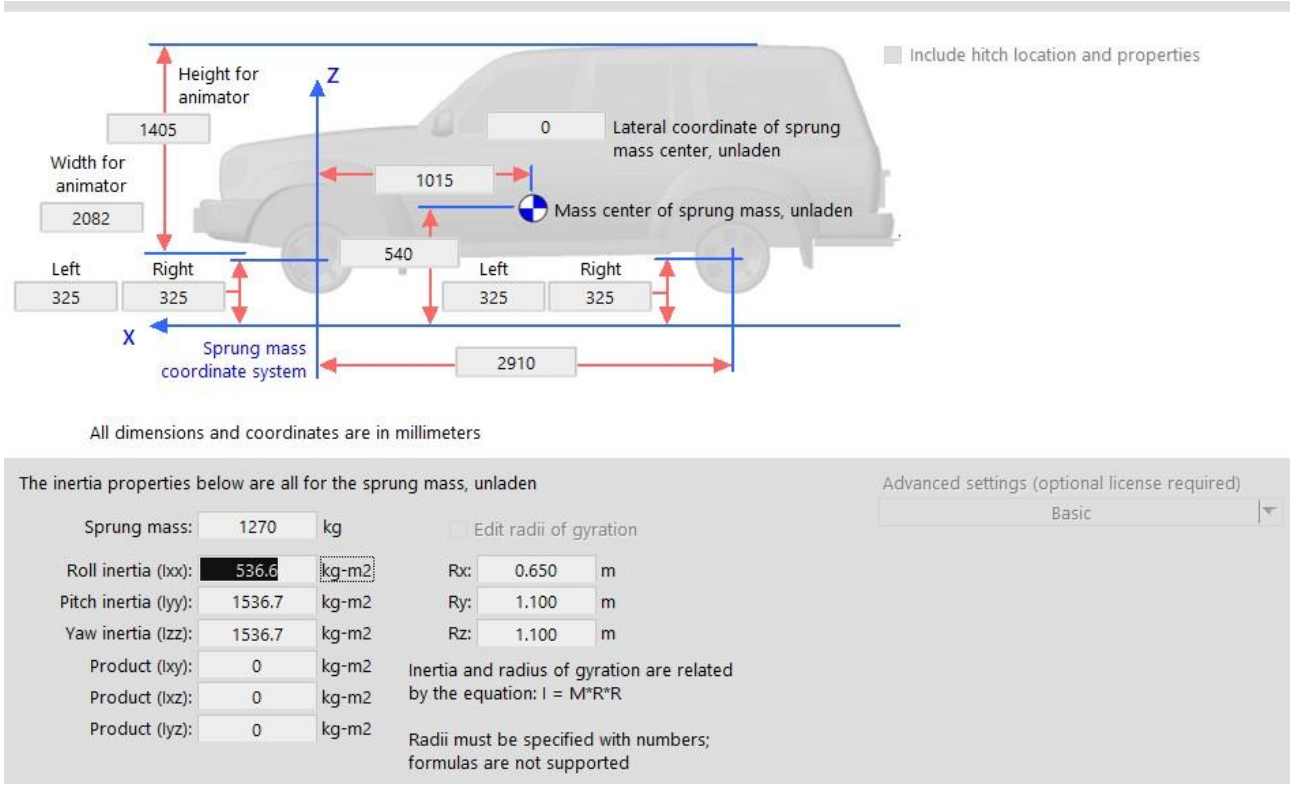

Figure 41: CarSim initial vehicle setting

Once this model has been set, it can be copied and pasted in the Simulink environment, to further investigate the dynamic response of the vehicle based on a more realistic dynamic model.

Tire model

One of the most important components of the vehicle system is the tire, it is the interface between the ground and the vehicle. The choice of the tire has been already discussed in the previous chapter, but an important point is represented by the mathematical model that can be adopted to simulate its behaviour. Many models have been defined, developed and reviewed through the years, some of them are mostly empirical models, others are more theoretical ones and, of course, more complicated, as can be noticed in the *Figure 42* below.

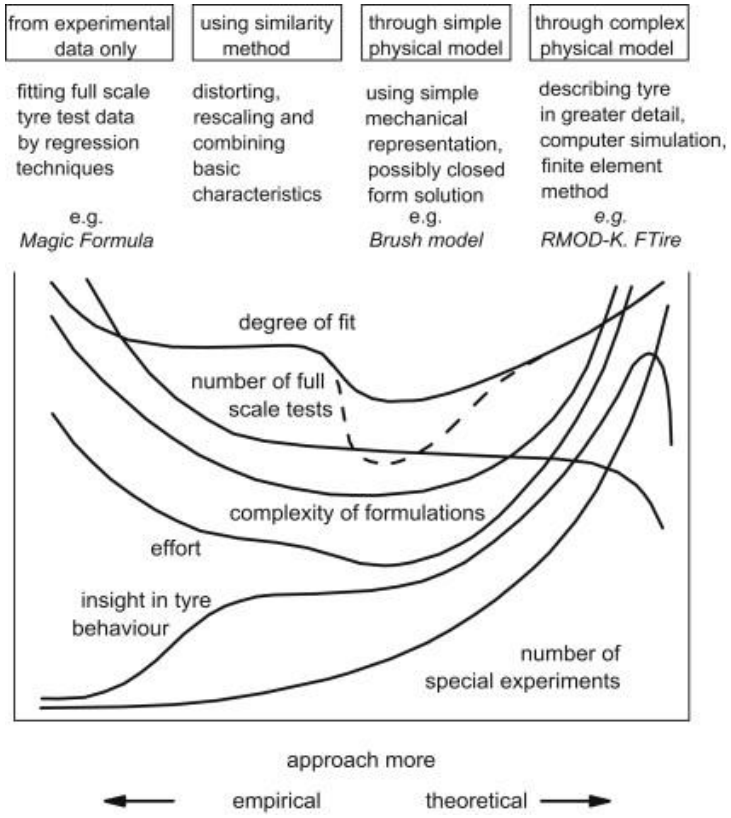

Figure 42: Parameters estimation for tire modelling

The father of all these models is the Pacejka model, also known as "Magic formula", because it is an empirical fitting of measured data of forces exchanged between tyre and ground and tyre characteristics. This formula has been subjected to many reviews and this is why many of them exist, according to the different year in which this has been revised. Among these, the Pacejka Magic Formula of 1989 is already

implemented in many software like MATLAB/ Simulink, CarSim or Adams Car, where some tyre parameters and constants must be set.

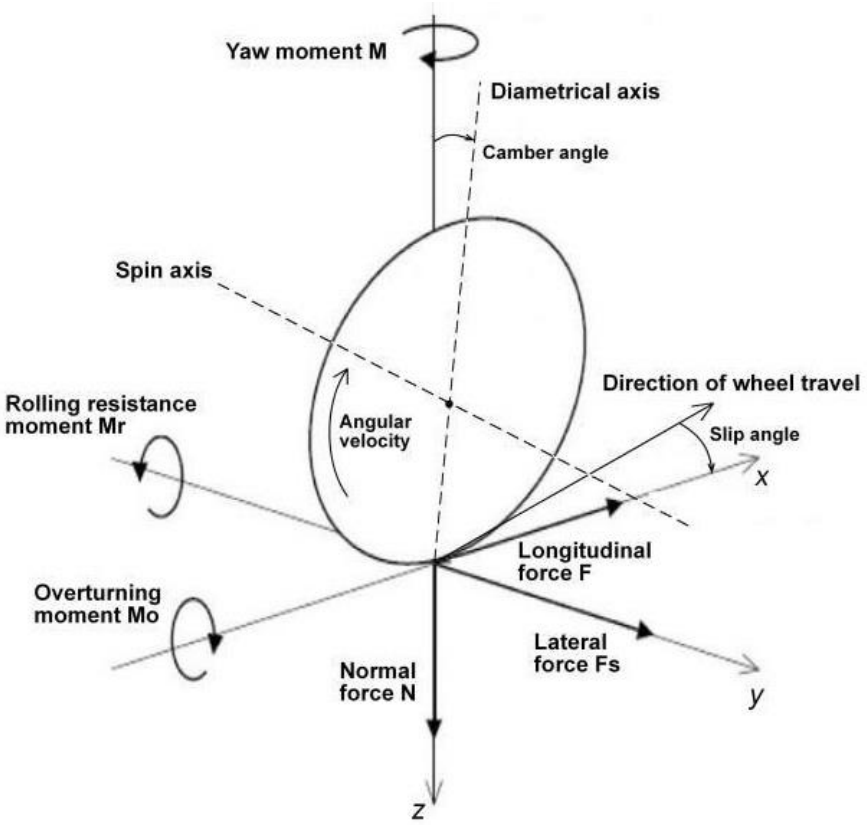

Figure 43: Reference system of the tire

Before starting outlining the Magic Formulae for longitudinal force, lateral force and self-aligning moment, a short kinematic analysis of the tire system is necessary.

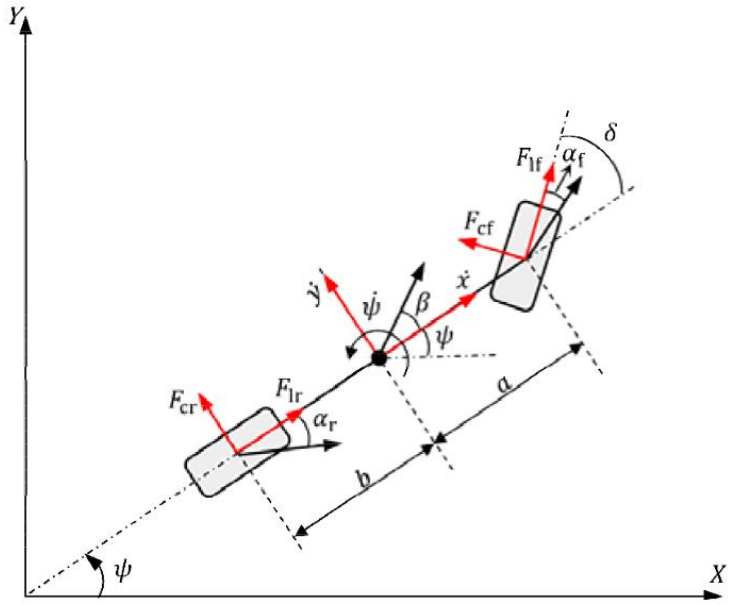

Figure 44: Dynamic single track model

The front speed and rear speed of the tire, along the longitudinal and lateral directions, can be computed from the vehicle speed as follows:

$$v_{x,f} = v_f \cos \alpha_f \qquad v_{x,r} = v_r \cos \alpha_r$$

$$v_{y,f} = v_f \sin \alpha_f \qquad v_{y,r} = v_r \sin \alpha_r$$

These speeds can be correlated to the speed of the vehicle:

$$v_{x,f} = v_x \qquad v_{x,r} = v_x$$

$$v_{y,f} = v_y + l_f \dot{\Psi} \qquad v_{y,r} = v_y - l_r \dot{\Psi}$$

The sideslip angle, which is the angle between the speed vector and the direction of the tire, can be expressed as

$$\alpha_f = \delta_f - \frac{v_{y,f}}{v_{x,f}} \qquad \alpha_r = \delta_r - \frac{v_{y,r}}{v_{x,r}}$$

Finally, the slip ratio of the wheel can be defined, it is the difference between the angular speed of a wheel that is in pure rolling and a wheel that is slipping on the ground

$$\sigma_f = \frac{r\omega_f - v_{x,f}}{v_{x,f}} \qquad \sigma_r = \frac{r\omega_r - v_{x,r}}{v_{x,r}}$$

$$\sigma_f = \frac{r\omega_f - v_{x,f}}{r\omega_f} \qquad \sigma_r = \frac{r\omega_r - v_{x,r}}{r\omega_r}$$

The first formula refers to braking, while the second one to driving conditions.

In the Pacejka model, the longitudinal force exerted between the tire and the ground is related to the longitudinal slip of the tire, the lateral force is related to the sideslip angle of the tire and the self-aligning moment is related to the sideslip angle, too.

In the following, the formula of the longitudinal force as a function the longitudinal slip is reported, in the definition of each curve the vertical load is considered as constant

$$F_x = D \sin\{C \operatorname{atan}(B(1-E)(\sigma + S_h) + E \operatorname{atan}[B(\sigma + S_h)])\} + S_v$$

In particular

$$C = b_0$$

$$D = \mu_{xp} F_z = (b_1 F_z + b_2) F_z$$

$$BCD_x = (b_3 F_Z^2 + b_7 F_z) e^{-b_5 F_z}$$

$$E = b_6 F_z^2 + b_7 F_z + b_8$$

$$S_h = b_9 F_z + b_{10}$$

$$S_v = 0$$

The coefficients indicated with b_x are experimental coefficients, while BCD_x is the slope of the resulting curve in the origin.

For the lateral force, the formula is a function of the slip angle of the tire, this will depend also on the camber angle. As in the previous case, each curve that will be obtained is for a constant value of the vertical load.

$$F_y = D\sin\{C\,\text{atan}(B(1-E)(\alpha+S_h)+E\,\text{atan}[B(\alpha+S_h)])\}+S_v$$

In particular

$$C = a_0$$

$$D = \mu_{yp}F_z = (a_1F_z + a_2)F_z$$

$$BCD_y = a_3\sin\left(2\,\text{atan}\left(\frac{F_z}{a_4}\right)\right)(1-a_5|\gamma|)$$

$$E = a_6F_z + a_7$$

$$S_h = a_8\gamma + a_9F_z + a_{10}$$

$$S_v = a_{11}\gamma F_z + a_{12}F_z + a_{13}$$

$$a_{11} = a_{111}F_z + a_{112}$$

The coefficients indicated with a_y are experimental coefficients, while BCD_y is the slope of the resulting curve in the origin.

The Magic Formula for the self-aligning torque depends on the side slip angle and on the camber angle. As in the previous cases the vertical load is considered constant for each of the resulting curve.

$$M_z = D\sin\{C\,\text{atan}(B(1-E)(\alpha+S_h)+E\,\text{atan}[B(\alpha+S_h)])\}+S_v$$

In particular

$$C = c_0$$

$$D = (c_1F_z + c_2)F_z$$

$$E = (c_7F_z^2 + c_8F_z + c_9)(1-c_{10}\gamma)$$

$$BCD_z = (c_3F_z^2 + c_4F_z)(1-c_6|\gamma|)e^{-c_5F_z}$$

$$S_h = c_{11}\gamma + c_{12}F_z + c_{13}$$

$$S_v = (c_{14}F_z^2 + c_{15}F_z)\gamma + c_{16}F_z + c_{17}$$

The coefficients indicated with c_z are experimental coefficients, while BCD_z is the slope of the resulting curve in the origin.

The Pacejka model can be considered suitable until each force that is exchanged between the tire and the ground can be considered singularly, whenever these forces act simultaneously on the tire, it happens that one limits the other and the ones that

have been obtained by means of the Pacejka Magic Formula represent the maximum forces that can singularly be exerted at the contact patch. For this reason, the elliptical model is the one that approximates the behaviour of the forces when there is interaction between the longitudinal and lateral forces.

$$\left(\frac{F_y}{F_{y0}}\right)^2 + \left(\frac{F_x}{F_{x0}}\right)^2 = 1$$

Where F_{x0} and F_{y0} are the maximum force that can be singularly exerted, computed by means of the Pacejka Magic Formula, at a given longitudinal slip and sideslip angle, respectively.

From the previous formula it is possible to evaluate the lateral friction coefficient, in relation to the longitudinal friction coefficient, and the cornering stiffness.

$$F_y = F_{y0}\sqrt{1-\left(\frac{F_x}{F_{x0}}\right)^2}; \qquad \mu_y = \mu_{y0}\sqrt{1-\left(\frac{\mu_x}{\mu_{xp}}\right)^2}; \qquad C = C_0\sqrt{1-\left(\frac{F_x}{\mu_{xp}F_z}\right)^2}.$$

For our purpose of dynamic simulation, the Pacejka Magic Formula results to give a satisfactory result.

Reasonable values for this purpose have been found, in literature[10], related to the tires mounted by the kick-off e-scooters.

Parameters for the longitudinal force evaluation		
B_0	Shape factor	1,67272
B_1	Peak factor	-9,46
B_2	Peak factor	1490
B_3	BCD calculation	30
B_4	BCD calculation	176
B_5	BCD calculation	0,0886
B_6	Curvature factor	0,00402
B_7	Curvature factor	-0,0615
B_8	Curvature factor	0,2
B_9	Horizontal shift	0,0299
B_{10}	Horizontal shift	-0,176

Table 11: Parameters for the longitudinal force evaluation [10]

In the following, the longitudinal force developed by the tire is reported depending on the amount of slip, reported in percentage, computed according to the Pacejka Formula of 1989, for different amounts of normal load.

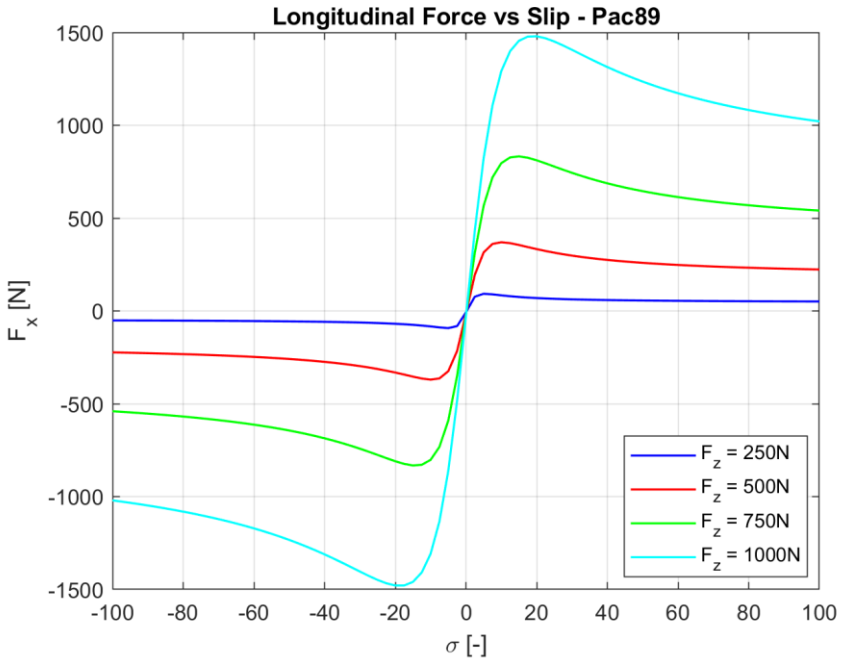

Figure 45: Longitudinal force vs slip

The maximum longitudinal friction coefficient has been computed for the same amounts of normal load that have been considered for the computation of the longitudinal force.

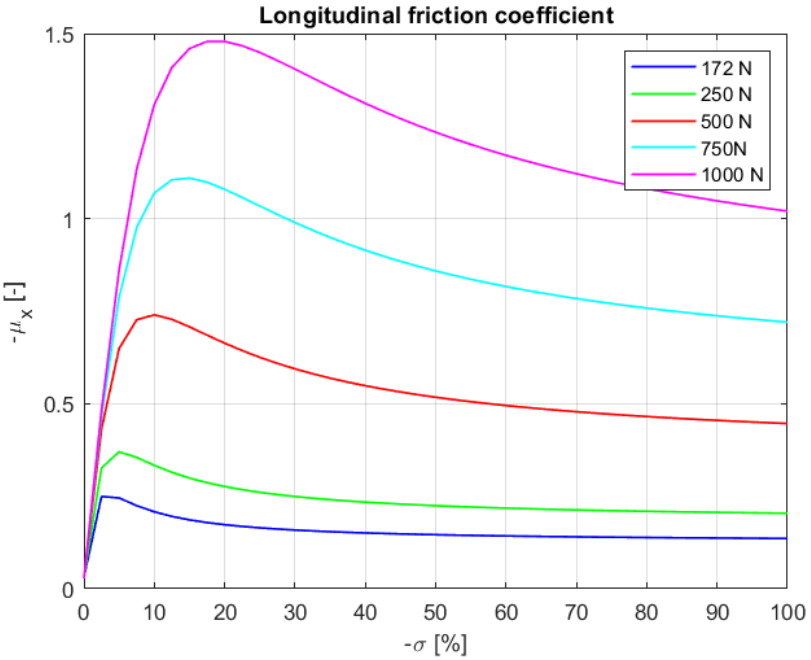

Figure 46: Longitudinal friction coefficient

Parameters for the lateral force evaluation		
A_0	Shape factor	1,65
A_1	Peak factor	-34
A_2	Peak factor	1250
A_3	BCD calculation	3036
A_4	BCD calculation	12,80
A_5	BCD calculation	0,00501
A_6	Curvature factor	-0,02103
A_7	Curvature factor	0,77394
A_8	Horizontal shift	0,0022890
A_9	Horizontal shift	0,013442
A_{10}	Horizontal shift	0,003709
A_{11}	Vertical shift	19,1656
A_{12}	Vertical shift	1,21356
A_{13}	Vertical shift	6,26206

Table 12: Parameters for the lateral force evaluation [10]

In the following, the lateral force developed by the tire is reported depending on the side-slip angle, computed according to the Pacejka Formula of 1989 reported above.

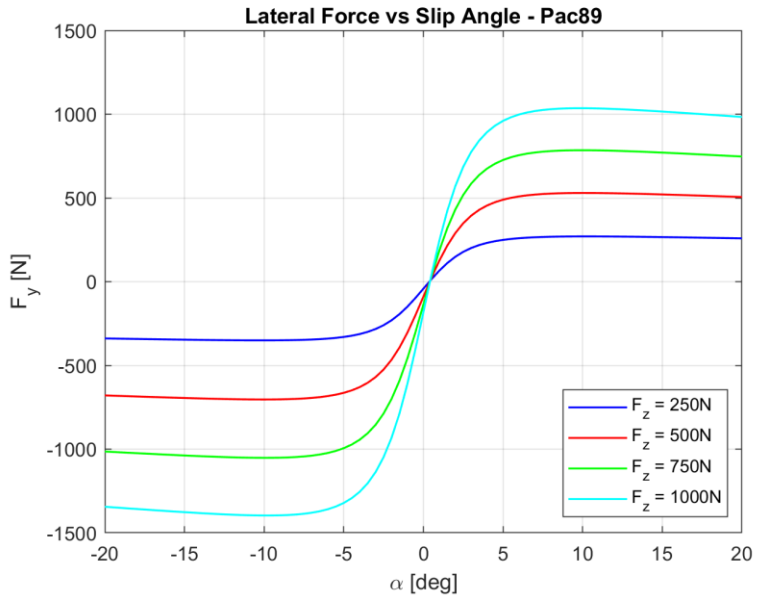

Figure 47: Lateral force vs side-slip angle

As done previously, also in this case the maximum lateral friction coefficient has been evaluated for different amounts of normal load.

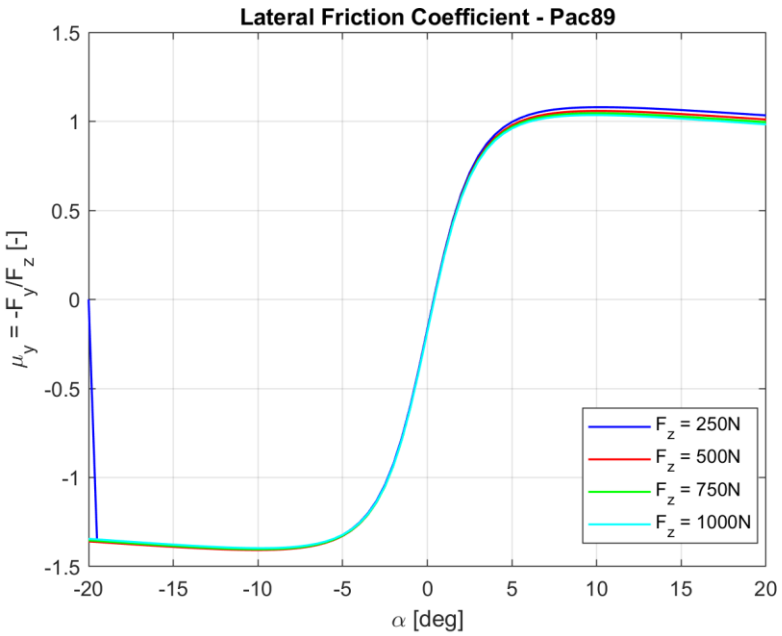

Figure 48: Lateral friction coefficient

As can be noticed, in this case, for the sideslip angle equal to -20 degrees the curve related to a normal load equal to 250N, reaches the adherence limit, this is why a peak comes out, reported in blue colour in *Figure 48*.

Controller design

The principles necessary to the autonomous driving are *perception*, *localization*, *motion planning* and *control*. Perception of the environment, of the obstacles and whatever is around the drone is necessary to avoid them and to guarantee a certain amount of safety. To detect what is around it, devices like Stereocamera, Sonar, Radar, LiDAR are necessary, some of them are more effective than other, in the case of Pacci, the presence of a LiDAR and Stereocamera revealed to be sufficient to travel in a real scenario. These two devices will be better outlined in the next paragraph. With the term "localization" it is intended that it is possible for the drone to orientee according to a specific path that has been planned in advance; in this case it is possible to mention a global path planning as the route that the drone has to accomplish to arrive to its prefixed destination and the local planning, which is the capability of the drone to avoid the obstacles that are present on the road that it has to travel, without exiting from the prefixed route defined during the global planning. To accomplish this latter task the previously mentioned devices are sufficient, while for the global path planning a GPS seems to be necessary, also because the drone has to send to the user real-time updates of its position. The motion planning is what defines the optimal speed to reach the destination, and this can be decided by a controller and all the actuators that must be driven by a decision-making device, which is the ECU. The

control is necessary to the decision making and to manage all the information coming from the sensors that are installed on the vehicle.

The first controller that has been considered is the PID. PID stands for Proportional, Integrative, Derivative controller, it is the most adopted control approach in the industrial field, because of its simplicity and its lower computational effort.

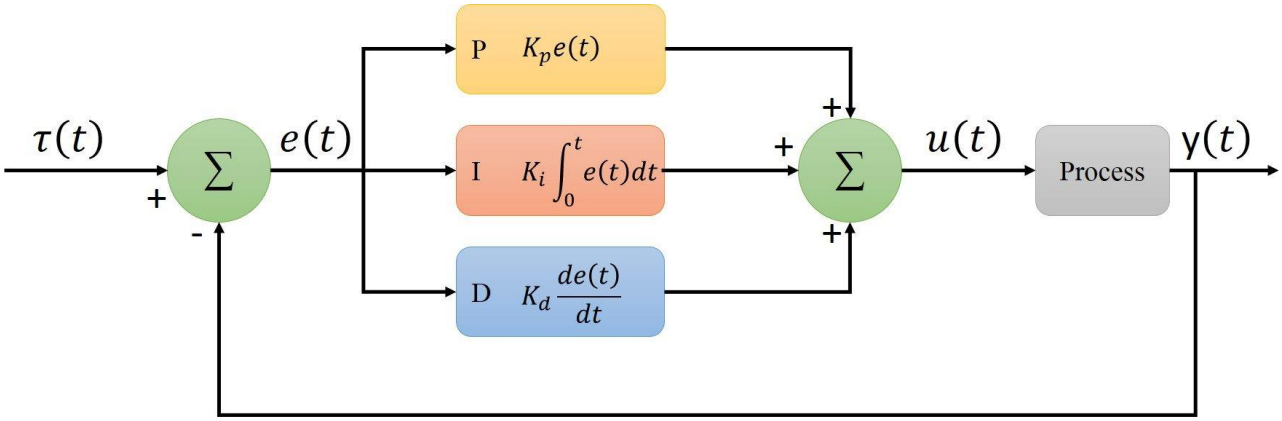

Figure 49: PID controller architecture

This controller acts on the errors that are provided in input as the difference between a reference and an actual value, which is generally the control variable at the plant output. The proportional action accounts for the present and its action is finalized at reducing the current tracking error; the integral action account for the past and permits a precise tracking error for references that are constant or slowly varying; then, the derivative action accounts for the future and improves the performance and robustness of the controller. Usually, an additional term is introduced in the derivative term, this is necessary to reduce the noise and it is a first-order filter. In order to design the controller, it is important to introduce how the increasing of a single parameter can affect the behaviour of the variables that are provided by the controller to the plant.

Parameter	Rise time	Overshoot	Steady-state error	Stability
K_P	Decrease	Increase	Decrease	Degrade
K_I	Decrease	Increase	Eliminate	Degrade
K_D	Minor change	Decrease	No effect in theory	Improve if "small"

Table 13: Effect of increasing the controller parameters

Several methods exist to design the controller; the Ziegler-Nichols' method is the most common and consists of tuning the single parameters according to the value of the proportional action of a "P controller" that provides system oscillations of constant amplitude and the oscillation period. This method resulted to be quite cumbersome, so that it has been opted for MATLAB PID tuning, in which, regulating the robustness and the speed of convergence of the signal, it has been possible to optimize the system behaviour. These steps will be better explained in the next chapter.

Another kind of controller, adopted for even more complex systems, is the Model Predictive Control (MPC) and this is able to provide the best trade-off between performance and command efforts.

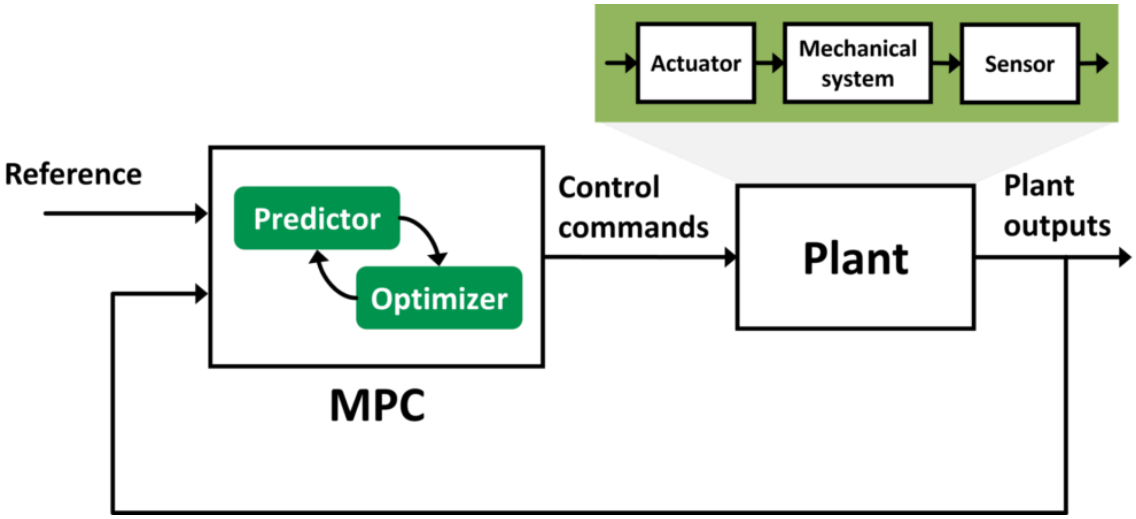

Figure 50: MPC controlled system

At each time of the duration equal to the sampling time, a certain estimation of the future state of the system is made over a finite time horizon, called prediction horizon. According to this, the optimal input command is provided to the plant at each sampling time. The idea is to solve real-time optimization problems to control the inputs to the plant and its performance, withstanding some constraints.

It can be associated to the driver behaviour: he or she can act on the accelerator pedal, adjusting the speed of the vehicle or even braking, and on the steering wheel, to adjust the trajectory, according to what can be seen in front of the vehicle; same for the MPC: it exerts control action on the plant according to prediction that has been made about the system, using a model which takes into consideration constraints. It is easily understandable that, like for a driver, if the MPC cannot "see" far enough from the vehicle, its performance could result in poor control, so a very first constraint can be the one of the prediction horizons, which must be equal or larger than the sampling time: $T_p \geq T_s$. In the following *Figure 51* it is graphically reported the operating principle of an MPC.

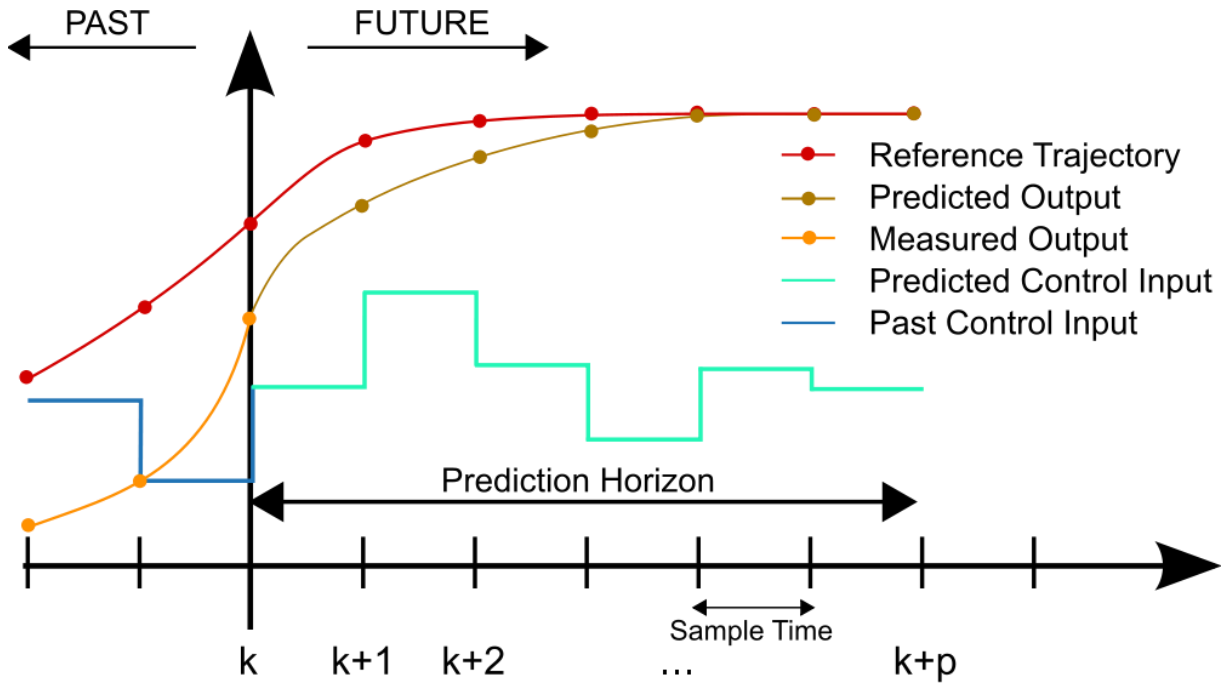

Figure 51: Operating principle of MPC

The autonomous vehicle control is based on longitudinal and lateral control, that the MPC can jointly perform. Some additional control algorithms can be added at higher levels, like the Decision Making Module (DMM), which can be necessary to allow vehicle to deal with intersections, for example, based on pre-defined policies, according to which all the possible scenarios can be faced. Since predictions made by MPC can be at manoeuvre level and at trajectory level, this controller results to be performant in trajectory planning and control, too. The trajectory planning can be lead as global, that is to find an optimal path to reach a destination, avoiding obstacles, or as local, that is to plan trajectory over a shorter time horizon, at each sampling time, and this must be consistent with the vehicle dynamics. In addition to the efficient management of the trade-off between performance and input activity and to the fact that constraints and saturations, which can vary with the time, are taken into consideration, this results to be an optimal controller for an autonomous vehicle, despite the computational efforts, which could be quite demanding. [11]

Sensors

Sensors are devices integrated in the vehicle system, which are devoted to the perception, as discussed above, this latter is one of the base principles of autonomous vehicles. Many types of sensors exist and a first distinction can be made between vehicle dynamic sensors and sensors for perception; to the first type of sensors belong the devices which are in charge of monitoring wheel speed, steering angle, steering torque, angular speeds and accelerations, brake pressure and virtual sensing, according to what has been detected by this sensors, a signal is sent to the ECU, which accordingly can send signals to the actuators to control and modify the state of the previously mentioned parameters, according to some references that are stored in it.

The second type of sensors consist of ultrasonic sensors, radar, LiDAR and camera, these are called perception sensors because they are in charge of monitoring and detecting what is outside and around the vehicle, as it happens for the previous type of sensors, according to what is sensed, a signal is sent to the ECU, which as a consequence drives the actuators.

Vehicle dynamic sensors

For what concerns the measurement of the wheel speed, this constitutes the basic evaluation for safety systems, stability control, deceleration control, estimation of the road friction coefficient, of the vehicle speed and of the slip of the wheel. It can be classified according to its operating principle on active or passive configuration, in the first case it is actuated by providing external power (typically from a 12 V device), while in the second case there is no external power supply. The toothed tone ring has a passive configuration and relies on the variable reluctance of a toothed wheel that is perceived by a magnetic circuit and according to this an alternated voltage is generated in the circuit. This kind of sensor can suffer the dirtiness which may deposit on the notch and the tooth of the wheel, affecting the performance of the sensor itself. Moreover, only angular speeds over a certain value can be perceived.

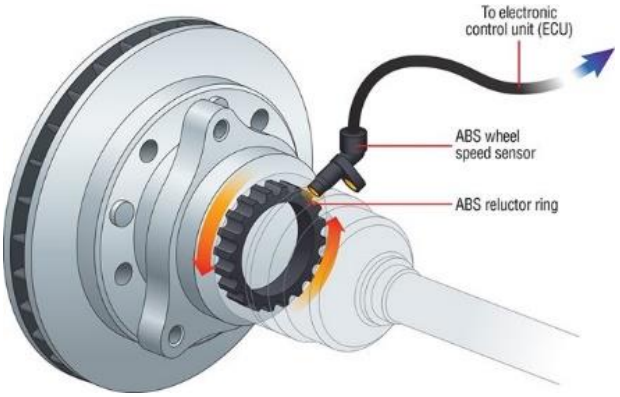

Figure 52: Toothed tone wheel

A similar sensor, but with an active configuration is the Hall sensor, which relies on the Hall Effect.

A more reliable way of measuring the angular speed is offered by a Magnetic Encoder, which relies on the magneto-resistive effect, it is similar to the Toothed tone ring, but in this case a magnetic tone ring is present; when the wheels rotate a square wave is generated and its frequency depends on the angular speed of the ring which is coupled with the rotating wheel and it is typically placed inside it.

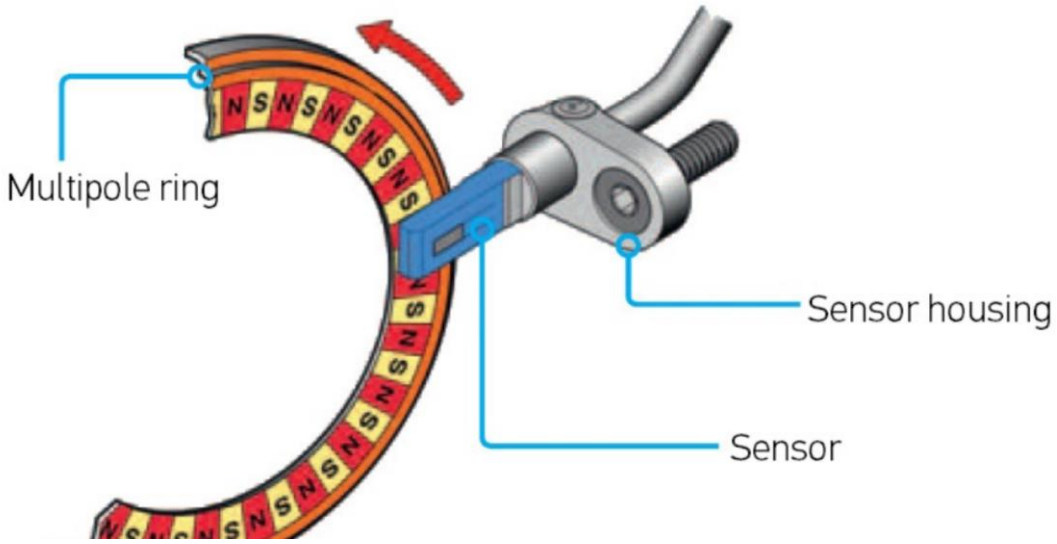

Figure 53: Magnetic encoder

Another sensor which reveals to be necessary in order to guarantee the stability of the vehicle is the Inertial Measurement Unit (IMU), which is a little device, similar to an accelerometer, that can measure the up to 6 units measurement dimension: longitudinal, lateral, vertical accelerations, roll, pitch and yaw; in order to obtain good results in the measurement, this must be installed on a stiff structure as close as possible to the CoG of the vehicle.

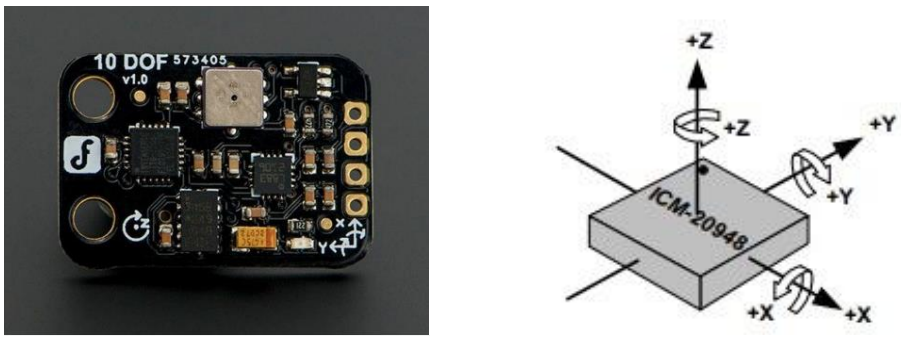

Figure 54: 10 DOF Inertial Measurement Unit

This sensor can be provided also with GPS, to obtain also a global information about where the vehicle is located.

Another kind of sensing is the virtual one, which means that there is no hardware in charge of measuring given quantities, because these cannot be directly measured or because they are difficult to measure, so that the virtual sensing can indirectly measure them; in particular, it is employed in the measure of the sideslip angle of the vehicle, of the vehicle speed and of the road condition. This estimation can be done on analytical techniques, which are model based, and employ state observer, based on the dynamic model of the vehicle, or on empirical techniques, which do not make reference to a model and this relies on the Artificial Neural Networks (ANNs).

Sensors for perception

The sensors for perceptions differ one from the other for the way they adopt to detect obstacles on the path. Nowadays, many of them can be found on modern vehicles to enhance active safety and each of them cover a specific area around the vehicle.

The ultrasonic sensor is typically adopted for short range detection and it was usually employed for the type of assisted parking sensors in previous stages. Their operating principle relies on the emission of a sonic wave by an emitter at a frequency of 16000 Hz, that is unperceivable for human ears, and the reception of the same wave, that is reflected back if an obstacle is present in front of the sensor, and it is registered by a receiver. These two devices are extremely sensible to these vibrations and the receiver can detect the distance from the obstacle simply knowing the time that the wave took to turn back to the sensor.

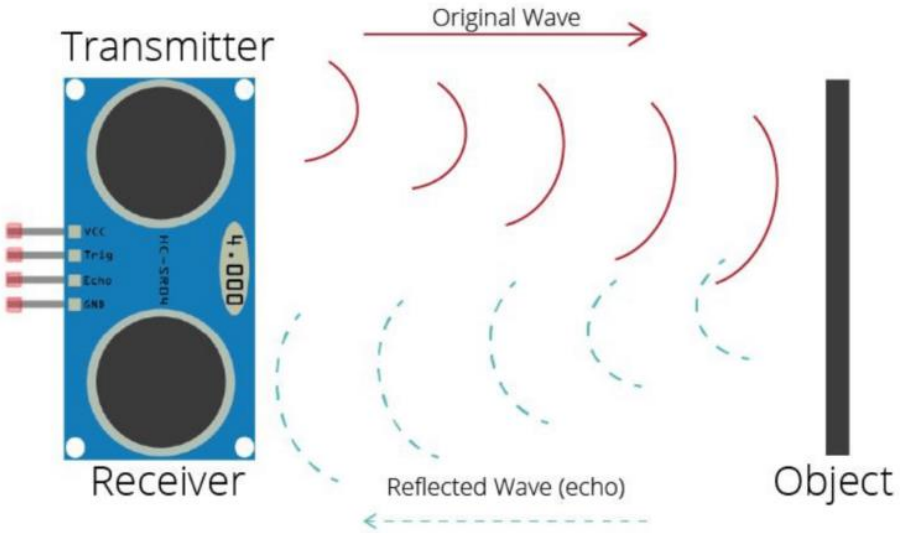

Figure 55: Operating principle of an ultrasonic sensor

Radar stands for Radio Detecting And Ranging; this kind of sensor relies on the emission of electromagnetic waves from an antenna: if some obstacles are present on the path, they reflects the beam back to the antenna; these devices are usually employed for distance and speed measurements, relying on the Doppler effect. Their measurements result to be robust even with poor visibility conditions due to severe weather conditions. Mounted on a vehicle, they perform the function of blind spot detection, lane change assist, forward collision warning, emergency braking and adaptive cruise control. They can be of various type according to the range they can cover, so it is possible to have short range radar (up to 30 meters), replacing la ultrasonic in parking assist manoeuvre, medium range radar (up to 60 meters) for blind spot detection and long-range radar (up to 200 meters) for collision warning, adaptive cruise control and automatic emergency braking.

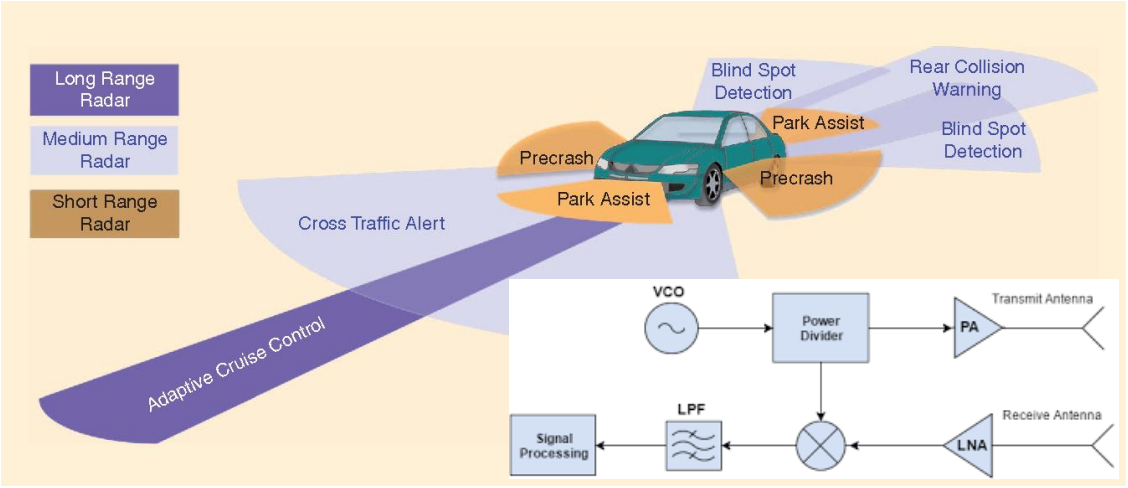

Figure 56: Different type of radars installed on a vehicle and working principle

LiDAR stands for Light Detection and Ranging; it is similar to a radar, but it uses laser light instead of radio waves; the strength of this kind of sensors is their high sampling rate and their high resolution, so that they can provide precise measures rapidly. They are used to examine the surface of the object and to measure the distance between an object and the sensor itself as the flight time multiplied by the speed of light and divided by 2; what is detected by a LiDAR constitutes a 3D reconstruction of the environment, called three-dimensional point cloud and this could be just in one direction (unidirectional LiDAR) or with a 360° horizontal field of view (motorized omnidirectional LiDAR). It can have up to 128 emitters and each detected point contains information about its position in a three-dimensional space. Differently from the radar, the LiDAR performance can be affected by severe weather conditions and they are not able to detect behind foliage or vegetation.

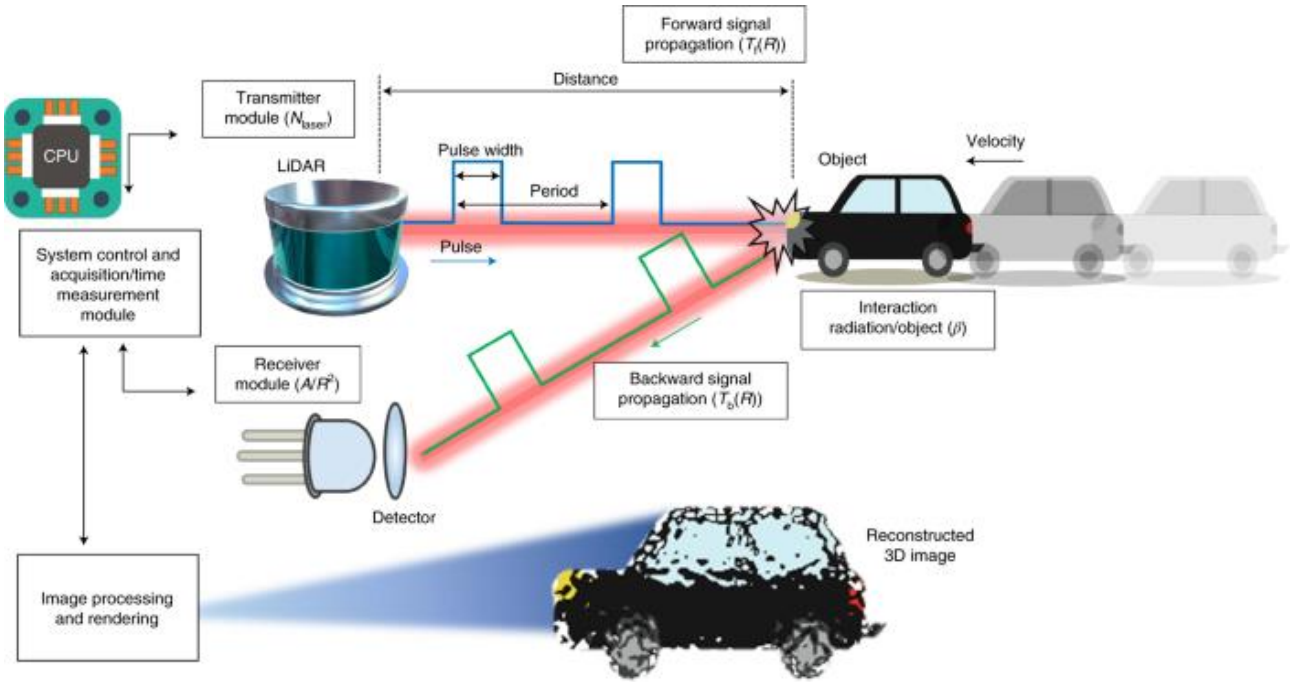

Figure 57: Working principle of a LiDAR

Moreover, the LiDAR is not able to detect the colours and this feature results to be fundamental whenever a vehicle has to detect the colour of a traffic light or the colour of some objects, for example, in order to classify them. The camera can solve this problem; they are fundamental also for lane detection. It is possible to have a single camera, but a stereocamera is preferable, since in a compact device with binocular vision it is able to detect blind spots by means of triangulation technique.

Figure 58: ZED stereocamera

The Pacci drone has been provided by a Magnetic encoder to monitor the state of the single wheel and this sensor resulted to be sufficient to control the overall dynamic of the vehicle at ground level. For what concerns the perception sensor, it has been chosen to provide the Pacci drone with LiDAR and Stereocamera to recognize and distinguish the type of obstacles that it could meet on its path.

Chapter 5

In this chapter it will be shown what has been developed in terms of dynamic simulations and analyses of the obtained results. The first part of this chapter is dedicated to the explanation of each single block that has been implemented in the MATLAB / Simulink environment to model each single part of the whole Pacci drone system, then a brief explanation of the tuning parameters that has been conducted on the controller until satisfactory results have been obtained and then the analyses of the results will follow.

Modelling

It must be specified that some assumptions have been adopted from the beginning which were suitable to the kind of vehicle that has been tested; due to the fact that the maximum speed of the Pacci drone is limited to 26 km/h, that it is a vehicle of reduced dimensions and masses, the DST model resulted to be sufficient for the purposes of dynamic simulations.

During these simulations, different situations have been taken into consideration. These have been assumed as standard cases that the Pacci drone will face during its missions. According to them, a PID controller has been evaluated, instead of a more sophisticated NMPC, because of the less complex structure of the robot and because of the reduced performance with respect to a vehicle like a car.

Thinking about the everyday life of the drone and the paths that it has to travel, two standard scenarios have been simulated:

1) A sinusoidal trajectory of reduced amplitude: it has been adapted to the dynamics of the Pacci drone, as it has to avoid multiple stationary obstacles on its path.

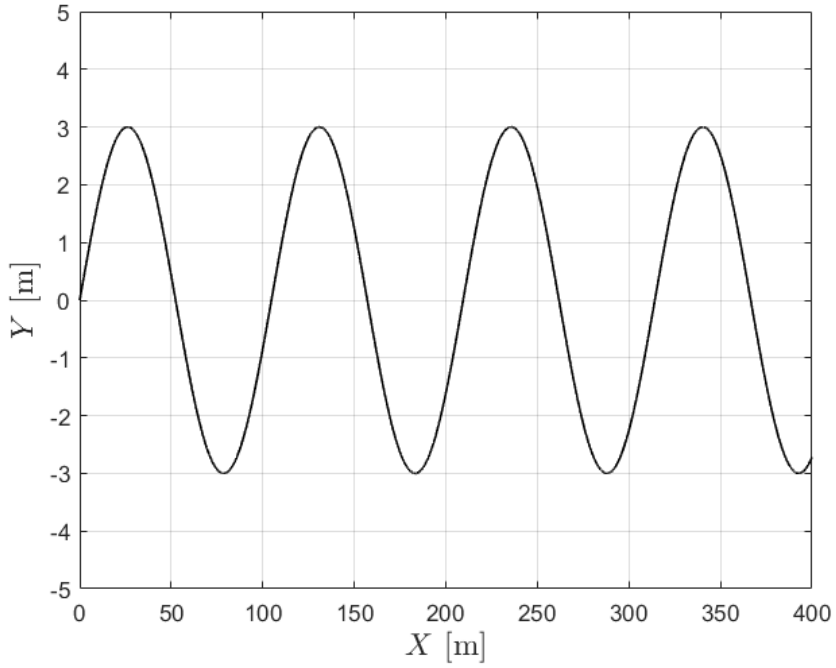

Figure 59: Sinusoidal reference trajectory

2) ISO double lane change manoeuvre: it has been tailored on the Pacci drone, which means a reduced amplitude of the trajectory which can resemble a direction to avoid sudden obstacles or an overpassing manoeuvre.

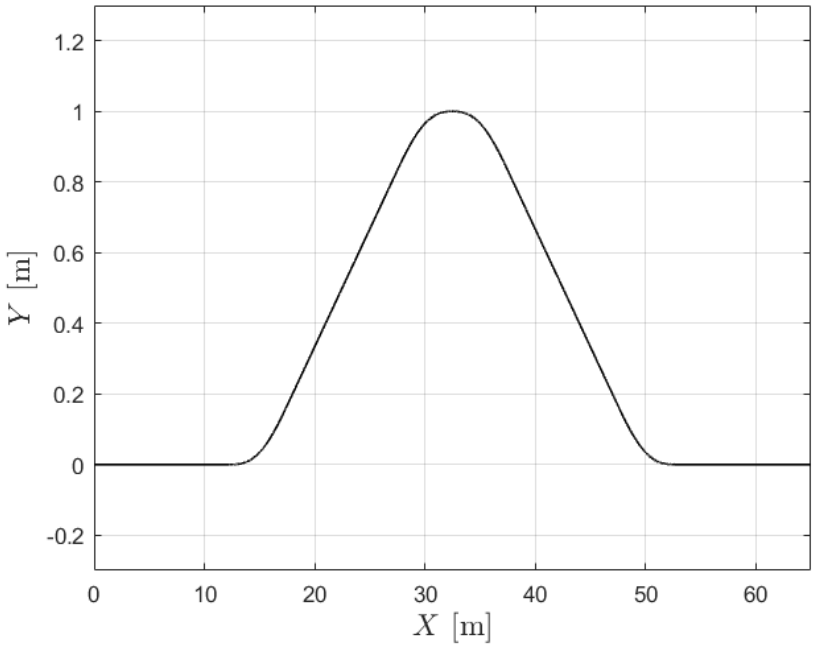

Figure 60: ISO double lane change reference trajectory

Longitudinal dynamic simulation

Before starting with the complete dynamic model, the very first approach concerns the study of the longitudinal dynamic behaviour of Pacci. This has been done by means of one tool of Matlab-Simulink that is Simscape. This kind of model has been elaborated after an online workshop led by MathWorks platform about "The formula student" competition.

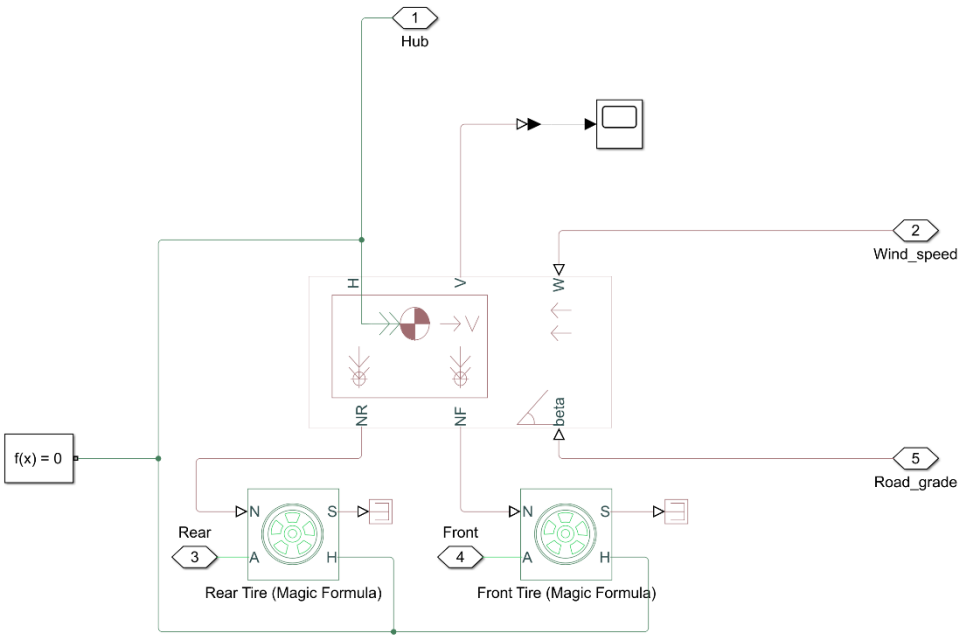

Figure 61: Vehicle body subsystem

Inside the vehicle block all the parameters reported in *Table 7* and related to the vehicle Pacci have been inserted, then, starting from the left bottom side, the normal load on rear and front axle has been provided as input to other two blocks related to the model of the tire, next, the gradeability of the road has been given as input; in the upper part, starting from the right, the wind speed has been provided as external input to the vehicle block, then the port "V" represents the vehicle speed and the port "H" provides the mechanical rotational conserving port related to the horizontal motion of the vehicle.

The tire Magic Formula linked to the "Vehicle body" block is reported in the *Figure 62* below.

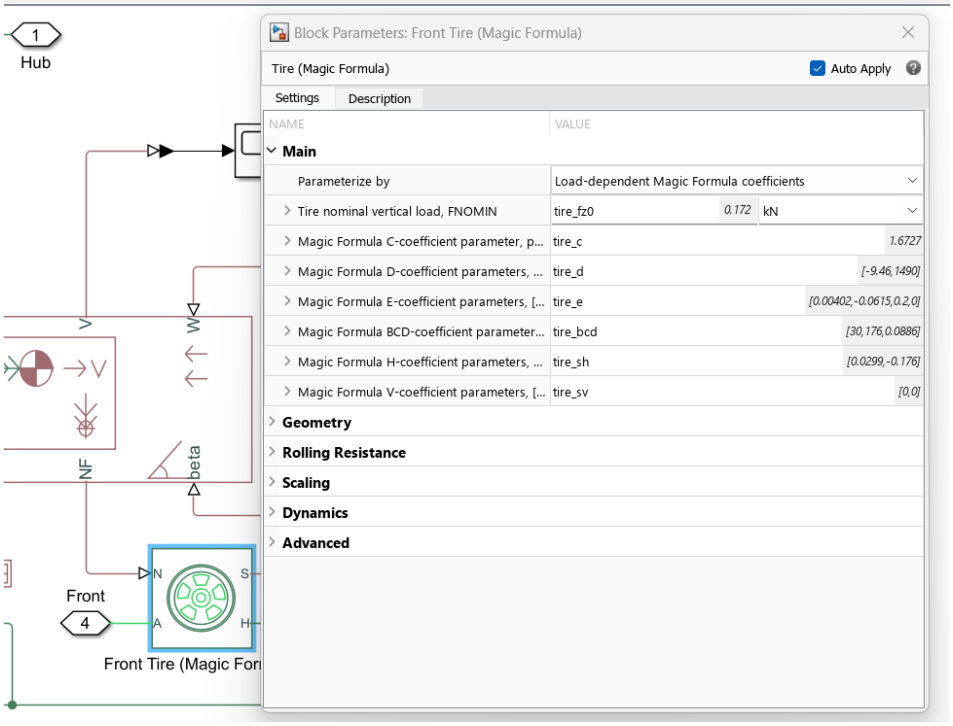

Figure 62: Tire block parameters

In this block the option "Load-dependent Magic Formula coefficents" has been chosen, so that the vectors containing the parameters reported in the *Table 8* are reported. In "Geometry" submenu the rolling radius has been inserted. In "Dynamics", instead, the longitudinal stiffness and compliance of the tire are considered, as reported in the following:

$$K_{tire} = 80\ \frac{N}{mm};$$

$$C_{tire} = 0.05\ \frac{Ns}{mm}.$$

Under "Rolling Resistance" menu, the rolling resistance coefficient equal to 0.005 has been considered; the other options have been left as default or as not present.

On this block four ports are present: The input port N carried from the vehicle body subsystem which represents the vertical load on one axle, the A port represents the mechanical rotational conserving port, the S port is the physical signal reporting the amount of slip of the tire and the H port is a mechanical rotational conserving port, too.

The manoeuvre that is going to be analysed is an emergency braking manoeuvre, so two blocks representing the front and rear brake tires have been inserted in the model described above. In particular, disc brakes have been modelled by means of a loaded-contact rotational friction to which the normal load acting on brake pads are given as input, by means of the port N. The forces that are provided have different trends in order to discretize between what happens when just rear brakes are acting and when

brakes on the front and rear axles are active. As can be seen in *Figure 64,* the rear braking manoeuvre has been implemented by means of a step input, which acts on brake pads after 20 seconds with a force equal to 100N, the front braking manoeuvre instead has been implemented by means of a step input which provides a force equal to 200 N after 25 seconds.

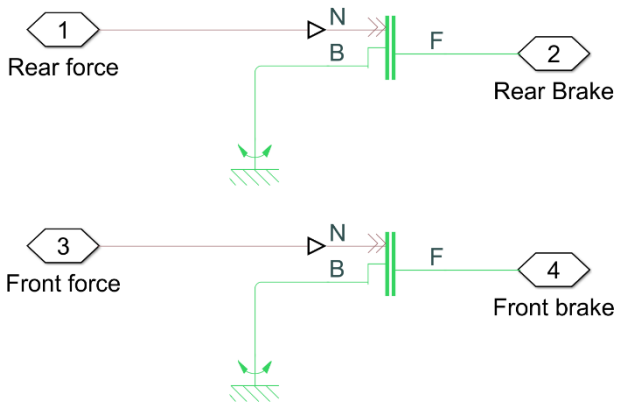

Figure 63: Brake subsystem

In *Figure 63*, the B port represents the rotational fixed reference, in this case the ground reference has been selected. The F port, instead, is the mechanical rotational conserving port, which gives the brake torque to the axle, by means of the radius of the disc, which is provided to the disc brake block, and the normal force acting to the pads, which will apply a certain braking force on the disc according to the friction coefficient of the pads material, too.

In the following *Figure 64*, the complete longitudinal dynamic model is shown.

As can be noticed, an additional subsystem has been added, it is called "Sensor Subsystem" and contains a motion sensor block which is in charge of measuring acceleration, speed or displacement with respect to the ground. This block is fundamental to analyse the final results.

The other blocks that are reported represent the external input to the vehicle body subsystem. The wind speed has been set equal to $0\ m/s$, while the road gradeability has been provided by means of a look-up table to which "Distance" input, corresponds a certain amount of slope, given in *radiants*.

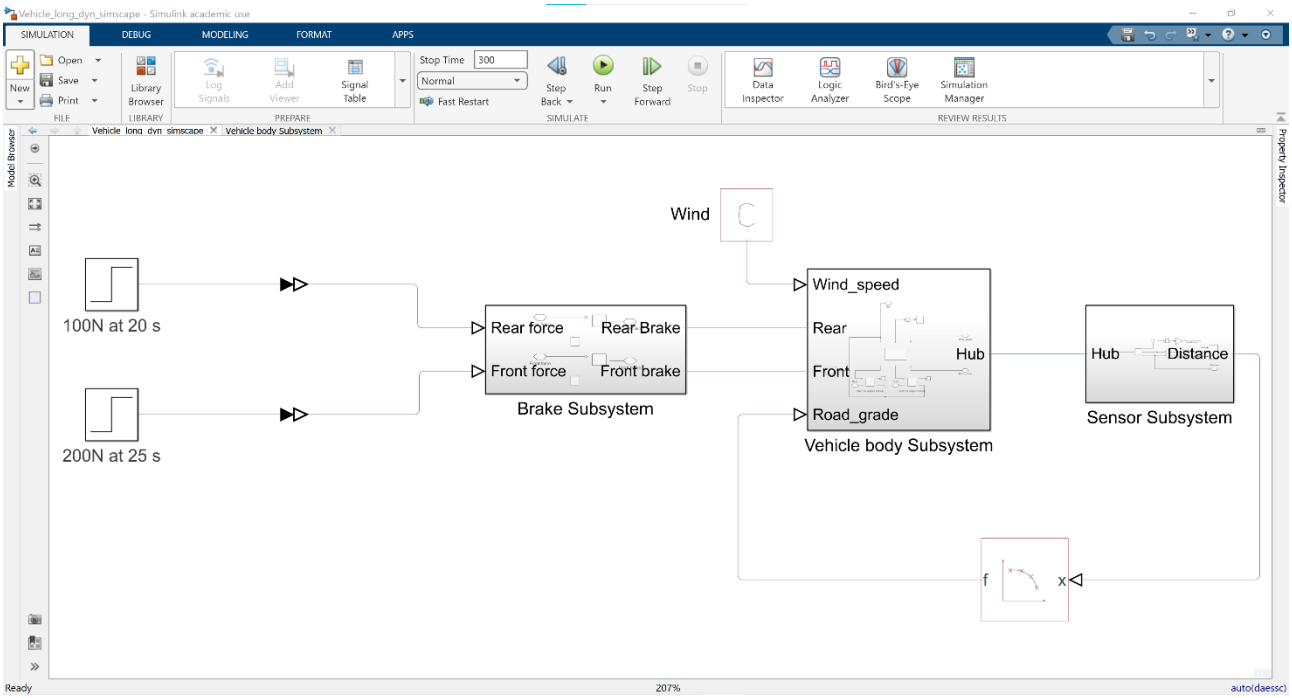

Figure 64: Simscape complete model of Pacci's longitudinal dynamics

In the following *Figure 65*, it is reported the slope of the terrain that has been provided as input to the Simulink model, to analyse the braking behaviour of the Pacci rover.

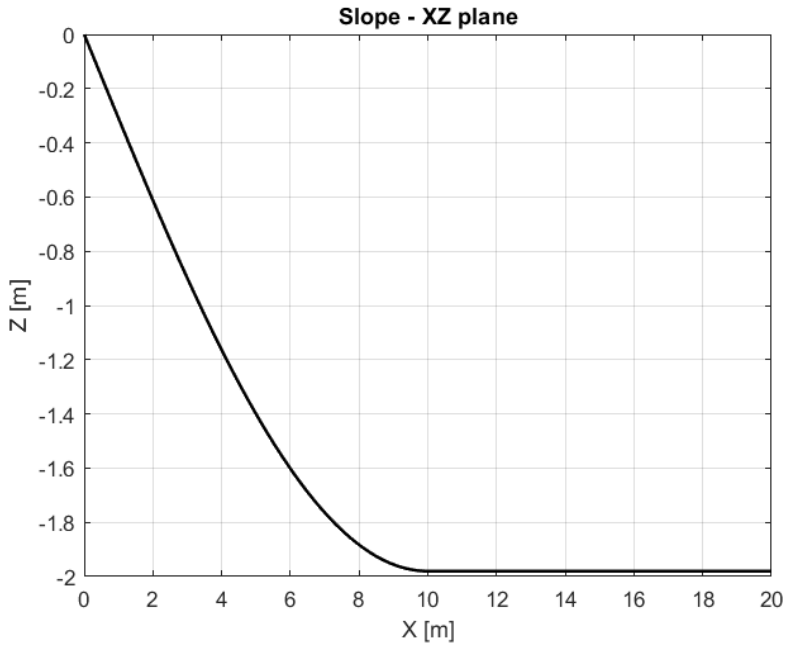

Figure 65: Slope of the modelled terrain

As it can be noticed, the vehicle will be launched in free rolling down to a declivity that will decrease its height of about 2 metres from the starting point, along a distance of about 9 metres.

Simulation results

With the action of the brakes after 20 and 25 seconds, it is expected to obtain a first part of the simulation in which Pacci from 0 m/s initial speed is pushed down the road and, due to the slope of this one and its inertia, the speed will increase, then, when the brake activates, it is expected to see a reduction of this speed in a double trend, the first representing the reduction of the speed due to the action of the rear brakes and the second one due to the action of both front and rear brakes. This is reported in the following *Figure 66*, which is the output of the "Sensor Subsystem" with respect to the time of the simulation.

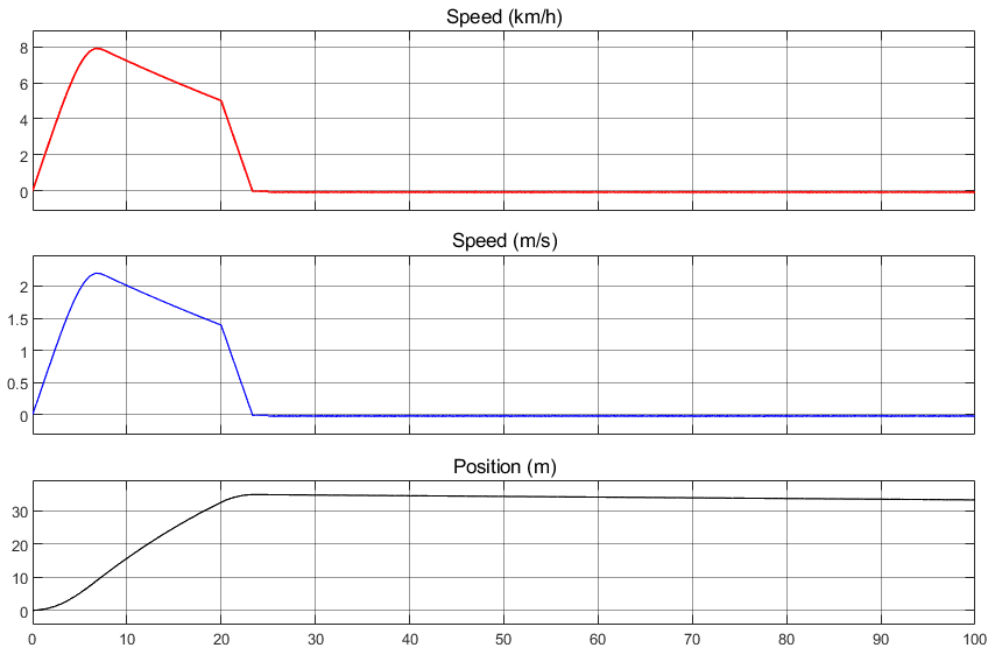

Figure 66: Speed and position results

What can be highlighted is the fact that the speed first reaches a maximum that is equal to $8\ km/h$ before brakes are activated, once the emergency braking manoeuvre is performed, then the speed drops to 0 km/h and the vehicle stops. For what concerns the position, this in a first moment increases, until brakes stop the vehicle. Due to computation reason, it is possible to see that the trend of the position slightly decreases after reaching 0 km/h, because, as can be seen in the *Figure 67* below, the speed has an irregular trend that is negative, so, according to the conventions stated by this simulation, seems that this vehicle is travelling backword very slowly. In

reality this behaviour is quite unfeasible, but it is just a matter of numerical simulation.

Braking simulation (ABS introduction)

In the previous simulation, the braking behaviour has been analysed, simulating an emergency manoeuvre to stop the vehicle. At tire level, in this case, it is possible to improve this manoeuvre and reduce the distance in which the vehicle stops, by means of an ABS system. In the following paragraph a comparison between a vehicle not provided with this braking strategy and another provided with it, is reported. The vehicle that has been simulated has the same characteristics of Pacci.

What limits the force that a tire can exert at the contact patch is the available traction. To exert a certain amount of longitudinal force, the tire works with a longitudinal slip, which is defined as

$$\sigma = \frac{v}{V}$$

Where at the numerator the average slip velocity of the tire is reported. As seen talking about the longitudinal force exerted by the tire, the longitudinal friction coefficient is linked to the slip of the tire by means of a non-linear relationship, according to which the maximum friction coefficient at the tire-ground contact can be obtained within a small range of slip percentage, which ranges typically between -20% and 20%, then the friction coefficient will decrease, due to the fact that the tire is slipping. This behaviour of the tire can deeply affect the handling of the vehicle and its stability. In traction, if this condition is reached the cornering capability of the tire practically drops and the forces exerted at the ground point in the same direction of the relative velocity at the contact patch, when the slip reaches a value near to 100%, the wheels lock and the vehicle becomes unstable and cannot be controlled. This unwanted behaviour can be prevented by means of an antilock system, which is capable of implementing a braking strategy that avoids the locking of the wheels, making the vehicle more controllable even in emergency situations. Practically it reduces the braking torque acting directly on the braking system.

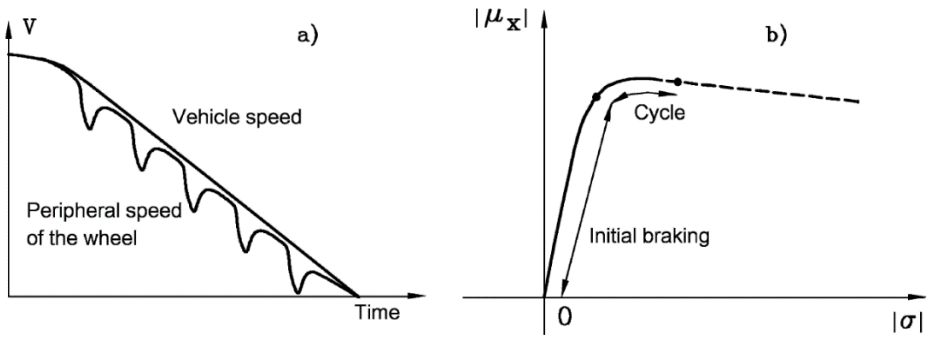

Figure 67: ABS working principle

Under the letter (a) the plot of how wheel speed and vehicle speed evolve during a braking manoeuvre is reported, it is noticeable that the trend of the peripheral speed is not regular due to the intervention of the anti-lock system, which acts on the braking circuit increasing and decreasing the braking force within a certain threshold. Under the letter (b) the working range of the ABS in terms of friction coefficient is showed, so that the purpose is to remain within the part of the curve that is denoted by means of the name “Cycle”.

In the following *Figure 68* and *Figure 69*, it is reported the Simulink model in which this braking strategy has been implemented. In the look-up table it has been reported the curve of the friction coefficient vs slip, the one reported in the previous *Figure 67* under the letter (b).

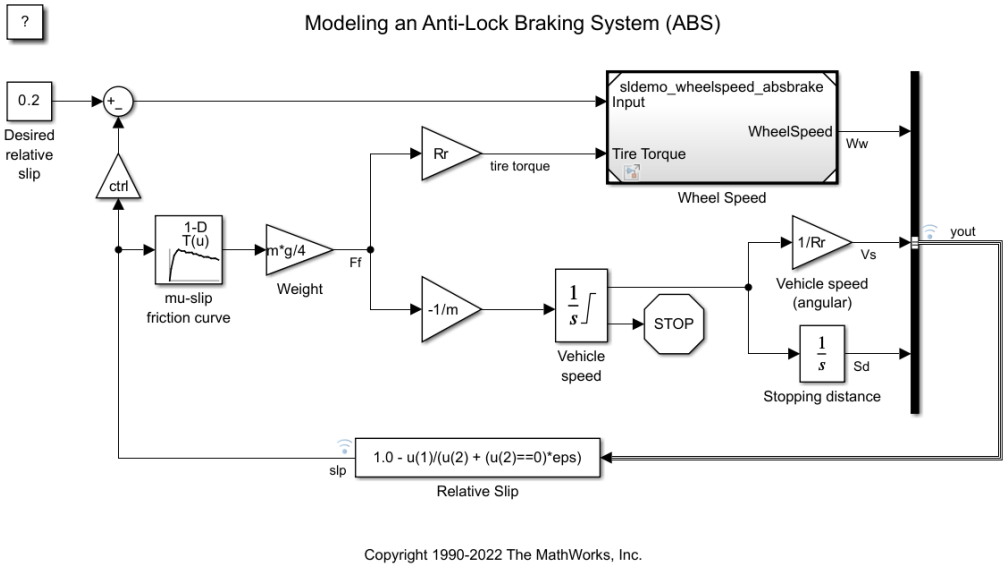

Figure 68: ABS modeling on Simulink

In the *Figure 69*, instead, it is reported the content of the “Wheel Speed” block and the particular control of the anti-lock strategy under the name of “Bang-bang controller”. This one works switching between two values of the slip of the tire, which is provided as input; the command coming from this controller is then provided to the brake circuit, which is modelled here as hydraulic and provides a certain braking pressure on the pads to pursue the scope of the anti-lock braking system. In particular, this controller operates on the slip value that is reached when the mu-slip curve reaches a peak value.

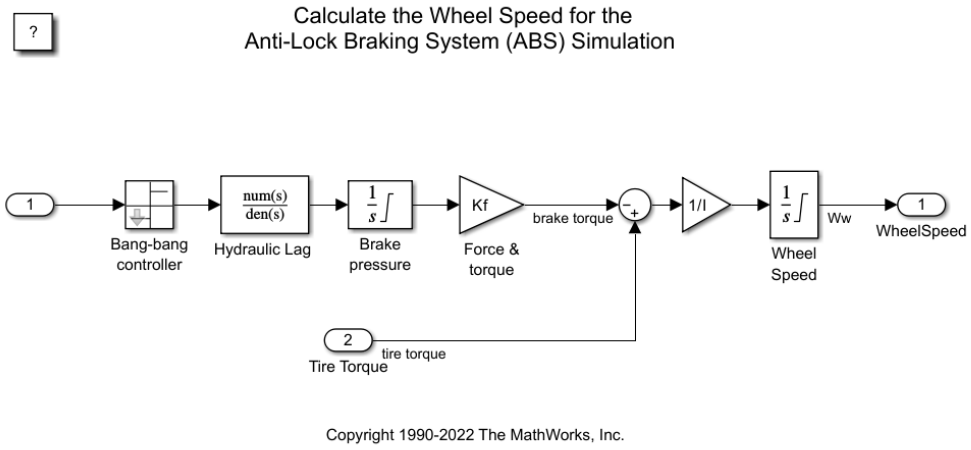

Figure 69: "Wheel Speed" subsystem

In the following figures, it is firstly reported the slip of the tire at the contact point with the ground and the vehicle speed and wheel speed evolution during the time of the simulation.

The purpose is to simulate an emergency braking manoeuvre, so it has been chosen to set the initial velocity equal to the maximum velocity that the rover can reach and evaluate the time needed to completely stop the vehicle with and without an anti-lock system.

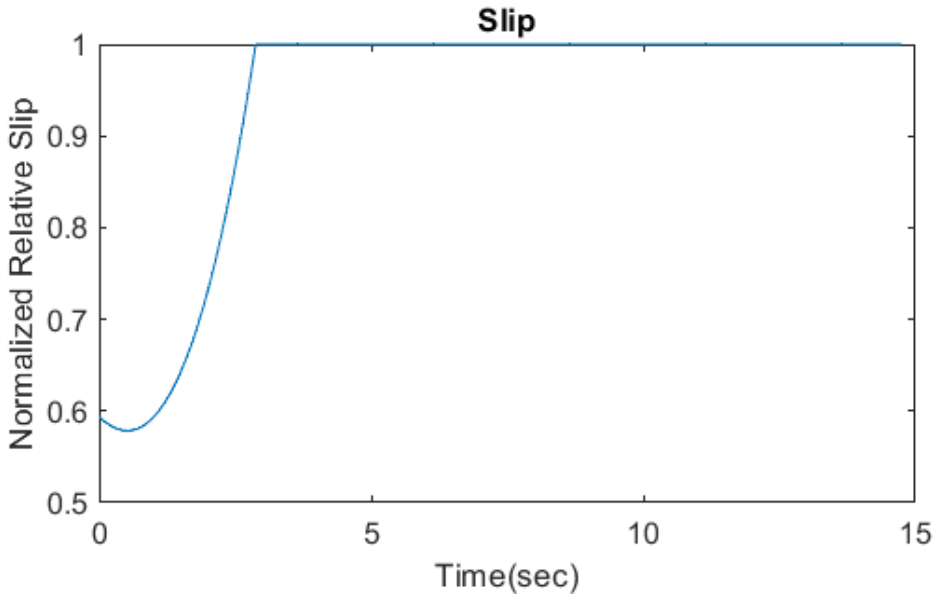

Figure 70: Tire slip during braking manoeuvre without ABS

As it can be clearly seen in the *Figure 70* above, the total slip condition of the tire is reached before 5 seconds of simulation have elapsed. In this condition, the tire is locked and the vehicle has a certain speed, as it can be seen in the following *Figure 71*.

It will take about 15 seconds to completely stop the vehicle, while the wheel appears locked well before 15 seconds have elapsed and the reaching of rest position of the vehicle. In this period of time the vehicle will be unstable and uncontrollable. This can represent a risk for all the people and objects that the rover Pacci can meet on its path, so the purpose is to avoid as much as possible this condition.

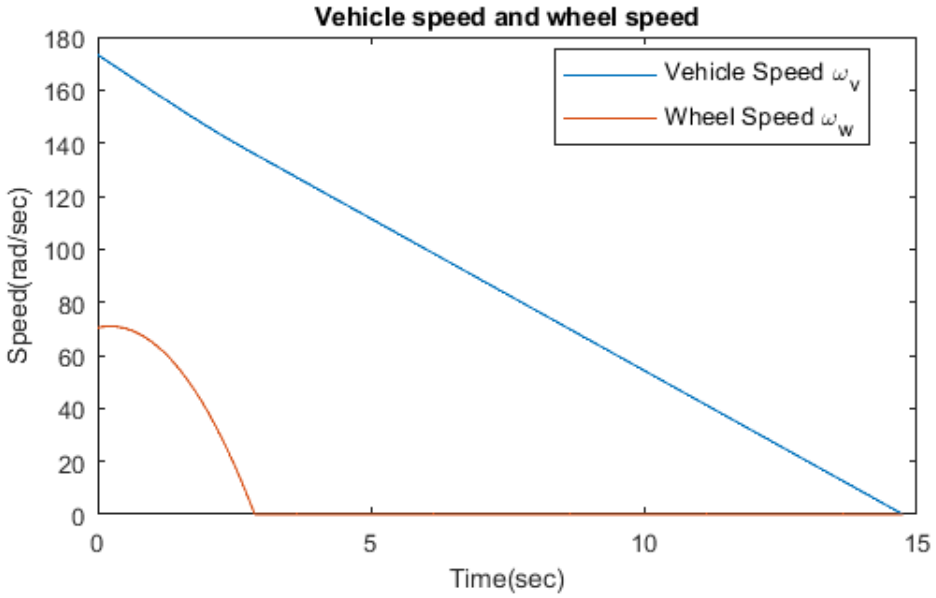

Figure 71: Vehicle speed and wheel speed without ABS

Now the braking strategy with ABS has been applied to the rover; the expected behaviour is an improved braking manoeuvre, which avoids the locking of the wheels and which brings the vehicle to rest position in less time with respect to the previous case.

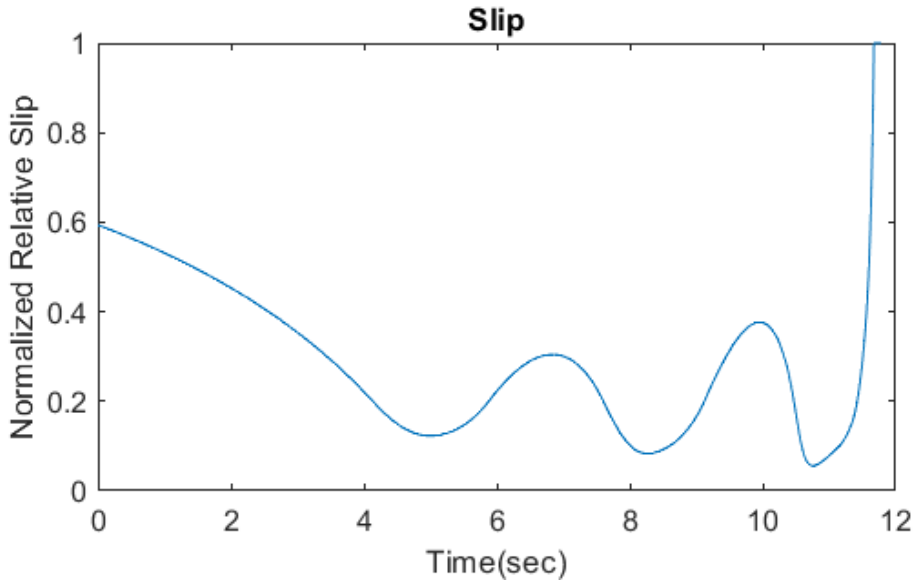

Figure 72: Tire slip during braking manoeuvre with ABS

In the *Figure 72* above, it can be noticed an oscillation of the relative slip, between the tire and the ground, around the value equal to 0,2, this is imposed in the braking strategy of this simulation and it reflects the real strategy implemented on vehicles. Around the simulation time of 12 seconds, it can be noticed that the slip arises to 1, here the wheels of the vehicle are completely locked. In the following picture it can be evaluated if they lock at the vehicle rest position or before the vehicle has reached zero speed.

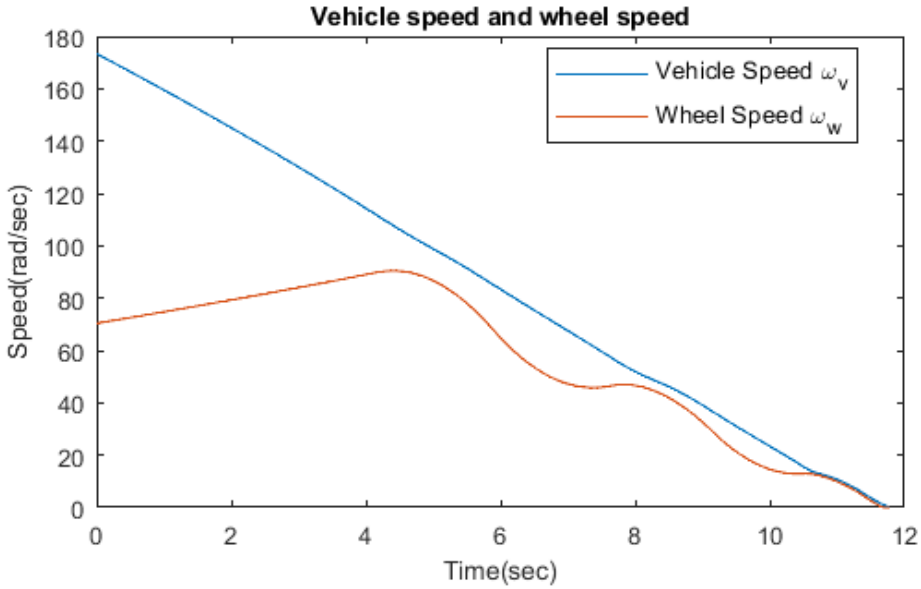

Figure 73: Vehicle speed and wheel speed with ABS

According to the *Figure 73* reported here, it can be stated that the vehicle will not reach an unstable condition, since the wheel speed and the vehicle speed reach the rest position at the same time, that is around 12 seconds of simulation time. The

locking of the wheels in this case is reached when the vehicle stops, as desired adopting the anti-lock system.

Lateral dynamic simulation

Before starting with the simulations of the lateral dynamics of the Pacci rover, it is necessary to study the lateral stability of the vehicle itself. The LTI system representing the drone has been designed in order to analyse the poles and zeros, the natural frequencies and all the variables that are involved in the study the lateral dynamic behaviour.

Starting from the equations of motion

$Hypothesis$:

$V = const;$

$\delta_r = 0;$

$$\begin{cases} \dot{\beta} = \left(\frac{-C_f - C_r}{mV}\right)\beta + \left(\frac{-C_f a + C_r b - mV^2}{mV^2}\right)\dot{\psi} + \frac{C_f \delta_f + C_r \delta_r}{mV} \\ \ddot{\psi} = \left(\frac{-C_f a + C_r b}{J_z}\right)\beta + \left(\frac{-C_f a^2 - C_r b^2}{J_z V}\right)\dot{\psi} + \frac{(C_f a)\delta_f - (C_r b)\delta_r}{J_z} \end{cases}$$

And knowing that the state space representation is of the type

$$\begin{cases} \dot{x} = Ax + Bu(t) \\ y = Cx + Du(t) \end{cases}$$

The states and inputs have been defined, as follows:

$$x = \begin{bmatrix} \beta \\ \dot{\psi} \end{bmatrix}$$

$$u(t) = \begin{bmatrix} \delta_f \\ \delta_r \end{bmatrix}$$

$$y = \begin{bmatrix} \beta \\ \dot{\psi} \\ \rho \\ \alpha_f \\ \alpha_r \\ a_y \end{bmatrix}$$

Where

$$\rho = \left(\frac{-C_r - C_f}{mV^2}\right)\beta + \left(\frac{-C_f a + C_r b}{mV^3}\right)\dot{\psi} + \frac{C_f \delta_f + C_r \delta_r}{mV^2}$$

$$\alpha_f = \delta_f - \beta - \frac{a}{V}\dot{\psi}$$

$$\alpha_r = \delta_r - \beta + \frac{b}{V}\dot{\psi}$$

$$a_y = V^2\rho = \left(\frac{-C_r - C_f}{m}\right)\beta + \left(\frac{-C_f a + C_r b}{mV}\right)\dot{\psi} + \frac{C_f \delta_f + C_r \delta_r}{m}$$

It is possible to obtain the following matrices A, B, C and D which are necessary for the study of the stability of the vehicle.

$$A = \begin{bmatrix} \frac{-C_f - C_r}{mV} & \frac{-C_f a + C_r b - mV^2}{mV^2} \\ \frac{-C_f a + C_r b}{J_z} & \frac{-C_f a^2 - C_r b^2}{J_z V} \end{bmatrix} \qquad B = \begin{bmatrix} \frac{C_f}{mV} & \frac{C_r}{mV} \\ \frac{C_f a}{J_z} & \frac{-C_r b}{J_z} \end{bmatrix}$$

$$C = \begin{bmatrix} 1 & 0 \\ 0 & 1 \\ \frac{-C_r - C_f}{mV^2} & \frac{-C_f a + C_r b}{mV^3} \\ -1 & -\frac{a}{V} \\ -1 & \frac{b}{V} \\ \frac{-C_r - C_f}{m} & \frac{-C_f a + C_r b}{mV} \end{bmatrix} \qquad D = \begin{bmatrix} 0 & 0 \\ 0 & 0 \\ \frac{C_f}{mV^2} & \frac{C_r}{mV^2} \\ 1 & 0 \\ 0 & 1 \\ \frac{C_f}{m} & \frac{C_r}{m} \end{bmatrix}$$

It is interesting to outline how the trend of the variables of interest change according to the parameters that describe the distance of the centre of gravity with respect to front and rear axles. This length can be different according to the different loading conditions of the Pacci rover, in order to outline the different cornering behaviour some limit cases have been considered.

In the first case the Pacci rover has been considered unloaded, so that

$$m = 35\ kg;$$

$$l_f = l_r = 0.35\ m;$$

In the second case the Pacci rover has been considered loaded on the rear axle only, so that

$$m = 65\ kg;$$

$$l_f = 0.32\ m;$$

$$l_r = 0.38\ m;$$

In the third case the Pacci rover has been considered loaded on the front axle only, so that

$$m = 65\ kg;$$

$$l_f = 0.38\ m;$$

$$l_r = 0.32\ m;$$

As the following study will underline, the cornering behaviour of the vehicle will change according to this loading conditions.

In all these cases, the front steering angle has been imposed equal to 1 degree, so that the different gains can be easily computed.

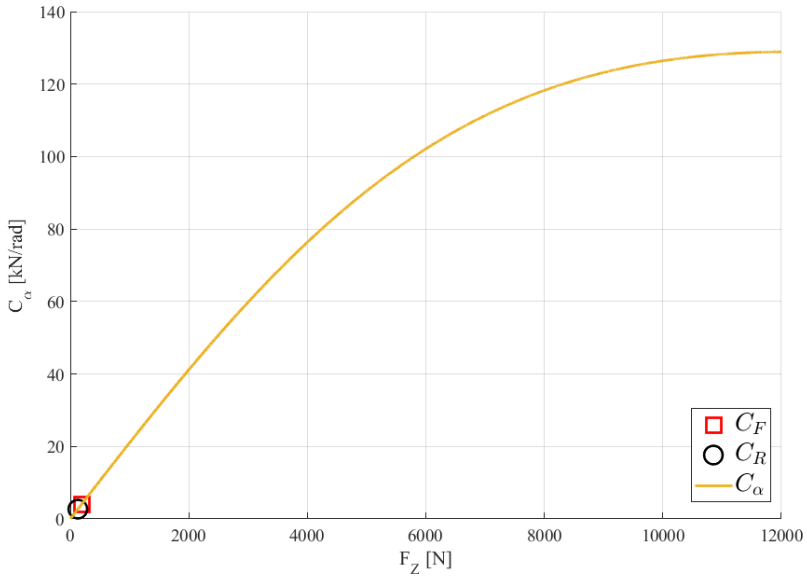

Figure 74: Cornering stiffness vs normal load

According to the different cases that have been studied, the cornering stiffnesses on front and rear axles change as well, in the following *Table 14* all their values are reported:

		C_F	C_R
Case 1	$l_f = l_r = 0.35\ m$	3629.09 N/rad	3629.09 N/rad
Case 2	$l_f = 0.32\ m$ $l_r = 0.38\ m$	7316.57 N/rad	6161.64 N/rad
Case 3	$l_f = 0.38\ m$ $l_r = 0.32\ m$	6161.64 N/rad	7316.57 N/rad

Table 14: Cornering stiffnesses of front and rear axles for different loading conditions

From these data it is possible also to compute the understeering coefficient, the results are reported in the following *Table 15*:

		K	
Case 1	$l_f = l_r = 0.35\ m$	0	rad/(m/s^2)
Case 2	$l_f = 0.32\ m$ $l_r = 0.38\ m$	2.5219e-07	rad/(m/s^2)
Case 3	$l_f = 0.38\ m$ $l_r = 0.32\ m$	-2.5219e-07	rad/(m/s^2)

Table 15: Understeering coefficient for different loading conditions

It is possible to notice that in the first case the Pacci rover has a neutral cornering behaviour, in the second case it has an understeering cornering behaviour and in the third case it has an oversteering cornering behaviour.

A clear understanding of what happens in these three cases is provided by the trend of the curvature gain, as reported in the following plot. In blue the neutral steering case is reported, in green the understeering case and in red the oversteering case.

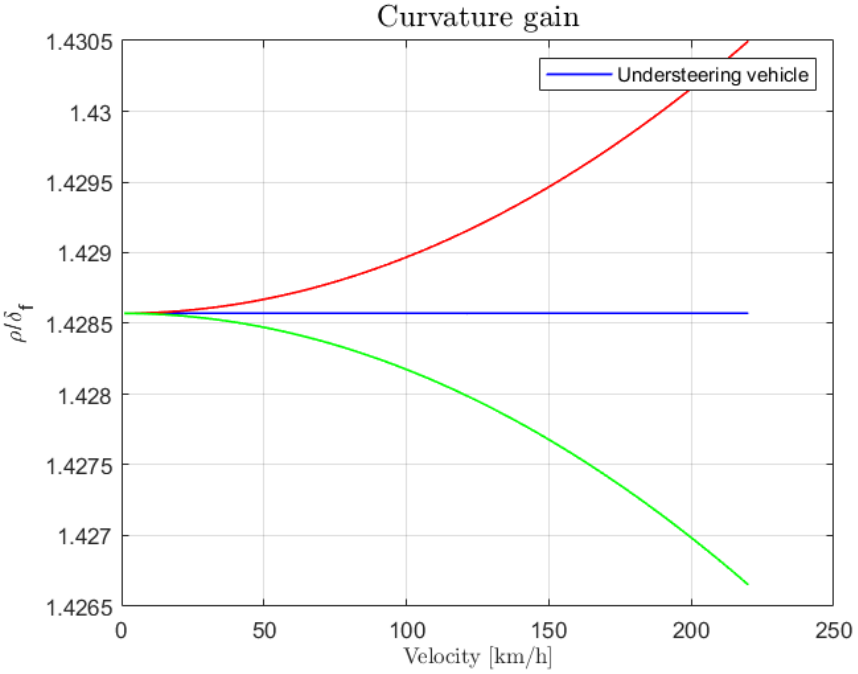

Figure 75: Curvature gain

It can be noticed that even for a wide range of speed, the curvature gain will not undergo a significant variation, even more in the region of the speeds that are practicable for the Pacci drone; this means that even in a limit loading condition the rover will be slightly understeering or slightly oversteering, but practically it can be said that the vehicle remains neutral. This characteristics reveals to be positive for a vehicle of that dimensions, tall and narrow, which can easily be subjected to rollover.

For sake of completeness, also the side-slip angle gain and the yaw rate gain have been reported in the following *Figure 76* and *Figure 77*; the trends are quite similar and not easy to distinguish since the cornering behaviour does not change significantly among these cases. Looking at the side-slip angle gain plot, for ß = 0 it is possible to individuate the speed at which the Pacci rover will be perfectly tangent to the trajectory, for all the three cases this speed is around 30 km/h, and more precisely

		$V_{\beta=0}$	
Case 1	$l_f = l_r = 0.35\ m$	30.67	m/s
Case 2	$l_f = 0.32\ m$ $l_r = 0.38\ m$	31.96	m/s
Case 3	$l_f = 0.38\ m$ $l_r = 0.32\ m$	29.32	m/s

Table 16: Speeds for which side-slip is null in different loading conditions

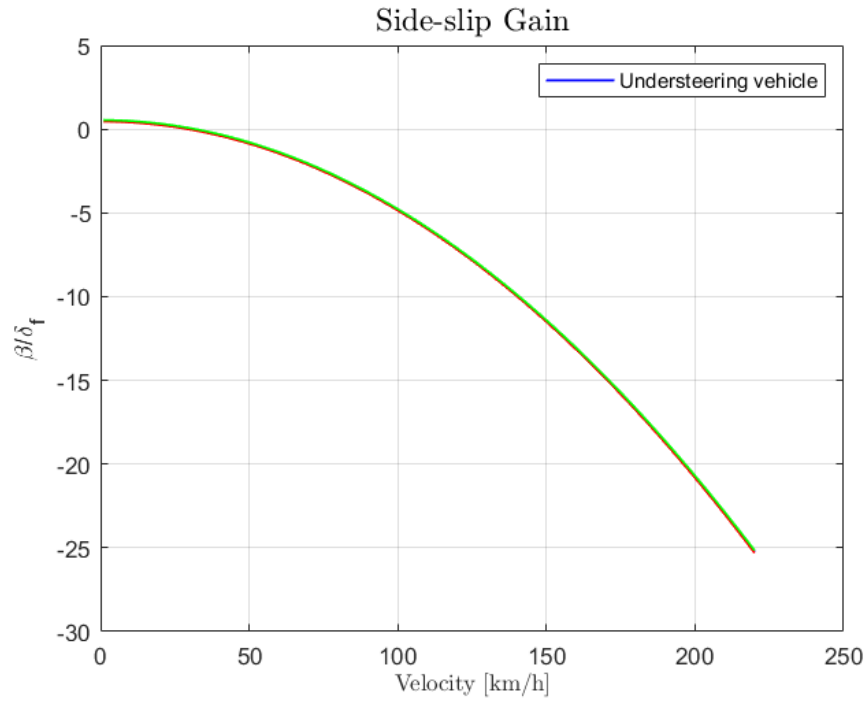

Figure 76: Side-slip gain

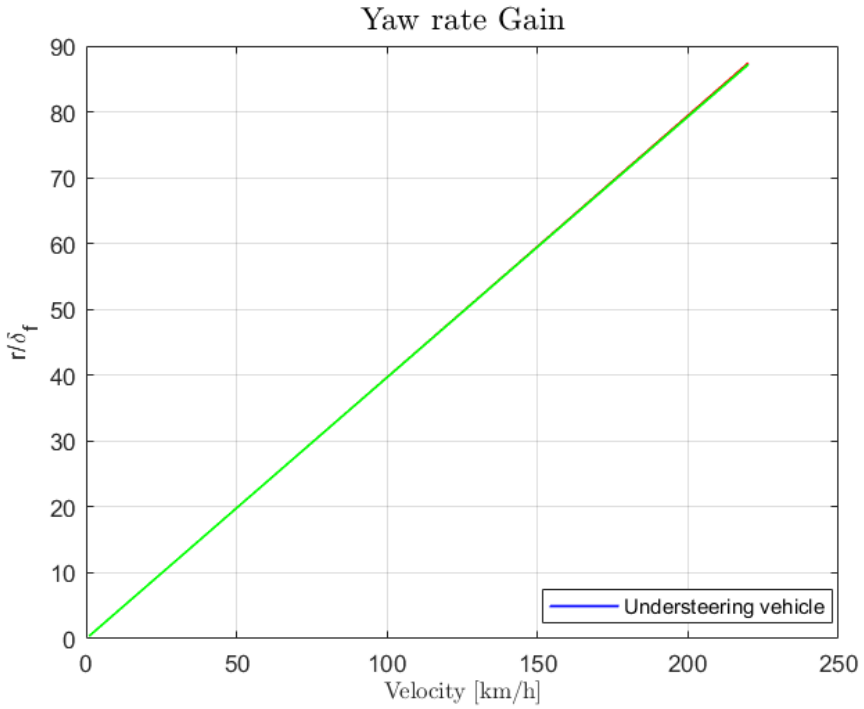

Figure 77: Yaw rate gain

For all these cases, the modal analyses have been carried out in order to study the stability of the Pacci rover. In the following there will be reported the natural frequencies, the damping ratios and poles.

Case 1: neutral steering behaviour

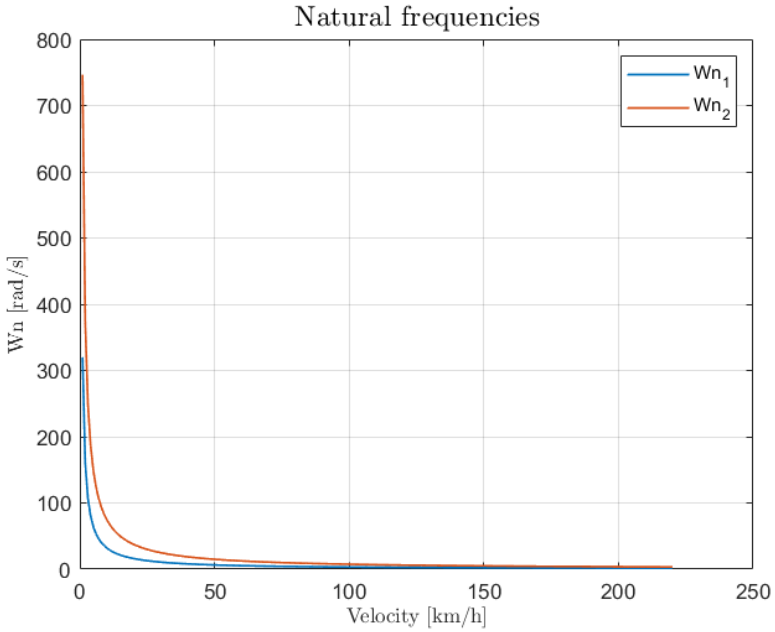

Figure 78: Natural frequencies of the neutral steering case

It can be noticed, here, that the vehicle is overdamped.

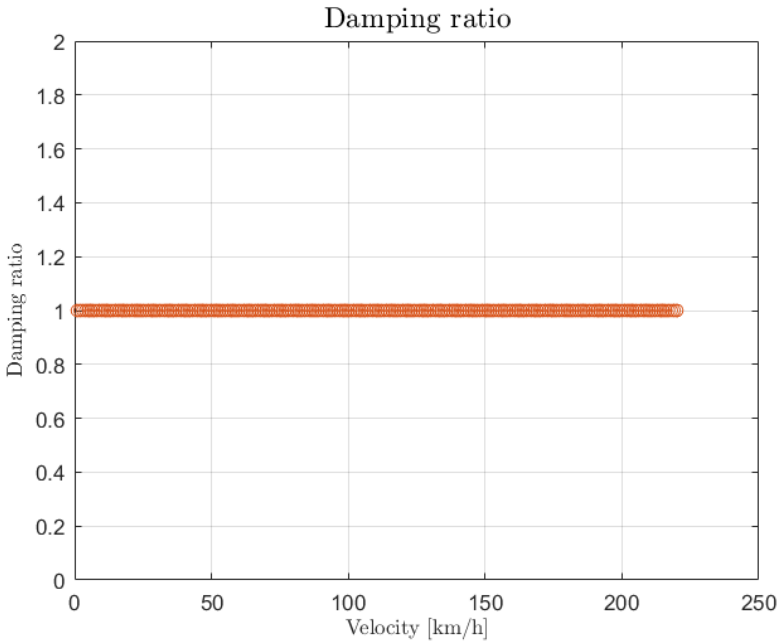

Figure 79: Damping ratio of neutral steering case

Here it can be noticed how the damping coefficient of the Pacci rover is equal to the optimal one.

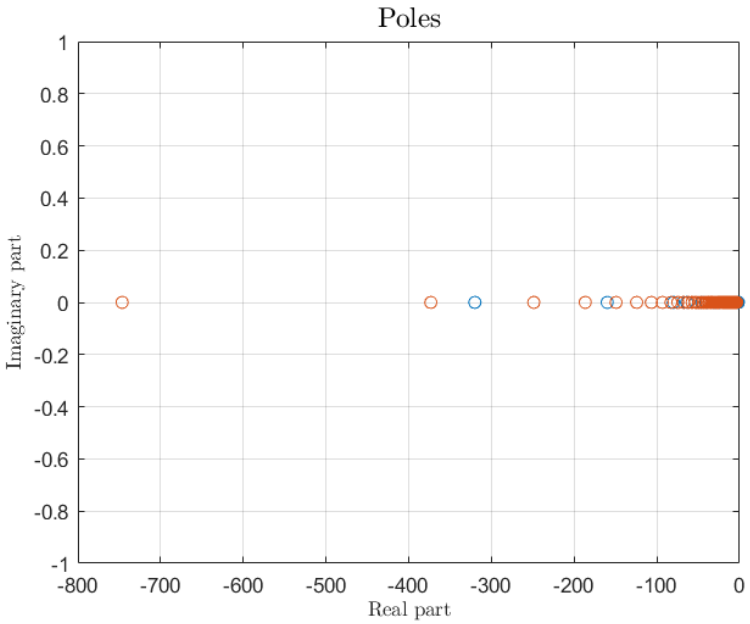

Figure 80: Poles of neutral steering case

From this latter plot, it can be seen that the eigenvalues of the matrix A, defined for the state space representation, have negative real part, so the result of this analyses is that the system is stable.

Case 2: understeering behaviour

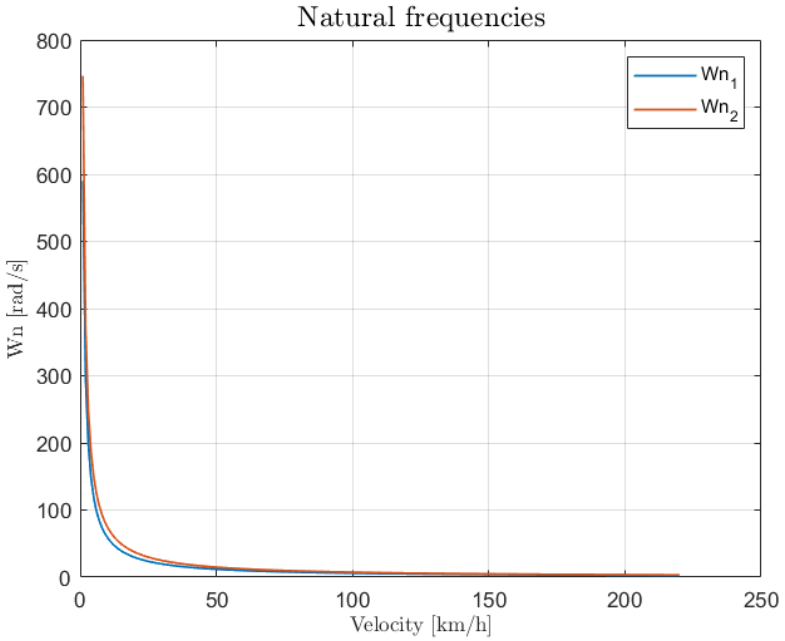

Figure 81: Natural frequencies of understeering case

Also in this case the system is overdamped.

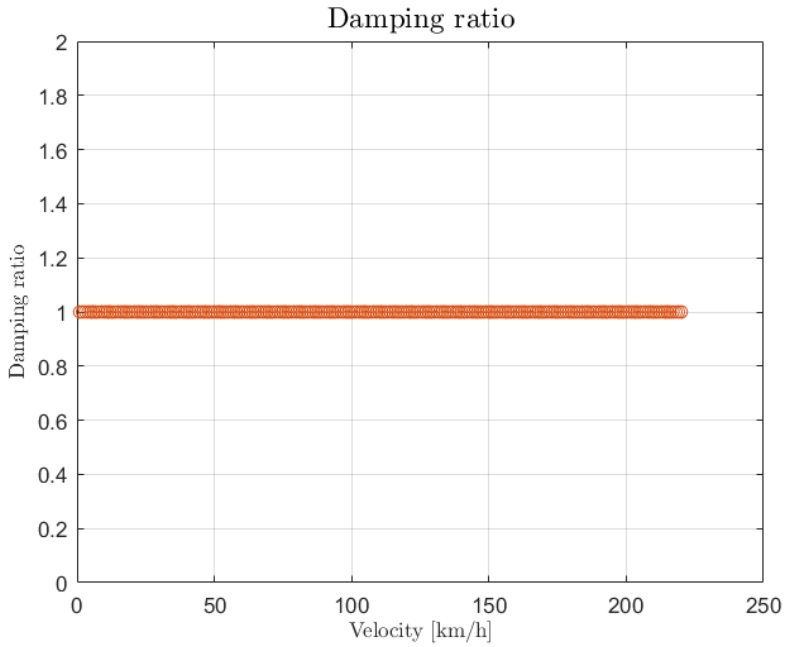

Figure 82: Damping ratio of understeering case

Here it can be noticed how the damping coefficient of the Pacci rover is equal to the optimal one.

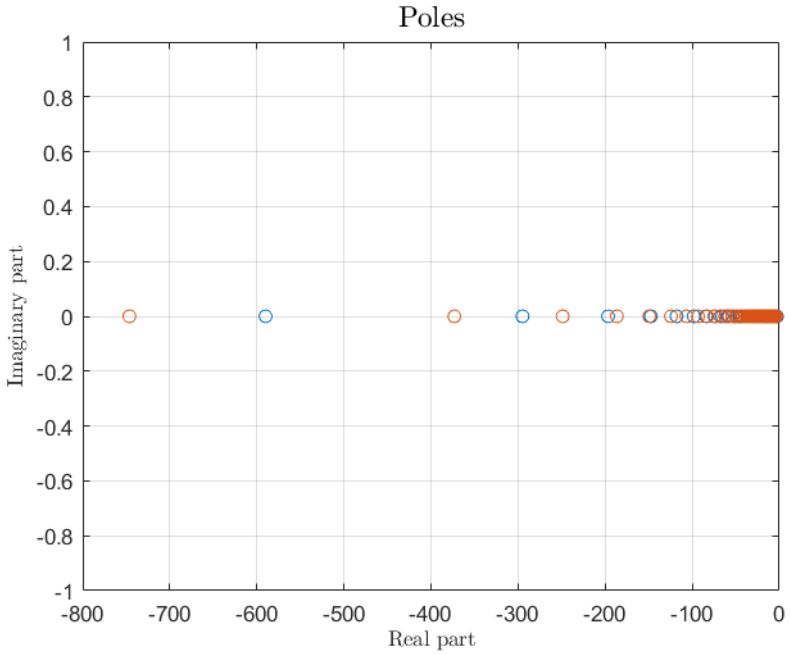

Figure 83: Poles of understeering case

From this latter plot it can be seen that the eigenvalues of the matrix A, defined for the state space representation, have negative real part, so the result of this analyses is that the system is stable.

Case 3: oversteering behaviour

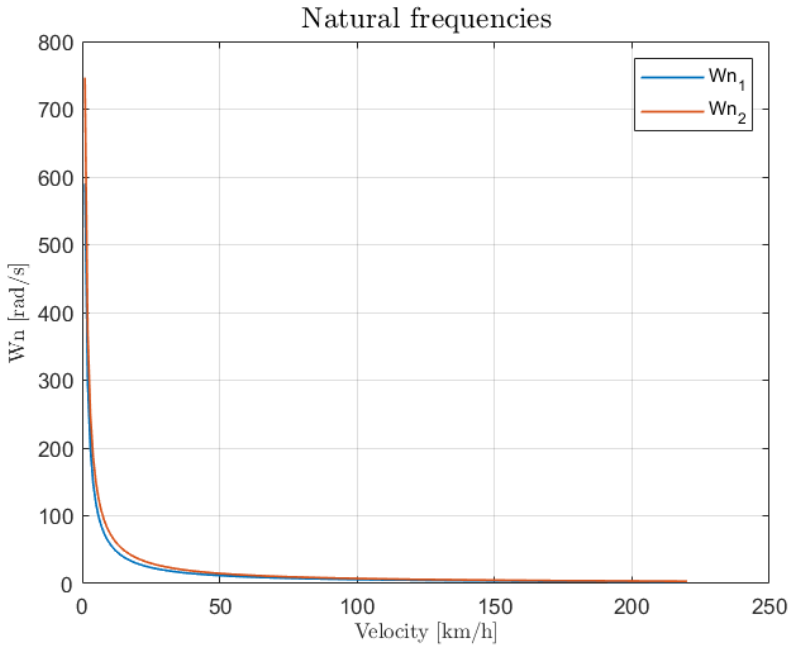

Figure 84: Natural frequencies of the oversteering case

Also in this case the system is overdamped.

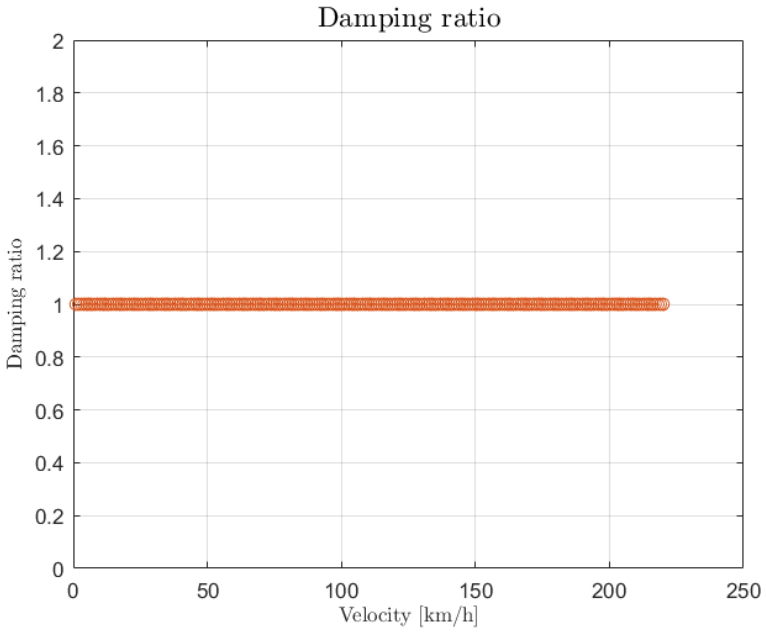

Figure 85: Damping ratio of oversteering case

Here it can be noticed how the damping coefficient of the Pacci rover is equal to the optimal one.

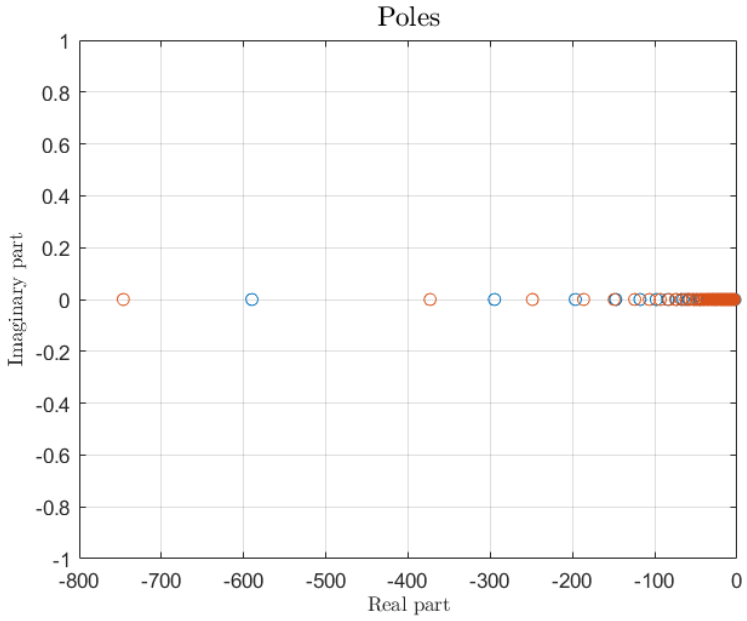

Figure 86: Poles of oversteering case

From this latter plot it can be seen that the eigenvalues of the matrix A, defined for the state space representation, have negative real part, so the result of this analyses is that the system is stable.

In *Figures 87, 88* and *89* the Bode plot reporting the magnitude and phase of the transfer function of lateral acceleration over the steering angle for the three cases is reported.

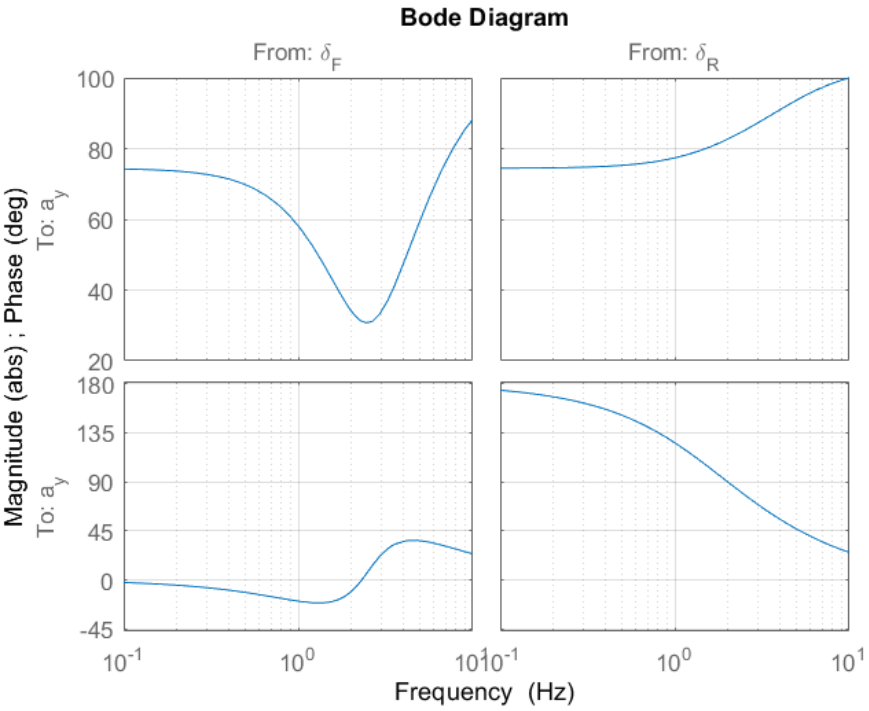

Figure 87: Bode diagram of neutral steering case @ V=26 km/h

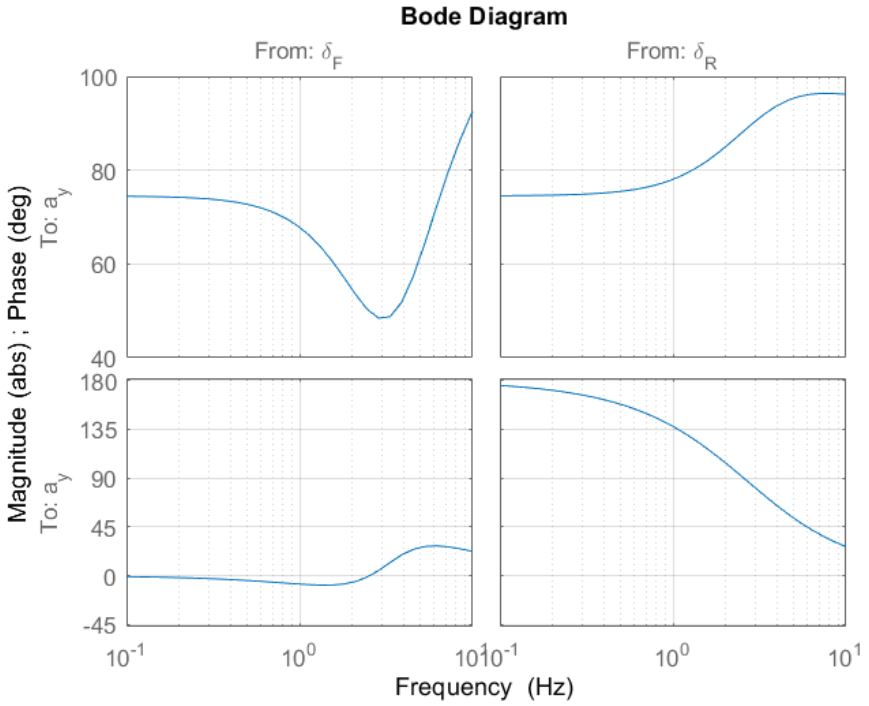

Figure 88: Bode diagram of understeering case @ V=26 km/h

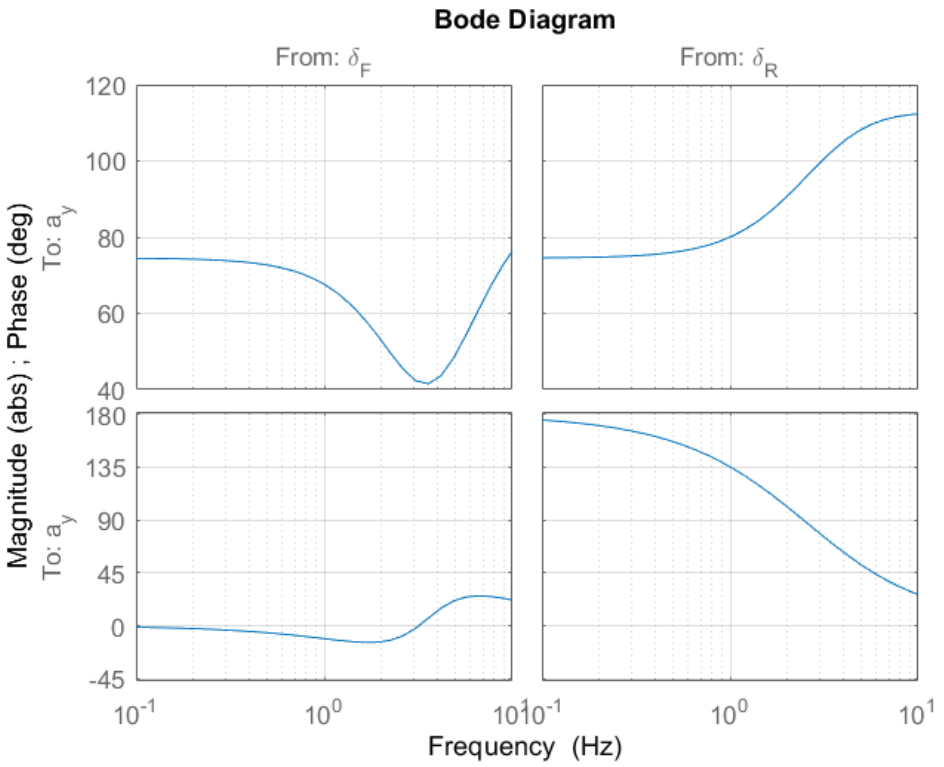

Figure 89: Bode diagram of oversteering case @ V=26 km/h

These diagrams have been evaluated for the maximum reachable speed of the rover at full load, that is equal to 26 km/h. The trends are quite similar, what is noteworthy to outline is the trough of the magnitude between 1 Hz and 10 Hz; this one has an increasing value in the order that goes from the neutral case, to oversteering and to understeering case.

Cornering simulations: step steering and ramp steering manoeuvres

Two cornering manoeuvres have been introduced in order to test the behaviour of the rover even under dynamic conditions; these two manoeuvres are step steering and ramp steering, they have been performed for all the three cases and for increasing amounts of steering angles and speeds. The most significant results will be presented.

Step steer ($\delta_f = 15\ deg; V = 30km/h$):

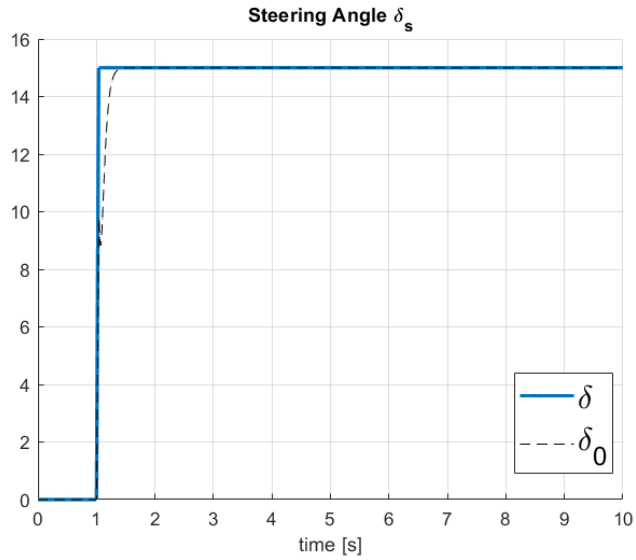

Figure 90: Front steering angle for step steer

Neutral vehicle case:

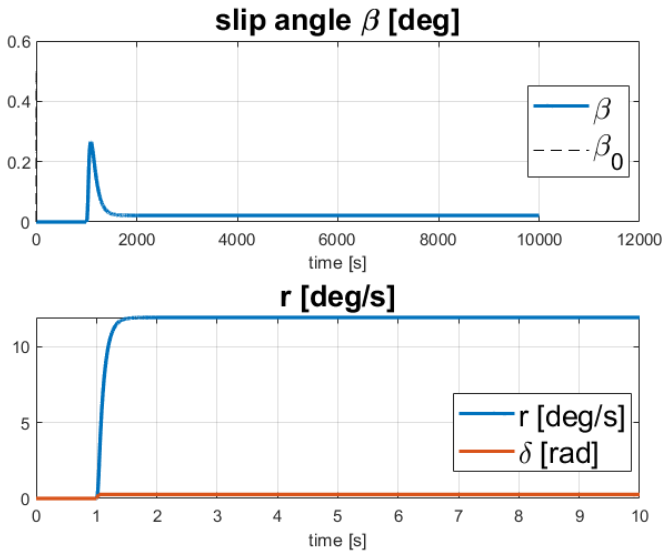

Figure 91: States of neutral vehicle performing step steering manoeuvre at 30km/h

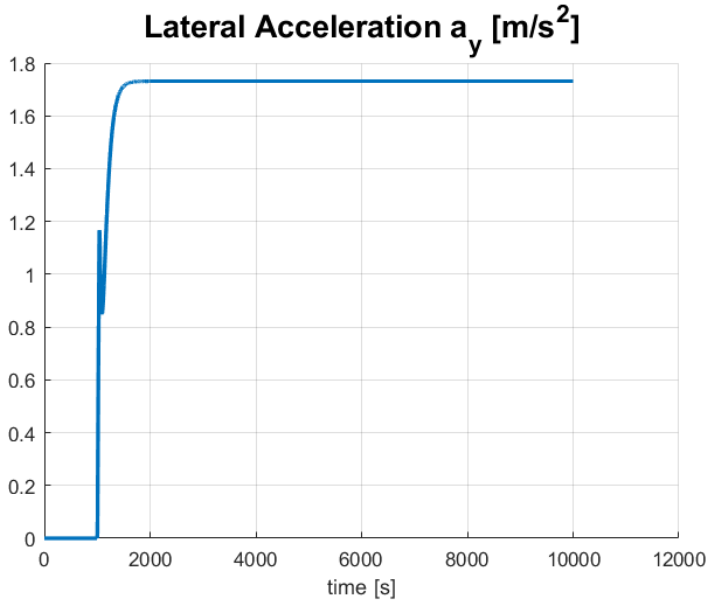

Figure 92: Lateral acceleration of neutral vehicle performing step steering manoeuvre at 30km/h

Understeering vehicle case:

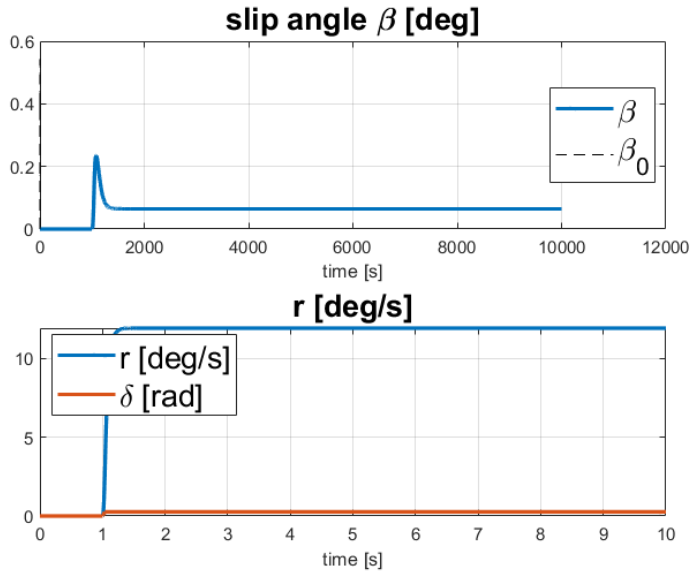

Figure 93: States of understeering vehicle performing step steering manoeuvre at 30km/h

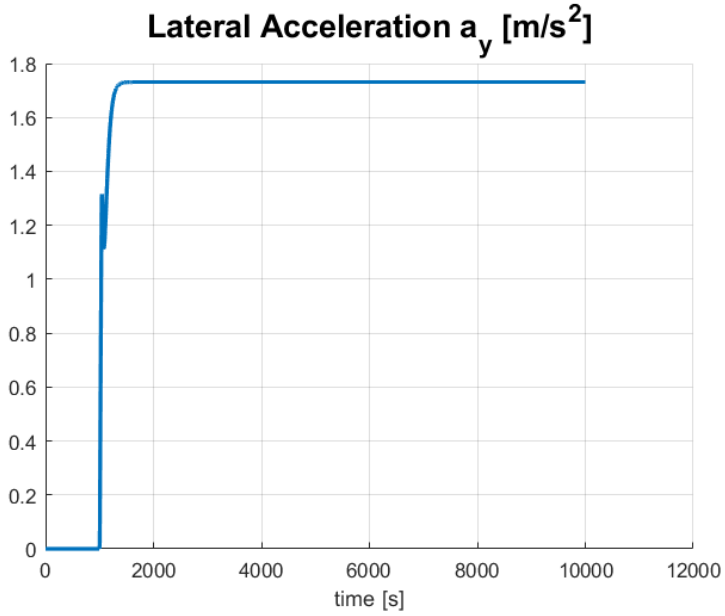

Figure 94: Lateral acceleration of understeering vehicle performing step steering manoeuvre at 30km/h

Oversteering vehicle case:

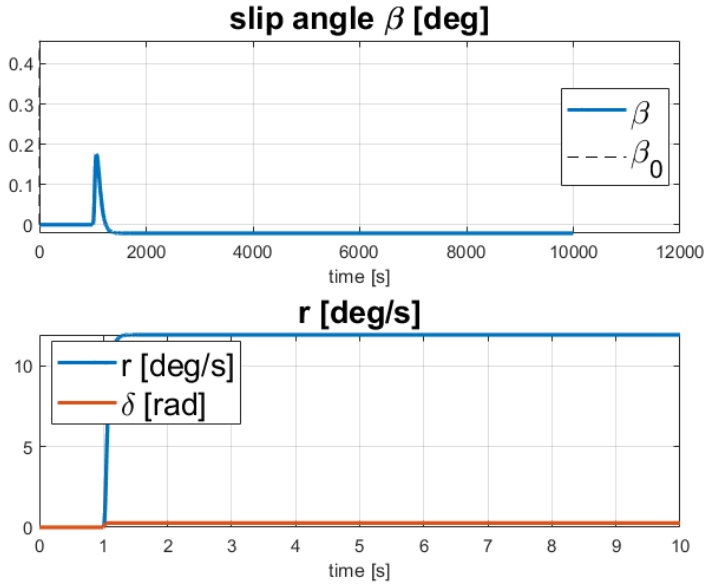

Figure 95: States of oversteering vehicle performing step steering manoeuvre at 30km/h

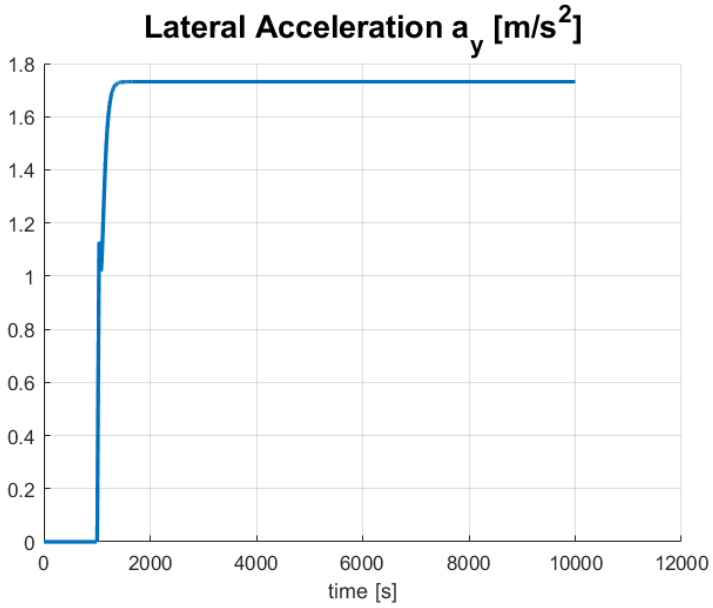

Figure 96: Lateral acceleration of oversteering vehicle performing step steering manoeuvre at 30km/h

What can be noticed among these three cases is that the trends do not change significantly: the side slip shows a peak which reaches about 0.2 degrees as the steering manoeuvre starts, the yaw rate settles around 12 deg/s and lateral accelerations reach a maximum value around 1,7 m/s^2.

In the following figures the path traced by the vehicle in the three different configurations is reported.

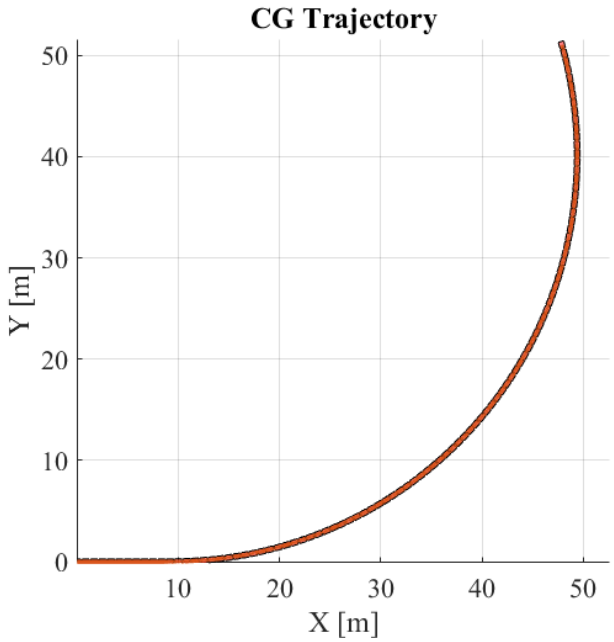

Figure 97: Trajectory of neutral steering vehicle performing step steering manoeuvre

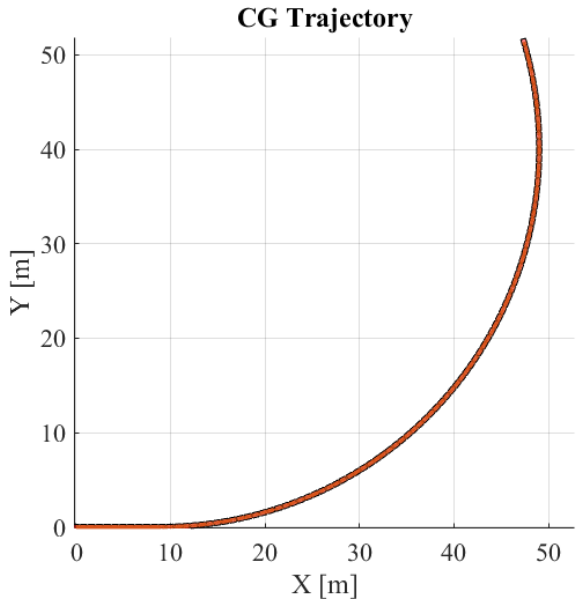

Figure 98: Trajectory of understeering vehicle performing step steering manoeuvre

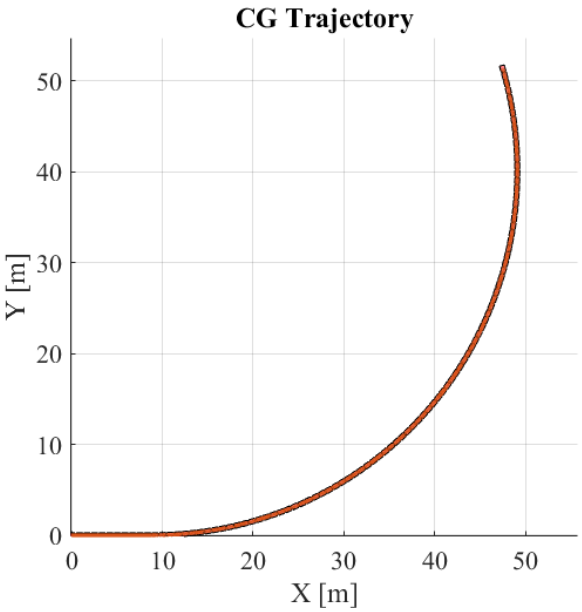

Figure 99: Trajectory of oversteering vehicle performing step steering manoeuvre

As expected by the analyses of the states and lateral accelerations, the trajectory can be considered the same for all the three cases, this as a remark of the fact that the vehicle can be considered practically neutral in all these loading conditions.

Ramp steer @ 15 deg/s ($\delta_{f,max} = 45\ deg; V = 30km/h$):

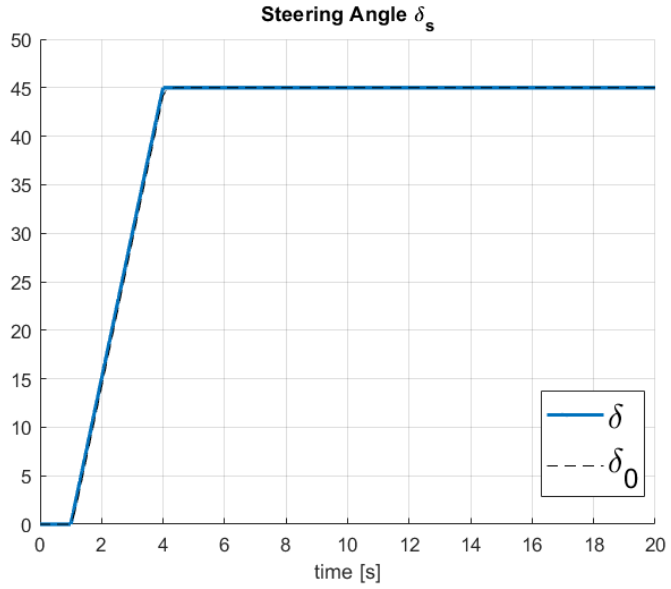

Figure 100: Front steering angle for ramp steer

Neutral vehicle:

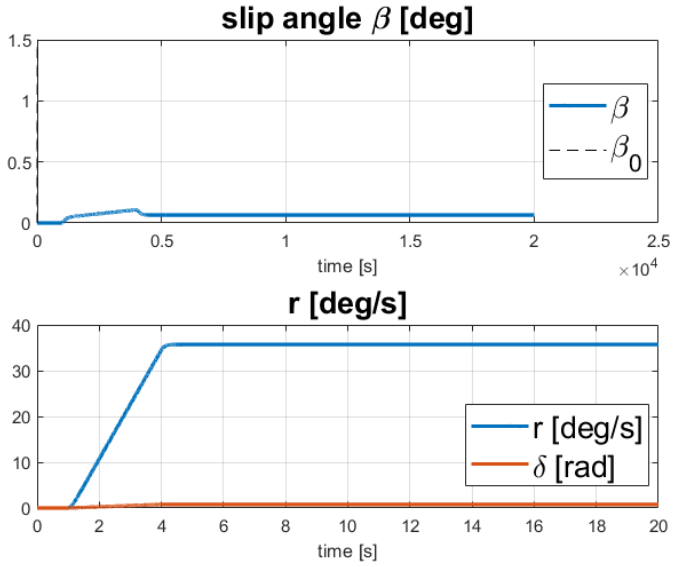

Figure 101: States of neutral steering vehicle performing ramp steering manoeuvre at 30km/h

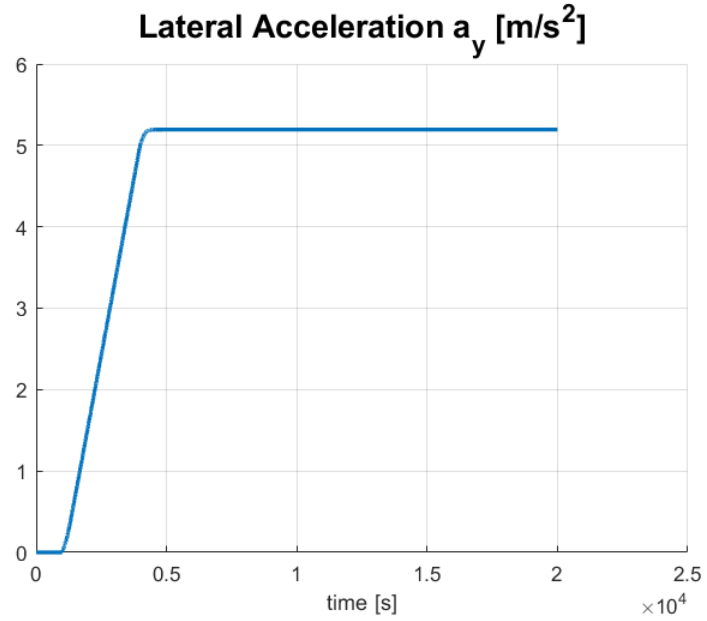

Figure 102: Lateral acceleration of neutral steering vehicle performing ramp steering manoeuvre at 30km/h

Understeering vehicle:

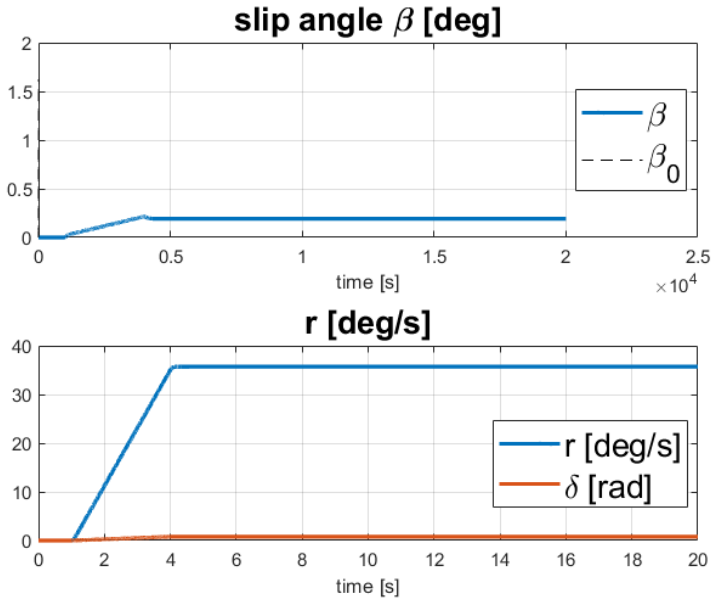

Figure 103: States of understeering vehicle performing ramp steering manoeuvre at 30km/h

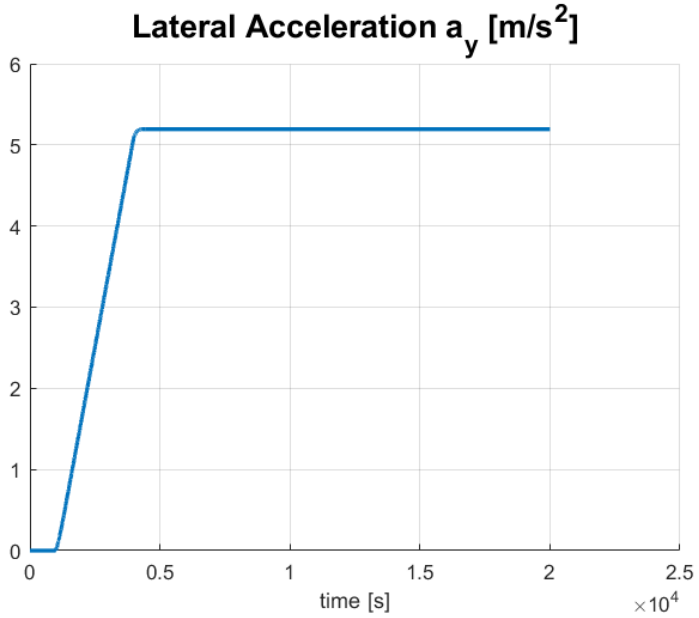

Figure 104: Lateral acceleration of understeering vehicle performing ramp steering manoeuvre at 30km/h

Oversteering vehicle:

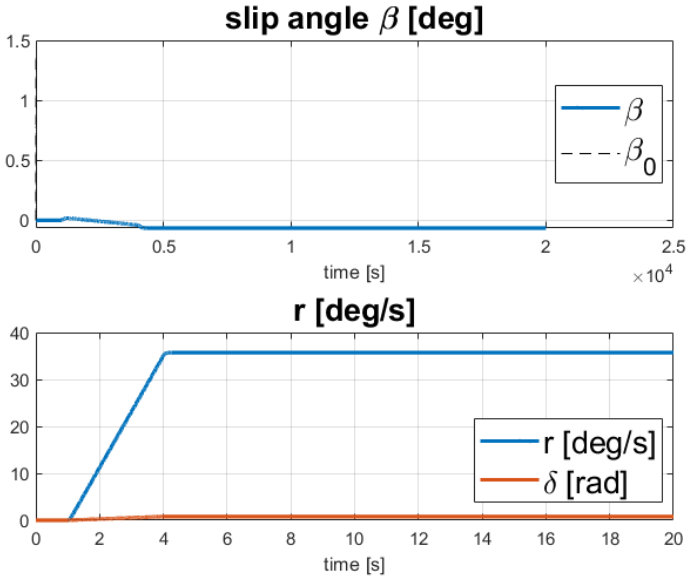

Figure 105: States of oversteering vehicle performing ramp steering manoeuvre at 30km/h

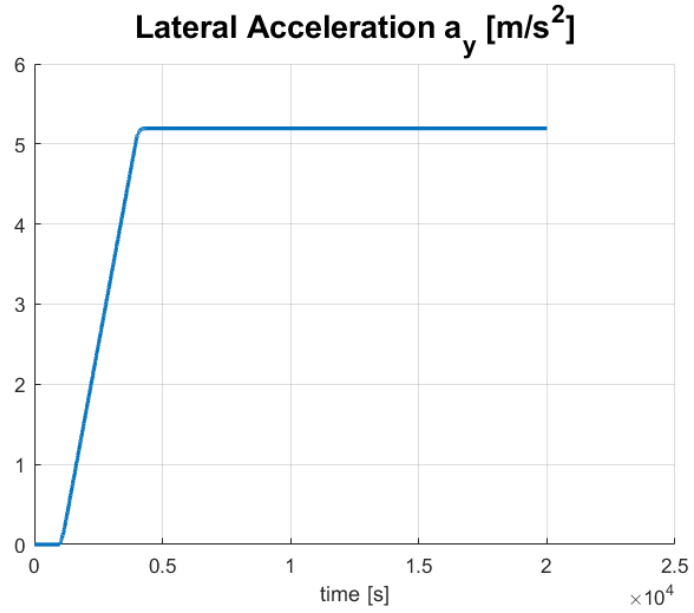

Figure 106: Lateral acceleration of oversteering vehicle performing ramp steering manoeuvre at 30km/h

What can be noticed among these three cases is that the trends do not change significantly: the side slip shows an almost flat trend, the yaw rate settles around 35 deg/s and lateral acceleration reaches a maximum value around 5 m/s^2, which is a below the limit lateral acceleration due to rollover, in fact, it was around 7 m/s^2.

In the following figures the path traced by the vehicle in the three different configurations is reported.

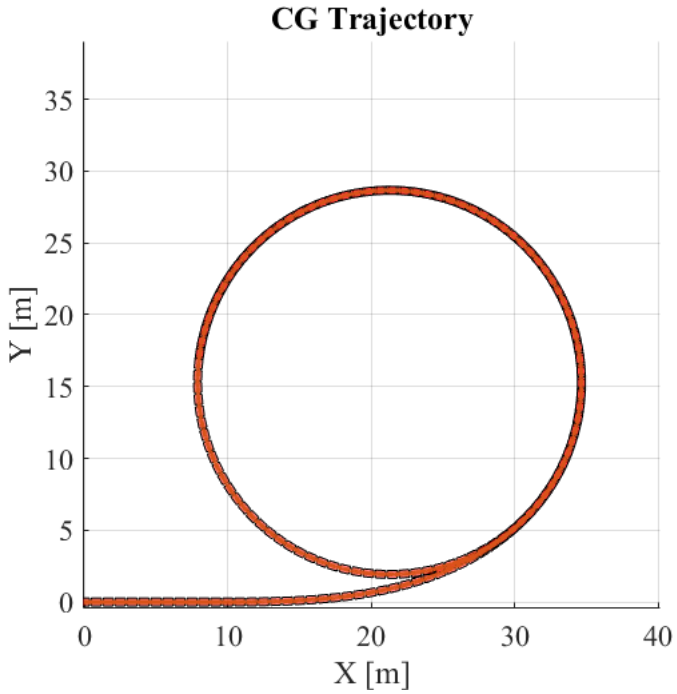

Figure 107: Trajectory of neutral steering vehicle performing ramp steering manoeuvre

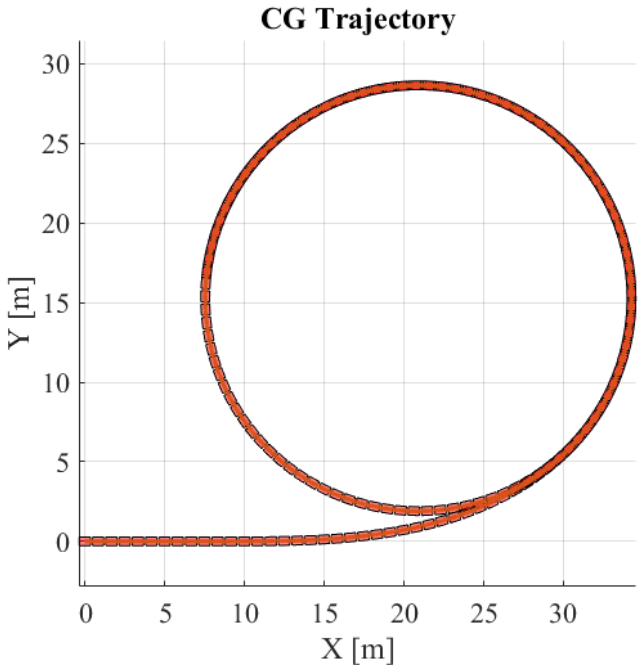

Figure 108: Trajectory of understeering vehicle performing ramp steering manoeuvre

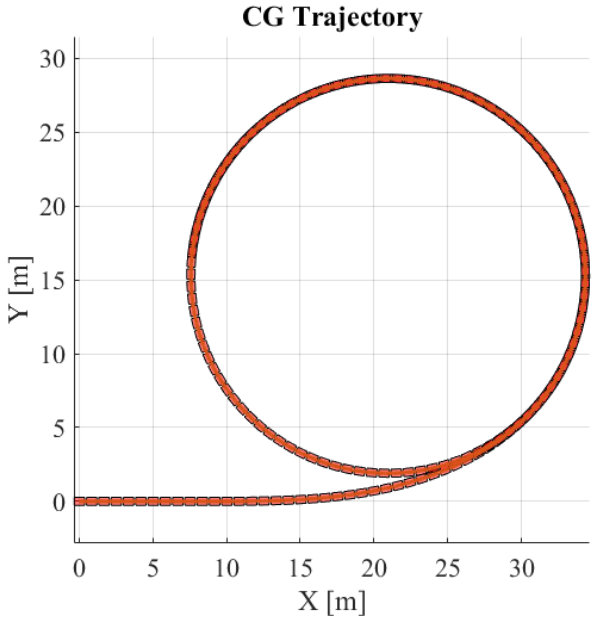

Figure 109: Trajectory of oversteering vehicle performing ramp steering manoeuvre

Comparing these results with the ones from the simulation of the step-steer, it is possible to notice how the trends of the variables of sideslip, yaw rate and lateral acceleration are smoother. What results from these two cornering simulations is that the vehicle is very responsive to any kind of input: more aggressive or more gradual; it is able to face these two situations without losing stability, increasing its robustness and reliability, which are two key factors to accomplish the mission of delivery in a mixed scenario.

Cornering behaviour simulation (4WS)

The manoeuvres proposed above have a certain level of simplification with respect to the real case of the Pacci rover, in fact, what has been neglected, in order to carry out the preceding analyses, was that fact that rear wheels can steer, too.

For this purpose, a sinusoidal manoeuvre has been proposed with the implementation of 4-wheel-steering mechanism, the non-linear equations of motions will be reported in the following.

Definition of the states:

$$x = \begin{Bmatrix} x \\ y \\ \psi \\ v \\ \beta \\ \dot{\psi} \end{Bmatrix}$$

Equations:

$$\dot{x_1} = v \cdot \cos(\psi + \beta)$$

$$\dot{x_2} = v \cdot \sin(\psi + \beta)$$

$$\dot{x_3} = \dot{\psi}$$

$$\dot{x_4} = \frac{F_{x,f}cos(\beta - \delta_F) + F_{x,r}cos(\beta - \delta_R) + F_{x,f}cos(\beta - \delta_F) + F_{x,r}cos(\beta - \delta_R)}{m_T}$$

$$\dot{x_5} = \frac{-F_{x,f}sin(\beta - \delta_F) - F_{x,r}sin(\beta - \delta_R) + F_{x,f}cos(\beta - \delta_F) + F_{x,r}cos(\beta - \delta_R) - m_T v\dot{\psi}}{m_T v}$$

$$\dot{x_6} = \frac{F_{x,f}asin\delta + F_{x,f}acos\delta - F_{x,r}b}{I_T}$$

Where

$$\alpha_F = arctan\left(\frac{v\ sin\beta + a\dot{\psi}}{v\ cos\beta}\right) - \delta_F$$

$$\alpha_R = arctan\left(\frac{v\ sin\beta - b\dot{\psi}}{v\ cos\beta}\right) - \delta_R$$

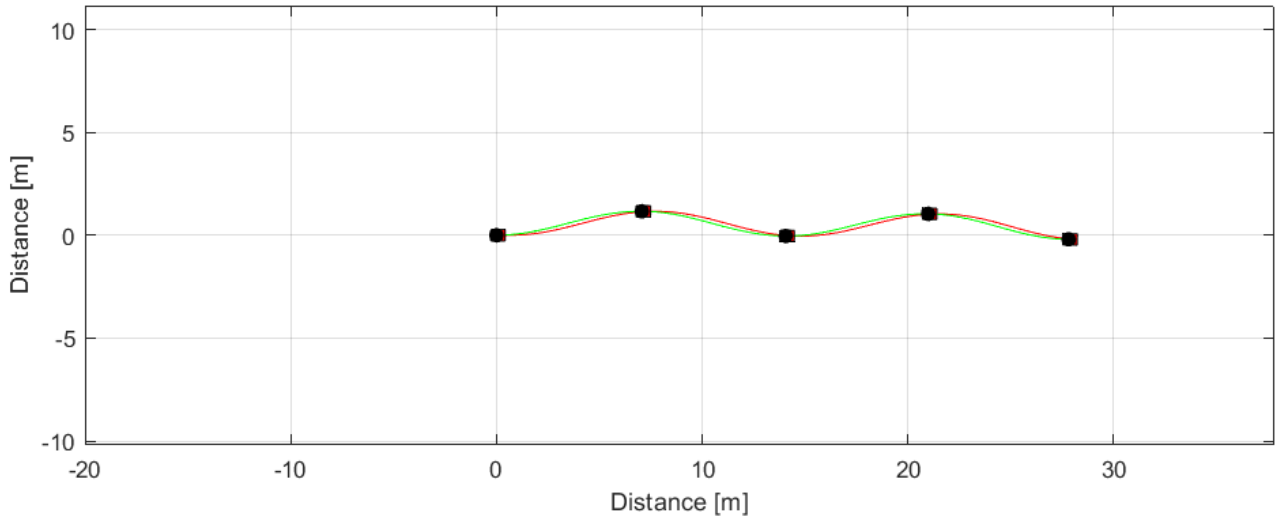

Figure 110: Sinusoidal trajectory of 4WS vehicle @ V=26 km/h

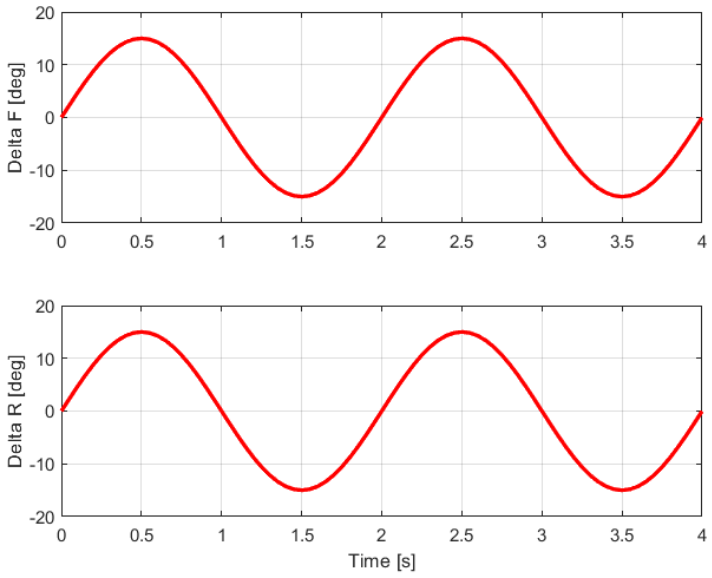

Figure 111: Sinusoidal input of front and rear steering angles

This simulation made possible to evaluate how the steering angles on front and rear wheels can work together in a ratio equal to 1:1 to follow the prescribed trajectory.

Control design: DSTP model implementation

Firstly, the initial conditions have been set up, in particular, it has been decided to test the Pacci drone at full load while running at its maximum speed, so that $v_{in} = const. = 26\frac{km}{h}$. All these initial conditions have been stored in a vector in which the first, the second and the third element are the variables X_0, Y_0 and Ψ_0, while the other three variables are $v_{x,0}$, $v_{y,0}$ and ω_0; the first of these latter has been set equal to the maximum speed of the drone, while the other two have been set equal to 0.

$$z_{e,0} = \begin{Bmatrix} X_0 \\ Y_0 \\ \Psi_0 \\ v_{x,0} \\ v_{y,0} \\ \omega_0 \end{Bmatrix}$$

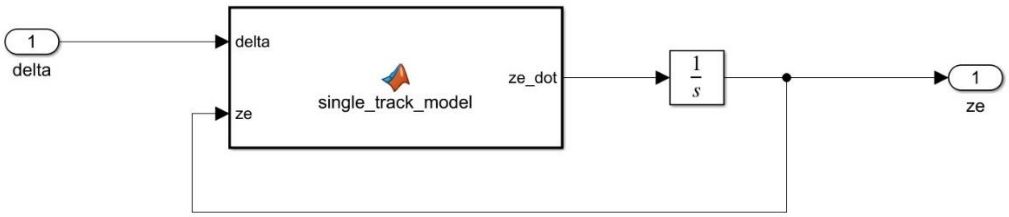

Figure 112: DST model implemented as a Matlab function

The dynamic model of the vehicle has been implemented by means of a MATLAB function in which the state vector z_e is obtained by means of integration of the output of the block which is the state derivative $\dot{z_e}$.

$$State\ vector \qquad z_e = \begin{Bmatrix} X \\ Y \\ \Psi \\ v_x \\ v_y \\ \omega \end{Bmatrix}$$

The state equations have been computed as:

$$\dot{X} = v_x \cos\Psi - v_y \sin\Psi$$

$$\dot{Y} = v_x \sin\Psi + v_y \cos\Psi$$

$$\dot{\Psi} = \omega$$

$$\dot{v_x} = v_y \omega$$

$$\dot{v_y} = -v_x \omega + \frac{2}{m}\left(F_{y,f} + F_{y,r}\right)$$

$$\dot{\omega} = \frac{2}{J}\left(l_f F_{y,f} - l_r F_{y,r}\right)$$

Here, the forces in the equation above have been evaluated by means of the Pacejka Magic Formula.

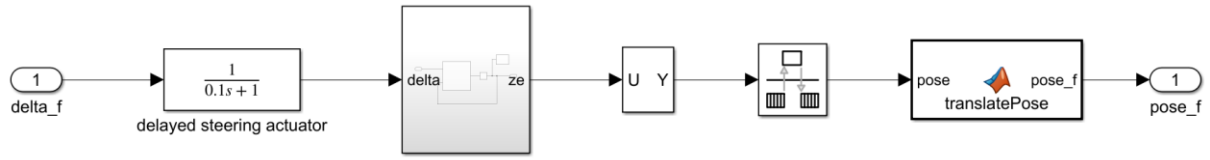

Figure 113: Simulink blocks accounting for the delay between command and actuation

In *Figure 113* it can be noticed that some additional blocks have been inserted in order to take into account a certain delay of the actuator devoted to steering, this is done in order to have a simulation as close as possible to reality; then the first three variables coming from the vehicle model are extracted which constitute the reference variables of the vehicle X, Y, Ψ; another MATLAB function is added to move these points from the CoG to the midpoint of the front axle, where the heading and cross-track error will be computed and then brought in a feedback loop, to compare them to the reference trajectory. This latter has been provided as input to the system, according to which different tests have been carried out.

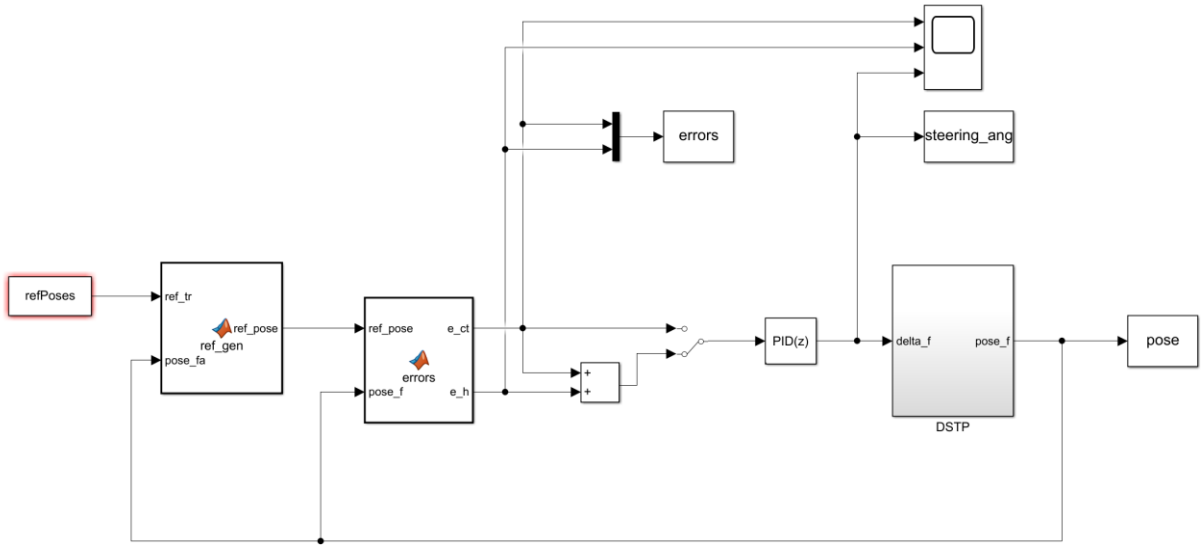

Figure 114: Simulink model of Pacci rover and PID controller

The following block is a MATLAB function in which a reference generator is created as the closest point of the vehicle to the reference trajectory; then, the cross-track and the heading errors have been computed and they are the ones on which the PID controller works, with the aim of minimizing them. The control variable is the steering angle that must be adjusted according to the heading and cross-track errors and it is provided to the vehicle system as output of the controller block. In order to obtain satisfactory results, the controller has been tuned by means of the MATLAB/Simulink tool, adjusting the response time and the transient behaviour of the signals.

Sinusoidal trajectory simulation

As first simulation, it has been chosen a sinusoidal trajectory of amplitude equal to few metres (*Figure 59*); this has been done in order to simulate a slalom path and verify the control dynamics of the Pacci drone.

By means of the tuner tool of MATLAB, the parameters of the PID controller have been set as the best behaviour that can be obtained.

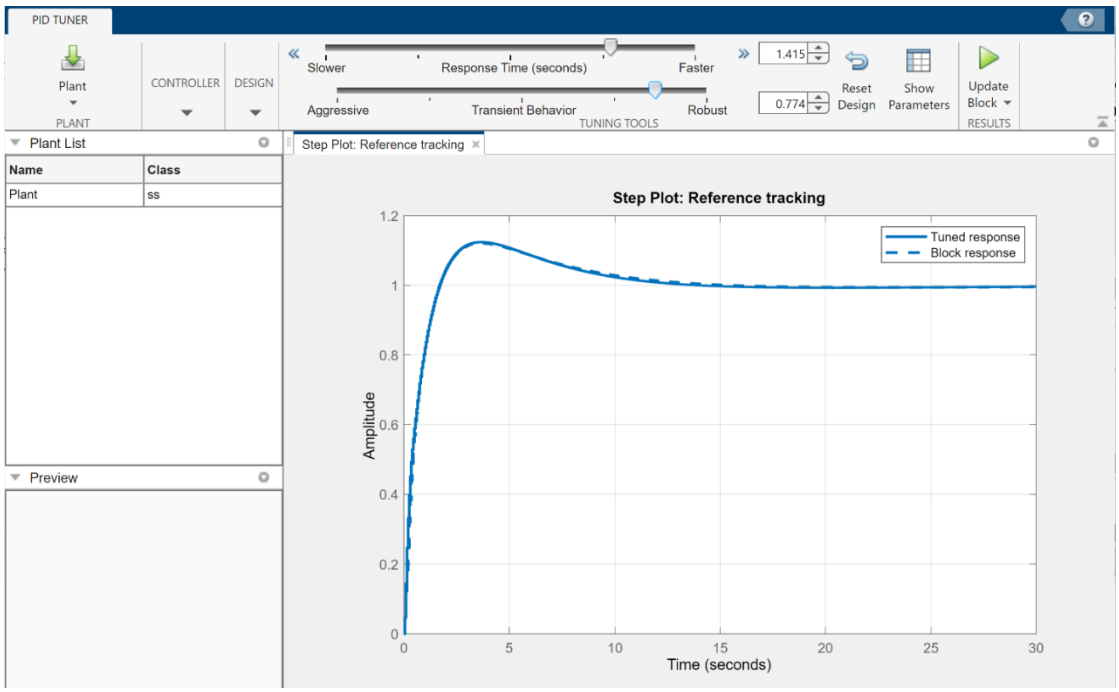

Figure 115: PID tuner tool by Simulink - Matlab

The parameters of the controller are reported in the *Table 17* below.

PIDF tuning	P	I	D
Value	0.0157	3.5095e-4	0.1557

Table 17: PID tuned parameters for sinusoidal manoeuvre

In the following *Figure 116* the cross-track and the heading errors of the Pacci drone are reported as results of the previous simulation, run with the tuned P, I, D parameters.

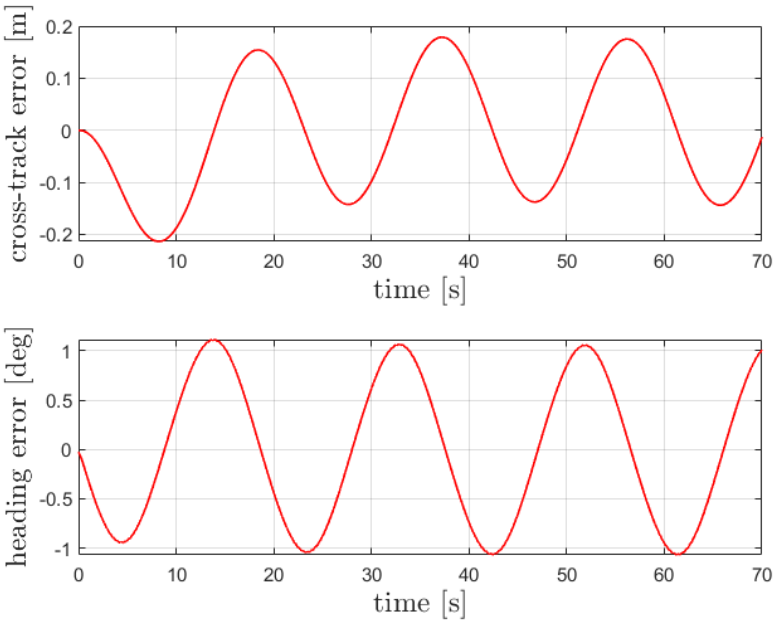

Figure 116: Cross-track and heading erors for sinusoidal manoeuvre

As can be noticed, these errors are quite small if compared to a situation in which a small vehicle is trying to avoid obstacles on its path, running at 20 km/h, an evidence of how the Pacci drone is following the reference trajectory is reported in the *Figure 119*.

As a further confirmation of the reliability of these simulations, the data of steering angle and lateral accelerations have been reported in the *Figure 117* and *Figure 118*. In particular, looking at lateral acceleration, this remains below the limit dictated by rollover, which means that the Pacci rover is able to travel on these trajectories without losing its stability.

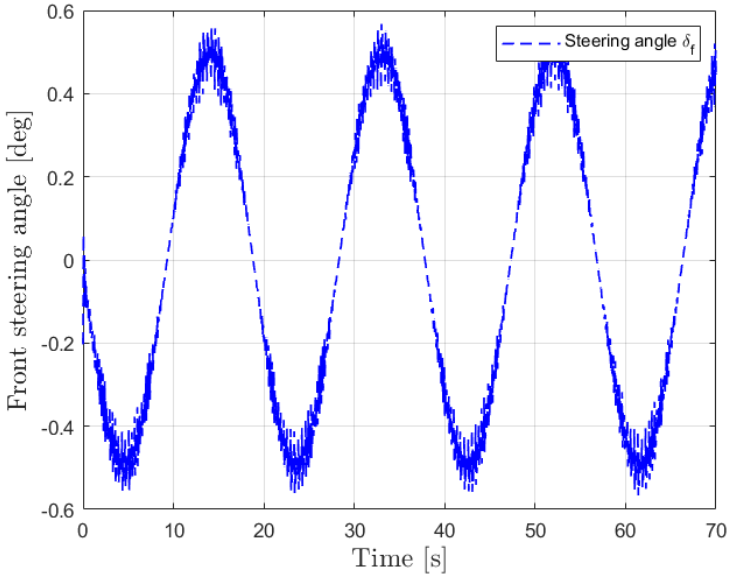

Figure 117: Front steering angle for sinusoidal manoeuvre @ V=20 km/h

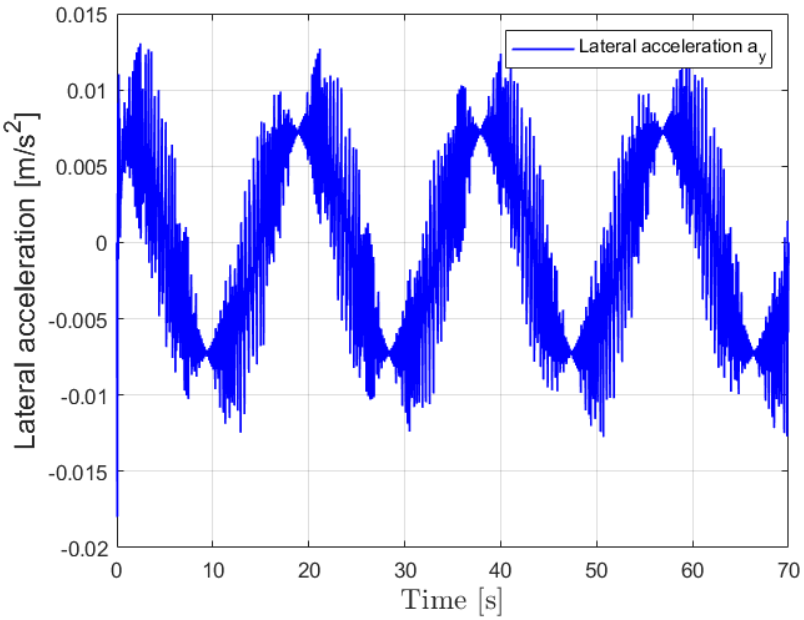

Figure 118: Lateral acceleration for sinusoidal manoeuvre @ V=20 km/h

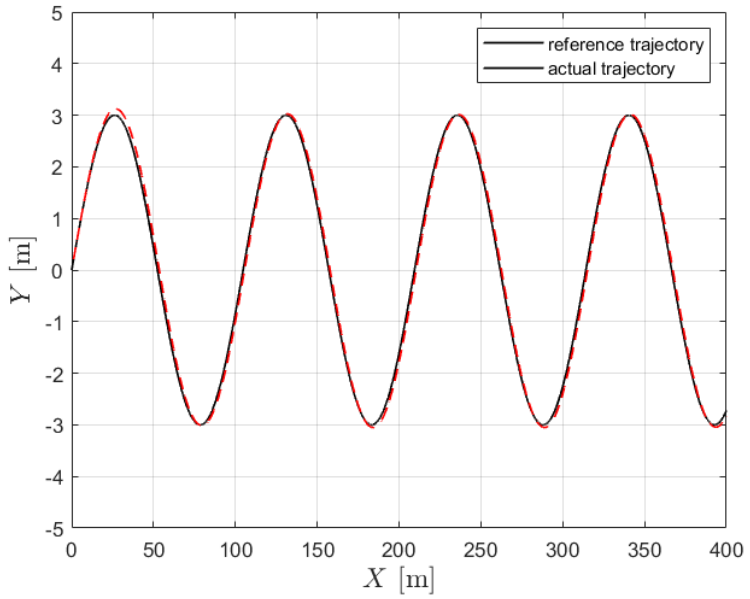

Figure 119: Reference trajectory vs actual trajectory in sinusoidal manoeuvre

Here with the black line is reported the reference trajectory, while with dashed red line is reported the actual trajectory that Pacci will follow. With a simple and not expensive controller as a PID, it is possible to obtain quite satisfactory results.

Double lane change simulation

The second simulation has been carried out with a more complex situation: a trajectory similar to a double lane change manoeuvre performed on a kind of bicycle lane.

The modelling phase remained unchanged, the building blocks of the Simulink environment, too apart from the reference trajectory and the controller.

As done for the previous simulation, the PID has been tuned with dedicated tool present in MATLAB/Simulink. The tuned PID parameters are reported in the *Table 18* below.

PIDF tuning	P	I	D
Value	0.0899	0.0040	0.2514

Table 18: PID tuned parameters for ISO double lane change manoeuvre

Once the reference trajectory has been displayed together with the path followed by the Pacci drone, as expected, the response is quite satisfactory, in fact, the drone, travelling at constant speed equal to 20 km/h is able to trace the reference manoeuvre, especially in the changes of direction.

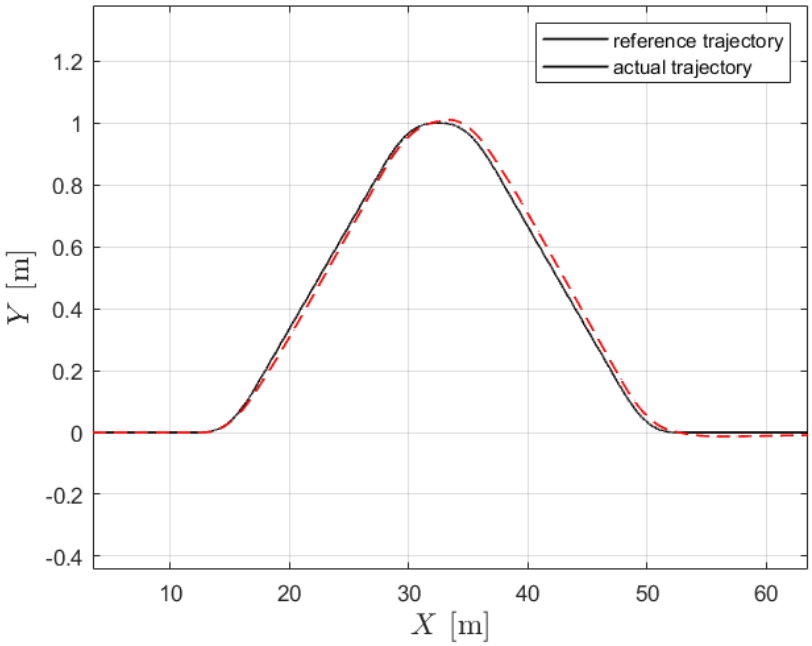

Figure 120: Reference vs actual trajectory in ISO double lane change manoeuvre

Also in this case, it is possible to notice that the heading and cross track errors are quite small and acceptable: the cross track error reaches a maximum of 0,04 m in absolute value, while the heading error registers a maximum of about 1 degree.

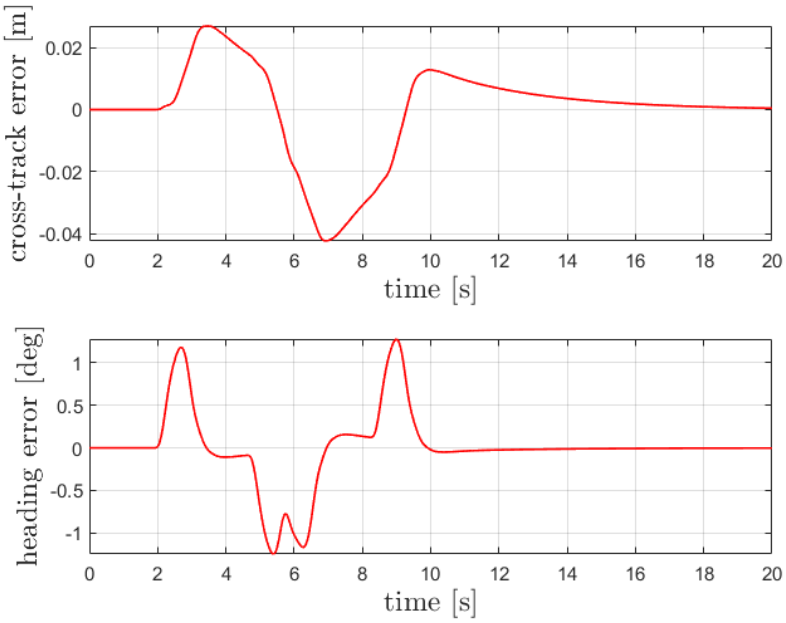

Figure 121: Cross-track and heading errors for ISO double lane change manoeuvre

Also here the data of steering angle and lateral accelerations have been reported in the *Figure 122* and *Figure 123*. Looking at lateral acceleration, this remains below the limit dictated by rollover, which means that the Pacci rover is able to travel on these trajectories without losing its stability and the steering angle has feasible values on the overall manoeuvre.

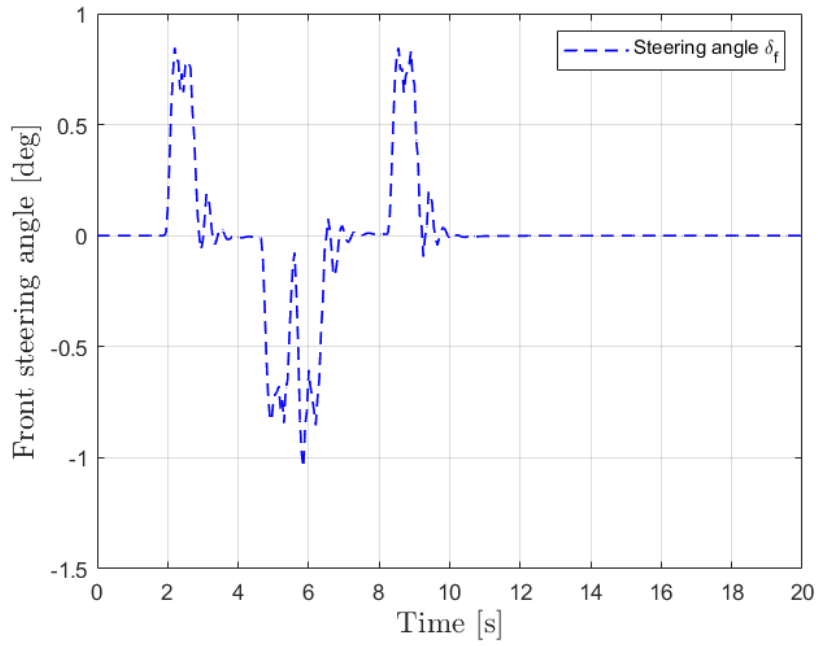

Figure 122: Front steering angle for ISO double lane change manoeuvre @ V=20 km/h

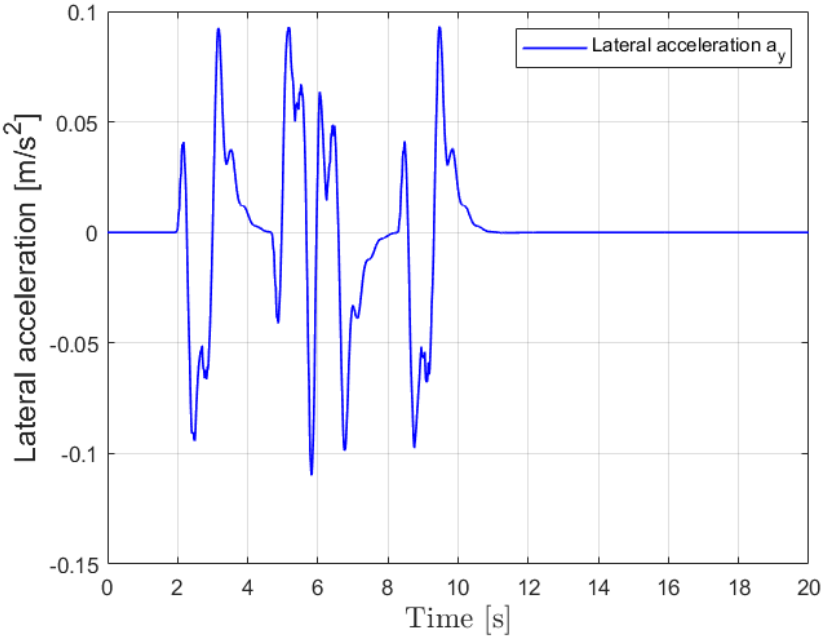

Figure 123: Lateral acceleration fos ISO double lane change manoeuvre @ V=20 km/h

Conclusions

All these simulations have been performed introducing a certain degree of simplification as the fact that the vehicle runs at constant speed in maximum adherence conditions and that the rear wheels are not steering ones. These characteristics would have brought to an increased level of complexity that would have been difficult to manage on common PCs, for this reason these have been studied singularly.

In these conditions, the study on longitudinal and lateral dynamics of the Pacci rover revealed how the vehicle has some limits in terms of maximum longitudinal and lateral accelerations, due to its dimensional characteristics, but according to the missions that it has to accomplish it results to be very stable and robust, even in limit loading conditions. The vehicle has a cornering behaviour that does not vary significantly in the range of the reachable speeds, avoiding any situation of poor controllability. The introduction of a controller as a PID made possible to manage the vehicle even in common situations of mixed scenario as avoidance of obstacles and of unpredictable object present on the road, performing a kind of sinusoidal manoeuvre, or overpassing in small spaces, performing a double lane change manoeuvre.

Bibliography

[1]: *(Ministero dell'Università e della Ricerca, "**PNR 2021-2027: Programma Nazionale per la Ricerca, grande ambito di ricerca e innovazione: Digitale, Industria e Aerospazio**", 13 July 2021, Rome).*

[2]: *(Moreno C., Allam Z., Chabaud D., Gall C., Pratlong F., **Introducing the "15-Minute City": Sustainability, Resilience and Place Identity in Future Post-Pandemic Cities**, Smart Cities, 8 January 2021, Paris).*

[3]: *(Data published by **Statista Research Department**, Apr 12, 2022).*

[4]: *(Inland Transport Committee of UNECE, **World Forum for Harmonization of Vehicle Regulations, Framework document on automated/autonomous vehicles**, November 2021).*

[5]: *(Westermark H., Gaeta M.C., Curran J., Polanco Lazo R., **Legal opinion on the Regulation of certain aspects of Automated Driving**, E-Avis ISDC 2022, 1 March 2022).*

[6]: *(Dawkins T., Wolf H., Al Abdelhamid S., Al-Bodour M., Ali-Sullivan A., Anthony C., Catania D., Khastgir S., Lichti T., Steiner R., Talon V., **Taxonomy for Segmentation of Autonomous Delivery Vehicles and Personal Delivery Devices**, World Economic Forum, September 2020).*

[7]: *(Guiggiani M., **The science of Vehicle Dynamics: Handling, Braking and Ride of Road and Race Cars**, Springer, February 2018).*

[8]: *A.Rodriguez, "**RC Car Modelling and Trajectory Tracking Control**", University of Southampton, September 2021*

[9]: *(D. Schramm et al., **Vehicle Dynamics**, Springer-Verlag Berlin Heidelberg 2014).*

[10]: *Porcelli N., MSc thesis in Mechanical Engineering "**Modellazione multibody di un monopattino elettrico**", Politecnico di Torino, a.a. 2021/2022*

[11]: *(Yonghwan Jeong, **Stochastic Model-Predictive Control with Uncertainty Estimation for Autonomous Driving at Uncontrolled Intersections**, Department of Mechanical and Automotive Engineering, Seoul National University of Science and Technology, Seoul 01811, Korea, 10 Oct 2021).*

[12]: C. Ronnapee and W. Witaya, Tire test for drifting dynamics of a scaled vehicle, Journal of Research and Applications in Mechanical Engineering, Bankok.

[13]: Kanwar Bharat Singh, Vehicle Sidedslip Angle Estimation Based on Tire Model Adaptation, MDPI, 2019.

[14]: Mattew Polley and Andrew G. Alleyne, Dimensionless Analysis of Tire Characteristics for Vehicle Dynamics Studies, American Control Conference, Boston, 2004

[15]: Video and Webinair: The Mathworks, Simulating Longitudinal and Lateral Vehicle Dynamics, 2020.